Study of DNA condensation for applications in nucleosome interactions and gene delivery with novel peptide vehicles
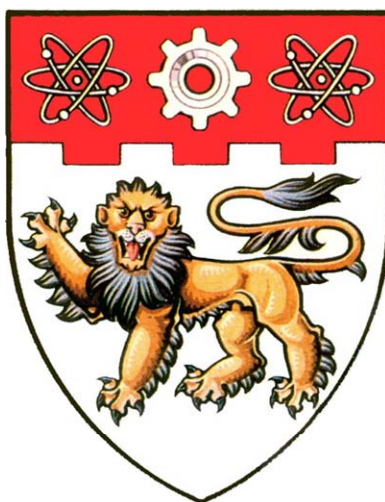
Huang, Dandan

2009

Huang, D. (2009). Study of DNA condensation for applications in nucleosome interactions and gene delivery with novel peptide vehicles. Doctoral thesis, Nanyang Technological University, Singapore.

https://hdl.handle.net/10356/15165

https://doi.org/10.32657/10356/15165

STUDY OF DNA CONDENSATION FOR APPLICATIONS

IN NUCLEOSOME INTERACTIONS AND GENE

DELIVERY WITH NOVEL PEPTIDE VEHICLES

HUANG DANDAN

SCHOOL OF BIOLOGICAL SCIENCES
NANYANG TECHNOLOGICAL UNIVERSITY

2009

Acknowledgements

This project was performed at School of Biological Sciences, Nanyang Technological University between January 2004 and November 2007 to fulfill the requirement for the PhD degree.

I would like to express my deep gratitude to Prof. Lars Nordenskiöld, my supervisor. Without him, this dissertation would not have been possible. I thank him for his patience and encouragement that carried me through difficult times, and for his insights and suggestions that helped to shape my research skills. In addition, he is always accessible and willing to help his students with their research.

A special thank goes to Prof. James P Tam, my co-supervisor. His insight to peptide synthesis is second to none. Besides, he sets an example of a world-class researcher for his rigour and passion on research.

I also thank Dr. Nikolay Korolev, who advised me and helped me in various aspects of my research. He is the one that I can always count on to discuss the tiniest details of a problem.

I thank all the members in my group. Thanks are also due to my postgraduate friends at School of Biological Sciences.

Last but not least, I would like to thank my parents for their everlasting love to me, and for always being there and supporting me through all these years.

Table of Contents

Summary

The basic idea of gene therapy is to replace abnormal genes with normal genes. To realize this replacement, carrier molecules called gene delivery vectors are needed. The shortcomings of viral gene delivery vectors have stimulated the development of nonviral vectors. In this work, a series of novel ε-polylysines with different chain length and side chains have been designed and characterized to be used as gene delivery agents.

I first physicochemically characterized DNA compaction by these novel ε-polylysines with Dynamic Light Scattering (DLS), Fluorescence Microscopy (FM) and Isothermal Titration Calorimetry (ITC). The ε-polylysines gave typical titration curves when added into DNA solutions. EC_{50} (the charge concentration of peptide at the midpoint of the scattering intensity curve) increased with the increase of ε-polylysine charge, indicating the electrostatic interactions between negatively charged DNA and positively charged ε-polylysines. For low charge ε-polylysines (n=5~7), EC_{50} increased as salt concentration increased in the solution. Among ε-K10 homologues with different side chains, ε-(LYR)K10 is the most efficient DNA compaction agent. EC_{50} of both ε-K10 and ε-(LYR)K10 increased with increase of the pH of the solution. With fluorescence microscopy, the free DNA molecules in extended coils and compacted DNA were clearly observed. The ITC results confirmed the behavior of DNA compaction.

I have also conducted studies of nucleosome core particles (NCP) aggregation using precipitation assay and DLS. NCP is the most regular central part of the nucleosome on which DNA mainly exists in the nucleus of eukaryotic cells. NCP precipitation curves were obtained with different cations, Mg^{2+}, Ca^{2+}, K^+ and Na^+ respectively and they are

consistent with reported work. HMGNs (high mobility group N) are a family of proteins found in the nuclei of all mammals and most vertebrate cells. Mg^{2+} or Spm^{4+} (cationic form of spermine) was used to test the effect of HMGN2 and its truncated form XN2 [fragment of HMGN2 (a.a. from 17 to 46)] on NCP aggregation. The results are rather complicated and different for different conditions. Therefore, more experiment need to be done to further explain the results.

Finally, *in vitro* transfection and cytotoxicity assay were carried out to evaluate the ε-polylysines for their ability to be used as gene delivery agents. Four cell lines, Hela, 293F, Mewo and A549 were tested. For Hela and 293F cells, combination of ε-(YR)K10, ε-(LYR)K10, ε-(LYH)K10, ε-(HK_4)K20, or ε-($LYHK_4$)K20 with DOTAP (N-[1-(2,3-Dioleoyloxy)propyl]-N,N,N-trimethylammonium methylsulfate, commercial transfection agent) dramatically increased transfection efficiency. Mixing of ε-(LYH)K10 and ε-(RGDP)K10 especially induced high transfection efficiency for 293F and A549 cells. ε-(LYH)K10, complexed with DOTAP, gave high transfection efficiency for all cell lines. MTT (3-(4,5-dimethylthiazol-2-yl)-2,5-diphenyl tetrazolium bromide) results showed all ε-polylysines tested displayed less cytotoxicity than the control DOTAP. All the findings indicated the promise of our ε-polylysines to be modified and applied as gene delivery vectors in the future.

List of Figures

List of Tables

Abbreviations

Boc-Lys(2-Cl-Z)-OH, N-(-tert-butoxycarbonyl-N-(-2-chloro-benzyloxycarbonyl-L-lysine;

Boc-Lys(Fmoc)-OH, N-(-tert-butoxycarbonyl-N-(-9-fluorenylmethoxycarbonyl-L-lysine;

cRGD, cyclic tripeptide sequence arginine-glycine-aspartic acid;

DAPI: 4,6-diamidino-2-phenylindole;

DCC, N,N'-dicyclohexylcarbodiimide;

DCM, dichloromethane;

DLS, dynamic light scattering;

DMF, dimethylformamide;

DMEM, Dulbecco's modified Eagle medium;

DMSO, dimethylsulfoxide;

DOPE, dioleoylphosphatidylethanolamine;

DOTAP, N-[1-(2,3-Dioleoyloxy)propyl]-N,N,N-trimethylammonium methylsulfate;

EC_{50}, the midpoint concentration of condensing agents in the titration curves;

EDTA, ethylenediamine tetraacetic acid;

FBS, fetal bovine serum;

FM, fluorescence microscopy;

GALA, glutamic acid-alanine-leucine-alanine repeat unit;

GFP, green fluorescence protein;

HK, histidine/lysine peptides;

HMG, high mobility group protein;

HOBt·H2O, N-hydroxybenzotriazole·water;

HPLC, high performance liquid chromatography;

ITC, isothermal titration calorimetry;

ε-K5… ε-K10: oligomers of ε-poly(L-lysines) with degree of polymerization from 5 to

10;

ε-(L)K10, ε-(Y)K10, ε-(R)K10, ε-(YR)K10, ε-(LYR)K10, ε-(LYH)K10, ε-(RGDP)K10 :

α-substituted ε-K10 homologues, amino acids in the brackets are the

substitution groups respectively;

ε-(LYR)K15, ε-(LYR)K20, ε-(HK$_4$)K20, ε-(LYHK$_4$)K20: other α-substituted ε-

polylysines, amino acids in the brackets are the substitution

groups respectively (for ε-(HK$_4$)K20 and ε-(LYHK$_4$)K20, K$_4$ in the

brackets denotes four lysines connected by ε-peptide bonds);

MALDI-MS, matrix-assisted laser desorption ionization mass spectrometry;

MBHA, 4-methylbenzhydrylamine;

MTT, 3-(4,5-dimethylthiazol-2-yl)-2,5-diphenyl tetrazolium bromide;

N/P ratio, molar ratio of nitrogen to DNA phosphate;

NBD, nucleosome binding domain;

NCP, nucleosome core particle;

NSBP1, nucleosomal binding protein;

PBS, phosphate-buffered saline;

PCS, photon correlation spectroscopy;

PEG, polyethylene glycol;

PEI, polyethylenimine;

α-PLL: α-poly(L-lysine) (degree of polymerization: 40 ~ 70);

ε-PLL: ε-poly(L-lysine) (degree of polymerization: 31) ;

PMMA, polymethylmethacrylate;

QELS, quasi elastic light scattering;

RGD, tripeptide sequence arginine-glycine-aspartic acid;

RP-HPLC, reversed phase-high performance liquid chromatography;

Spd^{3+}, cationic form of spermidine;

Spm^{4+}, cationic form of spermine;

TFA, trifluoroacetic acid;

TFMSA, trifluoromethanesulfonic acid;

XN2, fragment of HMGN2 (a.a. from 17 to 46).

Chapter 1. Introduction

1.1 DNA

1.1.1 DNA

Deoxyribonucleic acid (DNA) was first isolated in 1869 by the Swiss scientist Friedrich Miescher. He also showed that the new substance was derived from the nucleus of the cell alone and consequently named it "nuclein". By the late 1940s, scientists knew that DNA contained phosphate groups and four nitrogen-containing chemical "bases": adenine (A), thymine (T), guanine (G), and cytosine (C). But no one had thought out what the DNA molecule looked like.

In 1953, Linus Pauling, the American chemist, proposed the structure of DNA as a three-stranded helix with the bases facing out, but James Watson thought it was wrong when he saw Pauling's research paper (which had not been published) in January, 1953. A few days later at King's College in London, Watson was shown an X-ray diffraction photograph (Figure 1) of the DNA crystal taken by scientist Rosalind Franklin.

"The instant I saw the picture, my mouth fell open and my pulse began to race", wrote Watson in his book *The Double Helix* (1968). The photo ensured him that the DNA molecule must consist of two chains arranged in a paired helix, which resembles a spiral staircase or ladder.

Watson together with Francis Crick began to develop a stick-and-ball model of DNA's possible structure. The sides of the ladder were made up of alternating molecules of phosphate and the sugar deoxyribose, while each rung on the ladder was composed of a

pair of nitrogen-containing bases connected in the middle (Figure 2). At first, the scientists were not sure about how DNA's four bases---A, T, C, and G---link up with each other. Then with a suggestion from a colleague, they realized that the bases always join up with the same partners---A with T, and C with G.
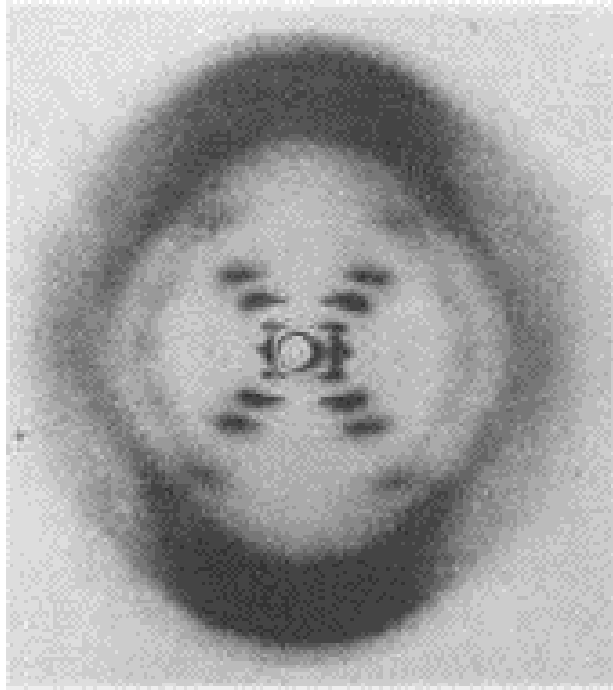
Figure 1. X-ray diffraction photograph of the DNA crystal taken by scientist Rosalind Franklin.
(Figure adapted from http://www.ocean.udel.edu/extreme2004/genomics/dnahistory.html)

In 1953, Watson and Crick finished their model which reached 6 feet tall. "A Structure for Deoxyribose Nucleic Acid" was published in *Nature* on April 25, 1953. By the late 1950s, their work had been widely accepted by the scientific community.

In 1962, Watson and Crick received the Nobel Prize for physiology or Medicine together with Maurice Wilkins, who had published important crystallography work relating to DNA at the same time as Watson and Crick.
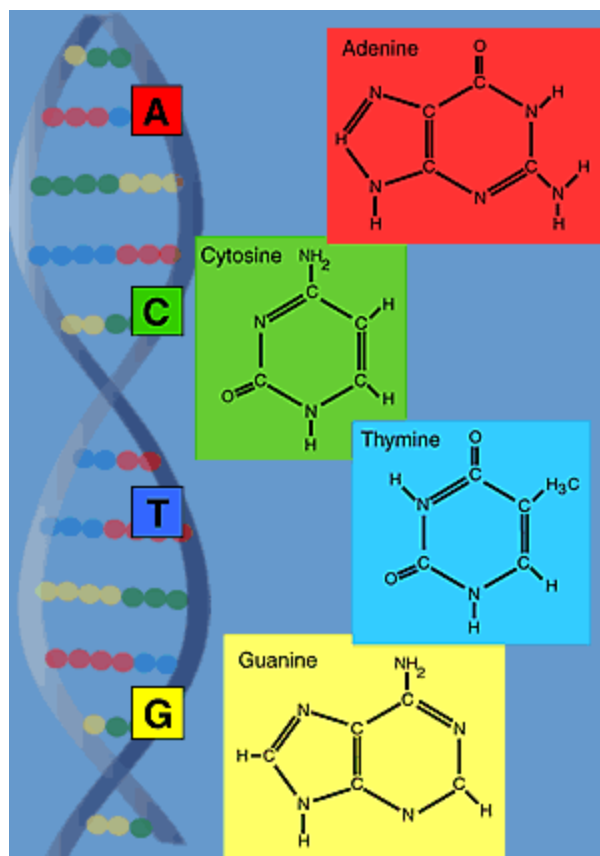
Figure 2. DNA double helix structure.
(Figure taken from http://www.ocean.udel.edu/extreme2004/genomics/dnahistory.html)

The DNA molecule resembles a spiral staircase or ladder. The sides of the ladders are made up of alternating molecules of phosphate and the sugar deoxyribose, while each rung is composed of a pair of nitrogen-containing chemical bases connected in the middle. DNA has four bases-Adenine, Thymine, Cytosine, and Guanine. These bases always join up with the same partners-A with T, and C with G.

The discovery of DNA structure has been called the most important biological work in the last 100 years and it opens a new door not only for the understanding of the fundamental basis of human life but also for the development of a novel group of therapeutics modeled on its endogenous structure (Patil *et al.*, 2005).

1.1.2 Nucleosome core particles (NCP)

The human chromosome 22 contains about 48 million nucleotide pairs, stretched from end to end, its DNA would extend about 1.5 cm. Yet, when it exists as a mitotic chromosome, chromosome 22 measures only about 2 μm in length, giving an end-to-end compaction ratio of nearly 10,000-fold (Alberts *et al.*, 2002).

The proteins that bind to the DNA to form eukaryotic chromosomes are traditionally divided into two general classes: the histones and the nonhistone chromosomal proteins. The complex of both classes of protein with the nuclear DNA of eukaryotic cells is known as chromatin. Histones are present in such enormous quantities in the cell (about 60 million molecules of each type per human cell) that their total mass in chromatin is about equal to that of the DNA (Alberts *et al.*, 2002).

Histones are responsible for the first and most basic level of chromosome organization, the nucleosome, which was discovered in 1974. When interphase nuclei are broken open very gently and their contents examined under the electron microscope, most of the chromatin is in the form of a fiber with a diameter of about 30 nm (Woodcock and Dimitrov, 2001; Hansen, 2002; Luger and Hansen, 2005). If this chromatin is subjected to treatments that cause it to unfold partially, it can be seen under the electron microscope as a series of "beads on a string" (Figure 3). The string is DNA and each bead is a "nucleosome core particle" that consists of DNA wound around a protein core formed from histones. The beads on a string represent the first level of chromosomal DNA packing (Alberts *et al.*, 2002).

Each individual nucleosome core particle consists of a complex of eight histone proteins-two molecules each of histones H2A, H2B, H3, H4---and double strand DNA

15

that is 146 nucleotide pairs long. The histone octamer forms a protein core around which

the double-stranded DNA is wound (Alberts *et al.*, 2002).
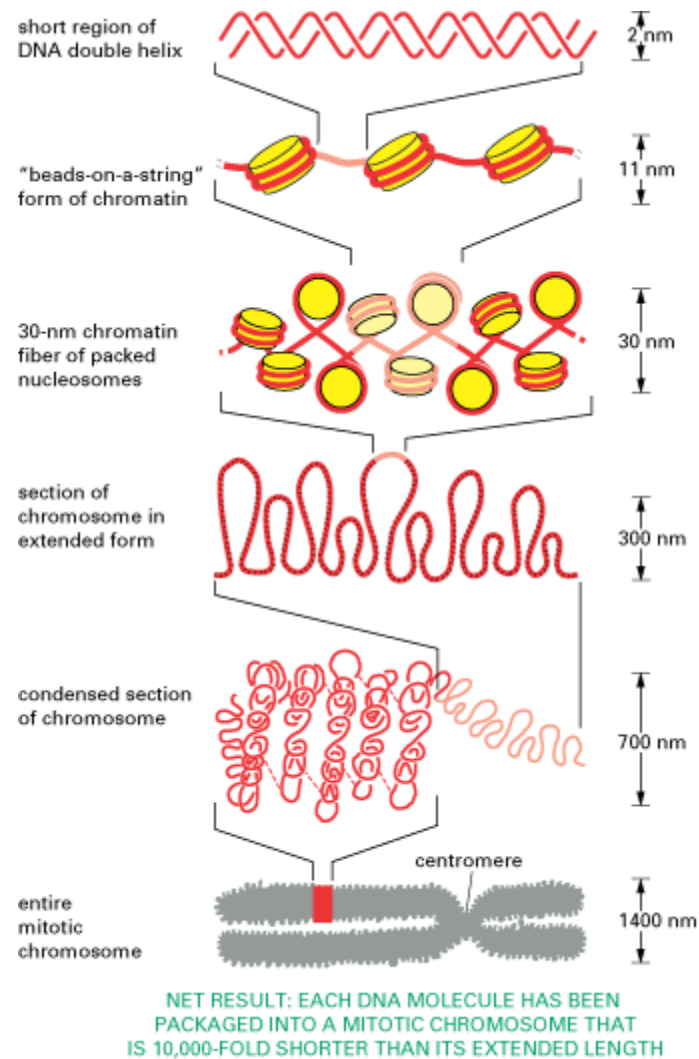
Figure 3. Chromatin packing.
(Figure adapted from (Alberts *et al.*, 2002)

This model shows some of the many levels of chromatin packing postulated to give rise to the highly
condensed mitotic chromosome.

The high-resolution structure of a nucleosome core particle, solved in 1997, revealed a

disc shaped histone core around which the DNA was tightly wrapped 1.65 turns in a left

handed coil (Luger *et al.*, 1997). All four of the histones that make up the core of the

nucleosome are relatively small proteins (102-135 amino acids), and they share a structural motif, known as the histone fold, formed from three α helices connected by two loops. In assembling a nucleosome, the histone folds first bind to each other to form H3-H4 and H2A-H2B dimers, and the H3-H4 dimers combine to form tetramers. An H3-H4 tetramer then further combines with two H2A-H2B dimers to form the compact octamer core, around which the DNA is wound (Alberts *et al.*, 2002).

The interface between DNA and histone is extensive: 142 hydrogen bonds are formed between DNA and the histone core in each nucleosome. Nearly half of these bonds form between the amino acid backbone of the histones and the phosphodiester backbone of the DNA. Numerous hydrophobic interactions and salt linkages also hold DNA and protein together in the nucleosome. For example, all the core histones are rich in lysine and arginine, and their positive charges can effectively neutralize the negatively charged DNA backbone (Alberts *et al.*, 2002).

In addition to its histone fold, each of the core histones has a long N-terminal amino acid "tail", which extends out from the DNA-histone core (Figure 4). These histone tails are subject to several different types of covalent modifications, which control many aspects of chromatin structure (Alberts *et al.*, 2002).
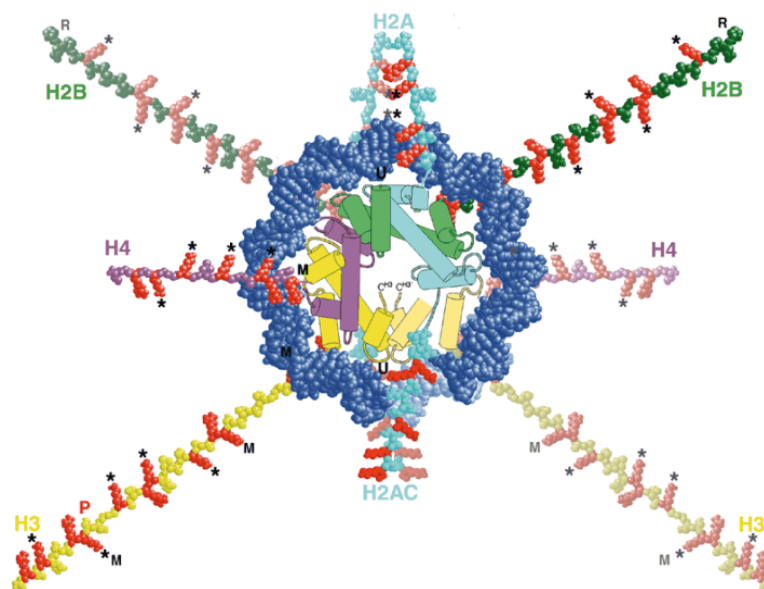
Figure 4. The detailed view of the histone tail domains and the nucleosome core particles along the superhelical DNA axis.
[Figure taken from (Wolffe and Hayes, 1999)]

The top and bottom superhelical turns of core DNA are colored blue and light blue, respectively. H2A, H2B, H3 and H4 are colored cyan, green, yellow and magenta respectively.

1.2 DNA condensation

1.2.1 Overview of condensation behavior

The mechanistic pathway for gene transfection includes the collapse of extended DNA chains into compact, orderly particles containing only one or a few molecules (Bloomfield, 1996; Blessing *et al.*, 1998). This process, known as DNA condensation, has received considerable attention in recent years due to its biological importance in DNA packaging in virus heads as well as in the development of gene delivery vehicles (Bloomfield, 1996; Blessing *et al.*, 1998; Duguid *et al.*, 1998; Xu *et al.*, 1999; Montigny *et al.*, 2001). Since DNA condensation is a prerequisite for gene delivery in cell transfection both *in vitro* and *in vivo*, it is worthwhile to begin with a brief overview of some broader aspects of DNA condensation (Bloomfield *et al.*, 1988; Bloomfield, 1991).

Condensation is defined as a decrease in the volume occupied by a DNA molecule from the large domain dilutely occupied by a wormlike random coil, to a compact state in which the volume fraction of solvent and DNA are comparable. In the condensed state, DNA helices may be separated by just one or two layers of water (Bloomfield, 1997).

In this thesis, I will use the notation compaction for the general phenomenon of a single molecule random coil to collapsed globular formation. The term condensation is often used for both intramolecular DNA collapse and/or intermolecular aggregation of many DNA molecules to a separate phase (Bloomfield, 1996), but since this terminology may be mixed up with the notion of condensation of cations on the charged DNA polyelectrolyte called "counterion condensation" (Manning, 1996), it should be avoided

in this context. Experimentally, this collapse transition to the compact state is often not a well defined event and it is common that several molecules are incorporated in the collapsed state, probably due to kinetic trapping or because the conditions correspond to coexistence of compacted and aggregated states. Thus condensation is difficult to distinguish rigorously from aggregation or precipitation. Use of the term condensation is generally confined to situations in which the aggregate is of finite size and shows orderly morphology (Bloomfield, 1997).

Genomic DNA is a very long molecule, which must fit it into a very small space inside a cell or virus particles. Fully extended, the 160,000 base pairs of T4 phage DNA span 54 μm. Yet the T4 DNA molecule has to fit in a virus capsid about 100 nm in diameter, a 540-fold linear compression. The 4.2 million base pairs of the *Escherichia coli* chromosome extend 1.4 mm (half this as a fully stretched circular chromosome), yet must fit into a nucleolar region about 1 μm across, a linear compression of about 1400. Thinking about the issue in a different way, the radius of gyration of the T4 wormlike coil is about 950 nm, so its volume compression ratio is about 6900. The molecular volume of the T4 DNA molecule, considered as a cylinder 2 nm in diameter phosphate-to-phosphate, is $1.7 \times 10^5 \text{ nm}^3$; the internal volume of the capsid is about $5 \times 10^5 \text{ nm}^3$, so the DNA occupies about 1/3 of the volume within the capsid (Bloomfield, 1997).

The decrease in size of the DNA domain in natural organisms is striking, so the phenomenon of DNA condensation has drawn much attention (Bloomfield, 1997). It is a considerable surprise that DNA collapse, or condensation, can occur spontaneously in the test tube, upon adding a low concentration of multivalent cation to low ionic strength

aqueous buffer (Gosule and Schellman, 1976). The morphology of the condensed DNA particles is most commonly that of a compact, orderly toroid, strongly reminiscent of the structure of intraphage DNA gently lysed from virus capsids (Klimenko *et al.*, 1967). The X-ray scattering shows that the surface-to-surface spacing between DNA helices is only about 1-2 water diameters (Schellman and Parthasarathy, 1984), so that the packing density of DNA condensed *in vitro* is entirely comparable to that of intraphage DNA (Bloomfield, 1997).

DNA condensation has become a lively field for research in diverse areas of science. In biochemistry, biophysics, and molecular biology it represents a process by which the genetic information is packaged and protected. In biotechnology and medicine, it provides a promising means whereby DNA containing genes of therapeutic interest can be prepared for transfer from solution to target cells for gene therapy applications (Bloomfield, 1997).

1.2.2 Condensing agents

Condensing agents generally work either by decreasing repulsions and even inducing attraction between DNA segments (e.g., neutralizing of phosphate charge, and/or reorienting water dipoles near DNA surface, by multivalent cations) or by making DNA-solvent interactions less favorable [e.g., by adding ethanol, which is a poorer solvent than water for DNA, or by adding another polymer, such as polyethylene glycol (PEG), which excludes volume to the DNA]. Multivalent cations may also cause localized bending or distortion of the DNA, which can also facilitate condensation (Bloomfield, 1997).

In aqueous solutions, condensation normally requires cations of charge +3 or greater. Those most commonly used in condensation studies are the naturally occurring polyamines spermidine[3+] and spermine[4+] (Gosule and Schellman, 1976; Chattoraj et al., 1978) and the inorganic cation $Co(NH_3)_6^{3+}$ (Widom and Baldwin, 1980; Widom and Baldwin, 1983). Others include cationic polypeptides such as polylysine (Laemmli, 1975), and basic proteins such as histone H1 and H5 (Hsiang and Cole, 1977; Garcia-Ramirez and Subirana, 1994). Divalent metal cations do not provoke DNA condensation in water at room temperatures except under special circumstances (Ma and Bloomfield, 1994), but they will do so in water-alcohol mixtures (Wilson and Bloomfield, 1979; Votavova et al., 1986; Arscott et al., 1995; Bloomfield, 1997).

Much attention has been paid recently to the condensation of DNA with cationic liposomes since the complex can be an efficient agent for transfection of eukaryotic cells. This is presumably because the condensed state of the DNA protects it from nucleases and allows it to pass more easily through small openings, while the lipid coating on the DNA increases its permeability through cell membranes (Duzgunes and Felgner, 1993; Huang et al., 1993; Bloomfield, 1996; Bloomfield, 1997; Lasic, 1997).

1.2.3 Morphology

When condensation is induced by careful addition of polyamines or $Co(NH_3)_6^{3+}$ to dilute aqueous DNA solutions, toroids and rods are the structures most commonly observed by electron microscopy. The toroids have similar size distributions regardless of DNA length, indicating that several small DNA molecules, or one large one, are incorporated in a single particle (Chattoraj et al., 1978; Arscott et al., 1990; Bloomfield,

1991). Torus-shaped particles of spermidine-condensed DNA exist under the hydrated conditions of freeze fracture electron microscopy, and DNA double-helical fibers can be seen circumferentially wrapped around the toroid (Marx and Ruben, 1983).

The toroidal conformation of condensed DNA, with a well-defined hole in the middle surrounded by circumferentially wound double-helical strands, is one of the most striking aspects of the condensation phenomenon. Given that solvent conditions are sufficient to cause collapse of the extended DNA chain, why are toroids formed, rather than spherical globules, or rods, or lamellae? Or indeed, why ordered particles at all, rather than random aggregates? Most of the answer lies in the stiffness of DNA, the rather weak attractive force between DNA segments, and the very low DNA concentrations at which condensation experiments are generally done (Bloomfield, 1997).

A tenable theory has been developed by Grosberg and Zhestkov, who consider that the total free energy of DNA is the sum of compressive, repulsive, and elastic contributions (Grosberg and Zhestkov, 1986). The relative importance of these free energy terms depends also on polymer chain length. The result is a complicated phase diagram, from which it is deduced that relatively short DNA molecules will form toroids, while very long molecules will form compact spherical globules. (Of course, very short DNAs cannot form toroids either, since they cannot bend sufficiently without kinking.) Greater compressive forces will favor spherical globules without an inner hole, while greater stiffness and excluded volume will favor toroids. These predictions have been verified experimentally for condensation by $Co(NH_3)_6^{3+}$ of DNA from bacteriophages λ [48 kilobase pair (kbp)] and T4 (166 kbp) (Vasilevskaya $et\ al.$, 1997). Toroids are seen with

both molecules at low $Co(NH_3)_6^{3+}$ concentration, but spherical globules become predominant as the concentration of condensing agent increases.

Rodlike particles are occasionally seen in electron micrographs of condensed DNA, but they are rarely in high proportion unless the solvent or the condensing agent is somewhat nonpolar. It seems likely that a nonpolar environment may lower the free energy of exposed heterocyclic bases, favoring sharp local kinking over gradual bending. The diameters and lengths of the rods are similar to the thickness and circumferences, respectively, of the toroids; but one does not seem to be the precursor of the other (Bloomfield, 1997).

The addition of larger volumes of alcohol produces ramified fibrous aggregates, accompanied by a B-A conformational transition of the plasmid DNA. The transition occurs at a lower concentration of either ethanol or $Co(NH_3)_6^{3+}$ than would be required with either alone, indicating that they act cooperatively (Arscott *et al.*, 1995). It is speculated that the A-DNA strongly self-adheres and rapidly aggregates into fibrous networks, disallowing the annealing required to form more compact and orderly condensates (Bloomfield, 1997).

Short DNA molecules do not normally form toroidal aggregates: their length is insufficient to nucleate such structures (Bloomfield, 1991). At very high concentration near 200 mg/mL, DNA of about one persistence length (~150 bp) spontaneously forms a liquid crystalline phase (Rill, 1986). This transition takes place in the presence of monovalent salt due to repulsive excluded volume interactions between the rod-like molecules. A liquid crystalline phase can also be formed by adding spermidine to a dilute

solution of mononucleosomal DNA (Sikorav *et al.*, 1994). In this case, formation of the ordered phase is due to attractive interactions between the parallel rods (Bloomfield, 1996).

1.2.4 Minimum DNA size

A striking feature of DNA condensation is that the dimensions and morphology of condensed DNA particles are largely independent of the size of the DNA. This generalization holds only above a minimum length, however. Widom and Baldwin found that DNA fragments shorter than about 400 base pairs will not condense into orderly, discrete particles (Widom and Baldwin, 1980). This indicates that the net attractive interactions per base pair are very small: at least several hundred base pairs must interact, either intramolecularly or intermolecularly, to form a stable condensed particle (Bloomfield, 1991; Bloomfield, 1997).

1.2.5 The importance of ionic interactions

Electrostatic forces must be important in condensation. The laws of physics require that the strong repulsive interactions must be substantially neutralized as negatively charged DNA segments approach closely. Ionic effects on condensation were investigated systematically by Wilson and Bloomfield (Wilson and Bloomfield, 1979), who studied condensation of T7 bacteriophage DNA with spermidine, spermine, and other multivalent cations by light scattering, which enabled convenient detection of condensation under a wide range of ionic conditions. They observed that the critical concentration of multivalent cation required to produce DNA condensation increases with increasing salt.

When the amount of binding of multivalent cation and simple salt to the DNA was calculated using Manning's counterion condensation theory (Manning, 1978), a striking regularity emerged that has since been confirmed under a wide variety of circumstances: approximately 90% of the DNA charge must be neutralized for condensation to occur (Bloomfield, 1997).

Widom and Baldwin (Widom and Baldwin, 1980; Widom and Baldwin, 1983) found that $Co(NH_3)_6^{3+}$ is a 5-fold more efficient condensing agent than spermidine^{3+}, despite equal binding of these isovalent compounds (Plum and Bloomfield, 1988), with collapse occurring at about 85% charge neutralization. However, the dependence of the critical $Co(NH_3)_6^{3+}$ concentration on added salt confirms the ion exchange behavior underlying the equations for competitive counterion condensation of two cations with different valences (Manning, 1978; Wilson and Bloomfield, 1979; Bloomfield, 1997). Electrophoretic light scattering shows directly that the condensation of λ DNA by spermidine^{3+} or spermine^{4+} is accompanied by a decrease in charge density to approximately 0.1 level (Yen and Ware, 1982). All of these results indicate that DNA condensation in the presence of multivalent cations is determined by the total charge neutralization of the DNA, rather than by the binding of the multivalent cation per se (Wilson and Bloomfield, 1979).

1.3 DNA compaction by proteins and polymers

The majority of DNA in all living organisms is present in a compact form. In higher organisms the histones are responsible for maintaining this packaging, and the interaction between DNA and histones is the subject of a lot of current research (Wilson and

Bloomfield, 1979). In viruses, several different molecules have been involved in the maintenance of a condensed form of DNA. These include internal proteins (Laemmli, 1975) and the polyamines such as putrescine, spermidine, and spermine (Ames and Dubin, 1960). Several studies have demonstrated the efficiency of these compounds in collapsing DNA *in vitro*. Collapse has been observed by using electron microscopy (Laemmli, 1975; Chattoraj *et al.*, 1978) and inferred from turbidity, circular dichroism, and hydrodynamic measurements (Gosule and Schellman, 1976; Gosule and Schellman, 1978). Collapse has also been induced by using neutral polymers such as poly(ethylene oxide) in the presence of high NaCl concentrations (Lerman, 1971).

1.4 NCP aggregation and HMGN proteins

In the nucleus of eukaryotic cells, DNA exists mainly as linear domains of uniform DNA-protein complexes, the nucleosomes. The most regular central part of the nucleosome is the nucleosome core particle (NCP), which consists of ~146-147 bp of DNA wrapped as a 1.75-turn superhelix around a wedge-like octamer of core histones formed by the core-histone protein octamer (Luger *et al.*, 1997; Davey *et al.*, 2002). Variable-length double-stranded linker DNA connects the NCPs with each other to form nucleosomal arrays that condense into 30-nm chromatin fibers (Woodcock and Dimitrov, 2001; Hansen, 2002; Luger and Hansen, 2005). Each of the core histones has unstructured, highly basic N-terminal domains called "histone tails" protruding through the DNA superhelix. The structure of the histone tails largely escapes detection by X-ray crystallography and other experimental methods, implying that they are highly flexible and dynamic (Luger *et al.*, 1997; Luger and Richmond, 1998). The histone tails are essential for maintenance of the higher-order compact folded structures of chromatin and

27

for regulation of transcription and replication (Wolffe, 1998; Horn and Peterson, 2002). These function of the histone tails are regulated by covalent modifications of the amino acids, which may change the net charge and distribution of the charged groups in the tails (Luger and Richmond, 1998; Ren and Gorovsky, 2003; Korolev *et al.*, 2006).

Many proteins have been shown to be involved in the remodeling of chromatin, which is suspected to be of great importance in the regulation of transcription or induction of mitosis for instance (Strahl and Allis, 2000). The aggregation of chromatin arrays has also been extensively studied *in vitro*. It has been demonstrated that the polyelectrolyte character of DNA, nucleosome, and chromatin was responsible for the aggregation of the fibers (Widom, 1986; Clark and Kimura, 1990). It was shown also that the aggregation of the fibers can be achieved by addition of cations in the absence of H1 histones, but the integrity of the histone tails is absolutely required (Fletcher and Hansen, 1996; Widom, 1998). The presence of divalent cations is also necessary to reach the ultimate states of aggregation of the fibers. Nevertheless, numerous questions remain open due to the complexity of the system.

HMGNs are a family of proteins found in the nuclei of all mammals and most vertebrate cells (Bustin, 1999; Bustin, 2001). The founding members of this family HMGN1 and HMGN2 (formerly known as HMG-14 and HMG-17; see (Bustin, 2001) for revised nomenclature of the HMG superfamily) are ubiquitous to most cells while the more recently discovered members HMGN3 (West *et al.*, 2001), HMGN4 (Birger *et al.*, 2001) and NSBP1 (nucleosomal binding protein) (Shirakawa *et al.*, 2000) have a restricted tissue distribution. On the average, a nucleus contains 1×10^5 HMGN1 and HMGN2 molecules, which is sufficient to bind to less than 2% of the nucleosomes (Johns,

1982). The protein bind to the 147 bp nucleosome core particle, the building block of the chromatin fiber, without any known specificity for the DNA sequence (Shirikawa *et al.*, 2000) and form homodimeric complexes of nucleosomes containing 2 molecules of either HMGN1 or HMGN2 (Postnikov *et al.*, 1995). In cellular chromatin, nucleosomes containing HMGN proteins are clustered into domains that on the average contain 6 contiguous nucleosome-HMGN complexes (Postnikov *et al.*, 1997). These domains are scattered throughout the entire non-nucleolar region of the nucleus and generate structural and compositional heterogeneity in the chromatin fiber.

Several types of *in vitro* experiments demonstrate that the interaction of HMGN with nucleosomes reduced the aggregation of the higher order chromatin structure and enhances the rate of transcription and replication. The ability of the proteins to enhance transcription and replication is linked to their ability to unfold chromatin (Trieschmann *et al.*, 1995; Trieschmann *et al.*, 1995; Ding *et al.*, 1997). HMGN mutants that do not unfold chromatin do not enhance transcription. Conceivably, domains of HMGN-containing nucleosomes disrupt the continuity of the 30 nm chromatin fiber, promote unfolding, and facilitate access to the nucleosome. Thus, the architectural changes induced in chromatin by HMGN proteins enhance the rate of DNA-related processes that are affected by chromatin aggregation.

HMGN are the only nuclear proteins that recognize structural features that are specific to the 147 bp nucleosome core particle. They do bind to nucleosome core particles better than DNA and interact with both the nucleosomal DNA (Alfonso *et al.*, 1994) and with the tails of core histone (Crippa *et al.*, 1992; Trieschmann *et al.*, 1998). These properties and the observation that nucleosomes containing HMGN proteins are clustered into

domains lead to the concept that HMGN are an integral part of the chromatin fiber, permanently associated with specific chromatin regions, perhaps marking them for transcription. Indeed, both confocal immunofluorescence and immunoelectron microscopy studies demonstrated that nascent transcripts colocalize with HMGN proteins (Hock *et al.*, 1998).

In a landmark study, Phair and Misteli (Phair and Misteli, 2000) used photobleaching techniques to analyze, in living cells, the intranuclear mobility of the chromatin binding protein HMGN2, of the RNA processing protein fibrillarin, and of the splicing factor SF2/ASF in living cells. All of these proteins were mobile and in constant motion; the fastest moving protein being HMGN2. Further analysis indicated that both HMGN1 and HMGN2 move rapidly throughout the nucleus in a random-type motion with an apparent diffusion constant of ~0.5 μm^2/s. It would take less than 1 min for one molecule of HMGN to traverse the entire 15 μm width of an average nucleus.

The high degree of mobility of the protein in the nucleus is an important aspect of the mechanism by which the proteins reach their target and affect chromatin function. Although the amount of the protein is sufficient to bind to only 2% of the nucleosomes, the rapid and constant movement ensures that all chromatin regions would have adequate access to HMGN proteins. In others words, HMGNs are everywhere. The biochemical studies using purified chromatin and isolated HMGN proteins do not always present the true picture on the interaction of these proteins with chromatin in the living nucleus. Conceivably the interaction of HMGN proteins with chromatin is more specific than previously imagined. HMGN proteins may bind to specific chromatin conformations, which are not preserved in isolated nucleosomes or chromatin, or recruited to specific

regions by histone modifications or by pre-bound chromatin factors. Alternatively, HMGN may reach their targets in association with other proteins (Lim *et al.*, 2002).

1.5 Gene delivery

1.5.1 Gene therapy

Genes, which are carried on chromosomes, are the basic physical and functional units of heredity. They are specific sequences of bases that encode instructions on how to make proteins. Although genes get a lot of attention, it is the proteins that perform most life functions and even make up the majority of cellular structures. When genes are altered so that the encoded proteins are unable to carry out their normal functions, genetic disorders can result.

Gene therapy is a technique for correcting defective genes responsible for disease development. In most gene therapy studies, a "normal" gene is inserted into the genome to replace an "abnormal", disease-causing gene. A carrier molecule called a vector must be used to deliver the therapeutic gene to the patient's target cells.

Early discussion of the possibility for gene therapy occurred at a symposium entitled "Reflections on Research and the Future of Medicine" that took place at Columbia University in May, 1966 (Tatum, 1967). Two papers in the early 1970s specifically discussed the possibilities and the ethics of gene therapy (Anderson, 1972; Friedmann and Roblin, 1972).

The science leading to gene therapy took a large step forward when Michael Wigler and Richard Axel succeeded in transferring a gene (thymidine kinase, TK) into mammalian cells (TK$^-$ L cells) in 1977 (Wigler *et al.*, 1977). The science underpinning gene therapy

began to be published in 1983 when Alan Bernstein (Joyner *et al.*, 1983), Dusty Miller with Inder Verma (Miller *et al.*, 1983), and Ted Friedmann (Wills et al., 1984) succeeded in using a retroviral vector to transfer a functional gene into cells, either murine bone marrow (Joyner *et al.*, 1983), 3T3 cells (Miller *et al.*, 1983), or a human HPRT⁻ B-lymphoblast cell line (Willis *et al.*, 1984). In 1984, other viral systems were being developed for gene transfer: adenovirus by Y. Gluzman (Van Doren *et al.*, 1984) and adeno-associated virus by Barrie Carter (Tratschin *et al.*, 1984) and Nicholas Muzyczka (Hermonat and Muzyczka, 1984).

In 1990, the first approved gene therapy clinical trial took place when a 4 year old girl with ADA-deficient Severe Combined Immunodeficiency, was given her own T cells engineered with a retroviral vector carrying a normal ADA gene by the NIH team of Anderson/Blaese/Rosenberg (Blaese *et al.*, 1995). The first non-viral gene therapy clinical trial also began in 1992 when Gary Nabel injected a DNA/lipocome complex (the DNA plasmid carrying an HLA-B7 gene) directly into HLA-B7⁻ tumors (Plautz *et al.*, 1992). A patient died in 1999 following intrahepatic infusion of an adenoviral vector as part of a Phase I/II toxicity trial.

The first gene therapy cure was reported in 2000 when Alain Fischer (Paris) succeeded in totally correcting children with X-linked severe combined immunodeficiency (SCID-X1) (Cavazzana-Calvo *et al.*, 2000). The patient's blood stem cells were incubated with a retroviral vector carrying a normal γc gene and the gene-engineered blood cells were re-infused into the patient. Unfortunately, ~30 months after treatment, 2 of the 10 patients developed a leukemia-like syndrome; the children were subsequently treated with chemotherapy. After considerable research, it has now been determined that the γc gene

itself can function as a cooperating factor in transformation if expressed from a retroviral promoter (Berns, 2004). These adverse events have prompted a reason for modification of current vector systems.

In 2003, Gendicine, the first gene therapy product to be approved for sale anywhere in the world was licensed in China. It is an adenoviral vector carrying a p53 gene for the treatment of cancer. As of March 2004, 619 gene therapy/transfer clinical protocols have been submitted to the NIH/FDA for approval (http://www4.od.nih.gov/oba/rac/documents.htm). Over 3000 patients have been treated with a gene therapy/transfer vector worldwide in clinical trials.

1.5.2 Viral gene delivery

Gene therapy has become a lively field due to the development of gene transfer technology. A major requirement for gene therapy is the efficient transport of DNA through the cell membrane by processes that are not well defined (Luo and Saltzman, 2000; Zuber *et al.*, 2001).

The principal strategies for gene delivery involve viral-mediated, chemical and physical mechanisms (Smith, 1995). Viral vectors are an obvious starting point because viruses have evolved efficient mechanisms to introduce and express their nucleic acid into recipient cells. By the same token the viral hosts have evolved sophisticated mechanisms to rid themselves of such pathogens (Smith, 1995).

Viral vectors are widely used since the molecular biology of recombinant viruses is well understood and they give high level of DNA uptake and expression. However, major disadvantages of viral vectors for gene transfer include a lack of cell type specificity, a

restriction in the size of DNA that can be used, safety considerations, and host immune response. For example, adenovirus-mediated gene delivery is highly efficient and can be used to transduce nondividing cells. There are, however, highly efficient host immune responses, which have evolved to contain viral infections that limit the usefulness of the recombinant adenovirus. The cells that contain the exogenous gene of interest are destroyed by a cellular immune response directed against the viral gene products that are also expressed in the target cells. Viral proteins stimulate neutralizing antibodies, so that the gene delivery system can only be used once in a given individual (Smith *et al.*, 1998). Furthermore, viral vector systems are rapidly cleared from the circulation, limiting transfection to 'first-pass' organs, such as the lungs, liver, and spleen (Lollo *et al.*, 2000).

1.5.3 Chemical nonviral DNA delivery

Among several methods of gene transfer, including cell-based and viral mediated approaches, nonviral gene delivery is becoming a major focus of research in the field of gene therapy due to complex and redundant anti-viral defenses (Ledley, 1994; Ledley, 1995; Rolland, 1996; Rolland and Tomlinson, 1996; Tomlinson and Rolland, 1996; Rolland, 1998). The objective of these research efforts is to construct self-assembling DNA complexes using synthetic chemical components that perform the roles of proteins in the viral vectors (Smith *et al.*, 1998).

This increased interest in nonviral gene therapy can be attributed to promising results both, *in vitro* and *in vivo*, in delivering genes using proteins (Wu and Wu, 1987; Wu and Wu, 1988; Wu and Wu, 1988; Wang and Huang, 1989; Cotten *et al.*, 1990; Wagner *et al.*, 1990; Wagner *et al.*, 1991; Plank *et al.*, 1992; Trubetskoy *et al.*, 1992; Wagner *et al.*,

1992; Cotten *et al.*, 1993), high-molecular-weight polypeptides (Cotten *et al.*, 1990; Wagner *et al.*, 1990; Wagner *et al.*, 1991; Midoux *et al.*, 1993; Monsigny *et al.*, 1994; Erbacher *et al.*, 1995), cationic lipids and liposomes (Felgner *et al.*, 1987; Wang and Huang, 1989; Legendre and Szoka, 1992; Trubetskoy *et al.*, 1992; Dowty and Wolff, 1994), novel synthetic polymers such as polylysine derivatives, and polyethyleneimine, polyamidoamine and polymethacrylate dendrimers which can condense anionic DNA molecules into compact and ordered nanoparticles that are ~50-200 nm in diameter (Haensler and Szoka, 1993; Boussif *et al.*, 1995; Kabanov and Kabanov, 1995), or combination thereof (Wagner *et al.*, 1991; Zhou *et al.*, 1991; Trubetskoy *et al.*, 1992; Plank *et al.*, 1994; Remy *et al.*, 1995).

The utilization of many of these delivery systems stems from their ability to interact with a plasmid and self-assembled into compact particles (Hirschman *et al.*, 1967; Olins *et al.*, 1967; Shapiro *et al.*, 1969; Haynes *et al.*, 1970; Lerman, 1971; Evdokimov Iu *et al.*, 1973; Laemmli, 1975; Evdokimov Iu *et al.*, 1976; Gosule and Schellman, 1976; Chattoraj *et al.*, 1978; Wilson and Bloomfield, 1979; Widom and Baldwin, 1980; Widom and Baldwin, 1983; Bloomfield *et al.*, 1992; Ghirlando *et al.*, 1992). The polycations reduce the size of the complex, and confer excess cationic charge to the complex, thereby enhancing their cellular uptake by an endocytosis pathway (Vijayanathan *et al.*, 2002; Schmidt-Wolf and Schmidt-Wolf, 2003). Some polymers have been conjugated to targeting ligands for cell-specific gene delivery, resulting in enhanced gene transfer efficiency via the route of receptor-mediated endocytosis (Wu and Wu, 1987; Wu and Wu, 1988; Wu and Wu, 1988; Wagner *et al.*, 1990; Wagner *et al.*, 1991; Plank *et al.*,

1992; Cotten *et al.*, 1993; Midoux *et al.*, 1993; Gottschalk *et al.*, 1994; Monsigny *et al.*, 1994; Erbacher *et al.*, 1995).

Nonviral vectors have several advantages over their viral counterparts: (1) they are easy to prepare and to scale-up; (2) they are more flexible with regard to the size of the DNA being transferred; (3) they are generally safer *in vivo*; (4) they do not elicit a specific immune response and can therefore be administered repeatedly; and (5) they are better for delivering cytokine genes because they are less immunogenic than viral vectors. However, intrinsic drawbacks with cationic carriers, such as solubility, cytotoxicity and low transfection effiency, have limited their use (Schmidt-Wolf and Schmidt-Wolf, 2003).

During gene delivery, the cellular uptake of polycation/DNA complexes can be gained by specific receptors, also the positive surface charge of complexes can serve to bind to cells via electrostatic interactions with the negatively charged cell membrane followed by endocytosis. After endocytosis, DNA may be released from endosome during cell division because of the de-compaction machinery of cells and then DNA will transport to nucleus.

The ideal nonviral DNA delivery system (Figure 5) should have the following properties:

(a) be a structurally well characterized, nontoxic, biodegradable, and nonantigenic system that protects DNA from degradation and is stable in biofluids;

(b) promotes cellular uptake mediated by cell specific plasma membrane receptors;

(c) favours rapid pH dependent release from the endosome;

(d) efficiently dissociates the DNA from the complex into the cytoplasm for transport

of DNA to the nucleus;

(e) exhibits controlled duration and magnitude of expression (Smith *et al.*, 1998).
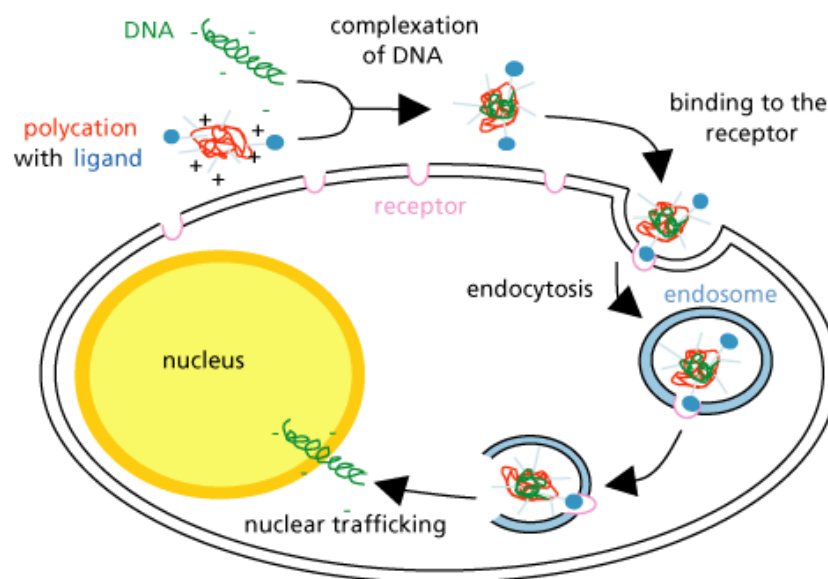
Figure 5. The typical process of gene delivery mediated by polycationic vectors.
(Adapted from: http://www.nano-lifescience.com/research/gene-delivery.html)

During gene delivery, therapeutic DNA is first compacted by polycations and then the cellular uptake of polycation/DNA complexes can be gained by specific receptors. The positively charged surface of complexes can serve to bind to cells via electrostatic interactions with the negatively charged cell membrane followed by endocytosis. After endocytosis, DNA may be released from endosome during cell devision because of the de-compaction machinery of cells and then DNA will transport to nucleus and be expressed into proteins.

1.6 RGD motif and pH-sensitive residue

Successful nonviral vectors should have multifunctional properties to overcome many

extracellular and intracellular barriers before they deliver therapeutic genes into desired

cells. One of the major advantages of polymeric gene delivery carrier development is that

various functional groups or molecules can be introduced into a cationic polymer

backbone, so as to get close to an ideal gene delivery carrier that should deliver

therapeutic DNA into target cells with high efficiency, be nontoxic and non-immunogenic, and be easily produced in large quantity (Cristiano and Roth, 1995). To satisfy these requirements, polymeric gene delivery carriers have been conjugated with diverse ligands that selectively target particular receptors on certain type of cells (Choi *et al.*, 1998; Kim *et al.*, 1998; Benns *et al.*, 2001; Suh *et al.*, 2001). The receptor-mediated gene transfer not only offers the possibility of targeted gene delivery, but also facilitates the internalization of DNA complex via a receptor-mediated endocytosis pathway.

Cancer remains an attractive target for gene delivery since conventional chemotherapy is often inefficient. Fast growing metastases, refractive to treatments such as radiation or chemotherapy, are associated with poor prognosis. Inhibition of angiogenesis, the development of new blood vessels from the endothelium of a pre-existing vasculature (Folkman and Shing, 1992; Hanahan, 1997; Carmeliet and Jain, 2000; Griffioen and Molema, 2000), was shown to suppress growth of metastases since new vessels are required for proliferation (Folkman, 1971).

Integrins are adhesion molecules involved in cell-cell and cell-matrix adhesion processes. The integrin family includes heterodimeric transmembrane glycoproteins made of α and β subunits (Buck and Horwitz, 1987; Springer, 1990; Hynes, 1992). The $\alpha\beta$ complex and the presence of divalent cations are required for ligand recognition. The vitronectin receptor $\alpha_v\beta_3$ is highly upregulated in vascular cells of tumors while minimal expression is found in resting or normal blood vessels (Varner and Cheresh, 1996). The tripeptide sequence arginine-glycine-aspartic acid (RGD), found in the active site of vitronectin, binds to $\alpha_v\beta_3$ and almost half of the 22 known integrins (Ruoslahti, 1996).

RGD peptides are exploited for cell entry by pathogenic microorganisms such as the foot-and-mouth disease virus (Logan *et al.*, 1993).

Short synthetic RGD-containing peptides can mimic the natural ligands (Pierschbacher and Ruoslahti, 1984; Pierschbacher and Ruoslahti, 1984; Akiyama and Yamada, 1985; Cheresh and Spiro, 1987) and integrin-mediated cells entry has been exploited to internalize DNA condensed with a RGD-containing peptide. For example, an integrin-binding peptide consisting of a cyclic RGD sequence and oligolysine has been shown to transfect Caco-2 cells effectively (Hart *et al.*, 1995). Erbacher *et al.* have synthesized conjugates of a non-cyclic RGD nonapeptide and PEI (polyethylenimine) and found that the transfection efficiency was enhanced by more than an order of magnitude in both Hela and MRC45 cells compared with PEI (Erbacher *et al.*, 1999). Woodle and colleagues synthesized a conjugate in which a cyclic RGD decapeptide was coupled to PEI via a PEG spacer; polyplexes formed by this RGD-PEG-PEI conjugate were more efficient in mediating gene expression than PEI/plasmid complexes, but no numbers or ratios for this increase were given in this report.

The pathways of nonviral-vector-mediated gene delivery presently believed to be cationic (Zabner *et al.*, 1995; Xu and Szoka, 1996) begin by endocytotic cellular uptake of the polymer/DNA complex (polyplex). The second step is DNA release from an endosome into the cytosol. The mechanistic detail of the release of DNA from endosomes into cytosol is still unknown. One possibilty is that disruption of endosomes liberates polyplexes into cytosol and that DNA dissociation from the liberated polyplexes follows as a separate event. Alternatively, DNA dissociation from polyplexes may happen before endosome disruption, during endosome disruption, or not at all. The endosomally

released DNA is then translocated into the cell nucleus so that it can get access to the nuclear transcription apparatus and is finally expressed into proteins in the cytosol (Singh *et al.*, 2004).

A key cellular barrier impeding the transfection efficacies of cationic polymers is the inefficient release of endosomally trapped DNA into the cell cytosol (Zabner *et al.*, 1995; Xu and Szoka, 1996). Assault from the various hydrolytic enzymes is, understandably, the fate of a therapeutic foreign gene if it remains endosomally trapped for a long time before being released to the cytosol. In order to protect DNA from such hydrolytic digestion by enhanced endosomal release, Wolff and his coworkers pioneered the design and synthesis of pH-sensitive, cationic transfection lipids containing weakly basic lysosomotropic imidazole head groups (Budker *et al.*, 1996). The rationale behind their approach was that the weakly basic imidazole head group, with its pK_a being within the acidity range of endosome lumens (pH 5.5-6.5), acts as a proton sponge while inside the endosome compartments. This so-called "endosomal buffering" is believed not only to inhibit the degradative enzymes (which perform optimally within the acidic pH range of the endosome-lysosome compartments) but also to induce stronger electrostatic repulsions among the protonated imidazole head groups of the cationic liposomes, leading to osmotic swelling and eventual endosomal bursting due to water entry (Budker *et al.*, 1996; Remy *et al.*, 1998). This elegant approach has subsequently been exploited in designing the next generation of cationic polymers (Midoux and Monsigny, 1999; Pichon *et al.*, 2000; Putnam *et al.*, 2001).

1.7 Review of existing polycationic nonviral vector systems

Viral DNA vectors have extremely high transfection efficiency in a variety of human tissues (Chamberlain, 2002; Lien and Lai, 2002; Martin *et al.*, 2002; Wolf and Jenkins, 2002), however, toxicity (Timme *et al.*, 1998; Favre *et al.*, 2001; Kay *et al.*, 2001) and the potential for generating a strong immune response have limited their use since safety is a major concern in human studies.

Nonviral delivery systems can circumvent some of the problems associated with viral vectors and are emerging as alternatives to viral vectors. Commonly used nonviral vectors for delivery of DNA-based therapeutics are polymers (Merdan *et al.*, 2002) and liposomes (Fattal *et al.*, 1999; Fattal *et al.*, 2001; Pedroso de Lima *et al.*, 2001).

Polymeric tranfection systems have advantages, but they are not ideal. In addition to low transfection capabilities, polymeric delivery systems suffer from problems in the control of molecular weight distributions, dispersities of the polyplexes, and other quality control issues (Merdan *et al.*, 2002).

Commonly used polymers include polyethylenimine (PEI) (Lemkine and Demeneix, 2001), poly-L-lysine (PLL) (Lollo *et al.*, 2002), chitosans (Borchard, 2001). The high transfection efficiency of PEI can be attributed to the buffering effect or the "proton sponge effect" of the polymer caused by the presence of amino groups in the molecule (Kamiya *et al.*, 2001). PEI can be very cytotoxic due to induction of apoptosis (Florea *et al.*, 2002). The cytotoxicity and transfection efficiency of PEI are directly proportional to its molecular weight (Godbey and Mikos, 2001).

Cationic PLL interacts with anionic DNA molecules and forms a positively charged complex that can interact with the negatively charged cell surface and undergo rapid

internalization (Merdan *et al.*, 2002). However, PLL has a low level of transfection efficiency, primarily owing to lack of rapid release of PLL-DNA complexes from endosome. Also PLL suffers from immunogenicity and toxicity caused by its amino acid backbone (Mumper, 1999).

Chitosan is a natural biodegradable polymer that has low toxicity (Koping-Hoggard *et al.*, 2001; Singla and Chawla, 2001). The transfection efficiency of chitosan is lower than that of other polymers such as PEI, as observed by a comparison study consisting of intratracheal administration of chitosan-DNA polyplexes to mice *in vivo* (Koping-Hoggard *et al.*, 2001). Chitosan at high dose can cause hypocholesterolemia in humans, thereby limiting its applications (LeHoux and Grondin, 1993).

The nonimmunogenic nature and ease of industrial production of cationic liposomes makes them appealing for gene transfer. Cationic liposomal formulations generally consist of mixtures of cationic and zwitterionic lipids (Felgner *et al.*, 1994; Hofland *et al.*, 1996; Godbey and Mikos, 2001). The cationic lipids serve as a DNA complexation and DNA condensation agent during the formation of the lipoplex. The positive charge also helps in cellular association. The zwitterionic lipids help in membrane perturbation and fusion. Proprietary formulations of cationic lipids such as Lipofectamine (Invitrogen, Carlsbad, CA), Effectene (Qiagen, Valencia, CA), and Tranfectam (Promega, Madison, WI) are commercially available (Kang *et al.*, 1999), but most of the transfection kits are useful only for *in vitro* experimentation due to their cytotoxicity. Despite the appreciable success of cationic lipids in gene transfer, toxicity is of great concern. Cytotoxicity of cationic lipids has been established in numerous *in vitro* (Lappalainen *et al.*, 1994; Patil *et al.*, 2004) and *in vivo* (Filion and Phillips, 1997; Dokka *et al.*, 2000) studies. Another

42

drawback in the use of cationic lipids is their rapid inactivation in the presence of serum (Hofland *et al.*, 1996; Audouy *et al.*, 2000). Some *in vivo* studies have revealed that the gene transduction responses obtained by cationic liposomes were transient and short-lived (Wheeler *et al.*, 1996; Liu *et al.*, 1997).

Previous reports have indicated that the non-chemical conjugation of an HK (histidine/lysine) peptide to a liposome (simple mixing) could increase transfection efficiency (Chen *et al.*, 2000; Chen *et al.*, 2001; Chen *et al.*, 2002). Yu and co-workers investigated the transfection activities by mixing the HoKC peptide with LipA and found that the mixing increased transfection efficiency in both DU145 and PANC-1 cell lines (Yu *et al.*, 2004). Scott et al. observed the great enhancement of gene delivery efficiency using a lipopolyplex containing both DC-Chol/DOPE (dioleoylphosphatidylethanolamine) and RGDK$_{16}$ (Scott *et al.*, 2001). Gao and Huang also shown that in the presence of PLL the level of luciferase gene expression was significantly enhanced in cells transfected with DNA and suboptimal dosed of DC-chol liposomes and Lipofectin (Gao and Huang, 1996).

Protein expression after delivery of plasmid DNA to the cell nucleus depends on the processes of transcription and translation. Cytotoxic gene-delivery systems may compromise these processes and potentially limit protein expression. This situation is perhaps the most prevalent in the nonviral polycationic gene-delivery class in which the polycationic nature of the delivery system can lead to cytotoxicity (Gad *et al.*, 1982; de Kruijff *et al.*, 1985; Elferink, 1985; Gatica *et al.*, 1987; Antonelli *et al.*, 1991; Elferink, 1991; Kato *et al.*, 1991; Kleinschmidt and Marsh, 1997), so interest has been directed on low molecular weight peptide delivery agents.

1.8 Research objective

The objective of the thesis is the study of electrostatically induced DNA compaction and DNA/DNA interaction with two applications: DNA condensation for application to gene delivery and DNA-DNA interaction in the NCP. The first part of this project aims to physically characterize and investigate a new class of peptide gene delivery agents that have not been tested before. These ε-oligolysines are polyamine mimics, containing epsilon hydrophobic peptide backbones tethered with charged moieties and basic amino acids. They are flexible since they can be designed with arbitrary net charge and length. These lower linear charge density carrier peptides are non-toxic and have potentially a high delivery effect, due to their ability to pass the cell membrane (Yu *et al.*).

It is our hypothesis that a design based on ε-oliogolysine peptides can act as effective DNA condensing agents resulting in nanoparticle complexes which are less toxic and more efficient in delivery as compared to standard α-oligolysine peptides. The objective is to investigate how such a flexible design with α-amino substituted pendent groups of short α-oligopeptides (Figure 9) can be modified to produce effective nonviral gene delivery vectors. It is proposed to study the effect on gene delivery exploiting three different mechanistic roles of the side chains: i) to improve delivery on the basis of improved compaction and cell surface binding due to increased charge (LYR side chain); ii) to improve delivery by incorporation of the histidine amino acid residue, which aids in endosomal release (LYH side chain); iii) to achieve cell targeting by attaching the RGD motif (RGDP side chain). These three variations will be studied separately with the aim to develop a block polymeric type of design in future work, where a linear chain of ε-oliogolysines having different pendent groups are combined.

Secondly, the multivalent cation induced aggregation of nucleosome core particles has been studied with dynamic light scattering and results from this method which is new in this context has been compared with those of precipitation assay. The DLS method is fast, convenient and requires low amount of sample. One objective is to establish this new methodology to study the Mg^{2+} and $Spermine^{4+}$ induced aggregation of NCP in the presence of high mobility group protein. Another purpose is to obtain an understanding of the importance of the basic physical mechanism in terms of electrostatic interaction that determines compaction of chromatin is affected by HMGN protein. Thus, understanding of the nature of the effect of HMG protein on chromatin compaction will be obtained. As a model system, recombinant NCP is used.

1.9 Experimental design

The behavior of DNA compaction by novel ε-oligolysines was first studied, and then *in vitro* transfection by those ε-oligolysines was conducted to investigate their potential to be applied as gene delivery agents. The experiment strategy is shown as followings.

1. Characterization of DNA compaction by novel ε-oligolysines.

a) Physicochemical characterization of DNA compaction and aggregation by ε-oligolysines using static light scattering (SLS) and dynamic light scattering (DLS), fluorescence microscopy (FM) and isothermal titration calorimetry (ITC). Salt concentration and pH were changed to obtain an understanding of these novel peptides in their ability of condensing DNA. SLS and FM were used to gain the DNA titration curves and measure the EC_{50} (the midpoint concentration of condensing agents in the titration curves). The particle size of condensed DNA was measured by DLS. Some of the basic features of DNA compaction have been verified.

b) Fluorescence microscopy was exploited to observe the morphology of free DNA and its compacted form.

2. Study of NCP aggregation by HMGN proteins and different cations.

I also studied the aggregation behavior of nucleosome core particles (NCP) in the presence of HMGN protein under different cationic conditions (Mg^{2+}, Spm^{4+}) by Precipitation assay and Dynamic Light Scattering. Precipitation assay was conducted to measure NCP concentration in NCP solutions with various amounts of cations. Aggregation curves and particle size information were obtained by DLS. In order to elucidate the possible role of the basic highly positively charged nucleosome binding domain (NBD) of HMGN protein, aggregation of NCP for both wild type HMGN as well as a truncated peptide XN2 containing this domain was studied.

3. *In vitro* transfection with ε-peptide vectors.

a) *In vitro* transfection was conducted with our novel ε-oligolysines. The cell lines used were Hela (cervical adenocarcinoma; human), 293F (embryonic kidney; human), Mewo (melanoma; human) and A549 (lung carcinoma; human). DOTAP (a commercially transfection agent) was used as positive control. Flow cytometry (FACS) was used to measure the transfection efficiency.

b) DOTAP and ε-oligolysines were mixed together to improve the efficiency of transfection (Gao and Huang, 1996; Chen *et al.*, 2000; Chen *et al.*, 2001; Chen *et al.*, 2002; Yu *et al.*, 2004). The concentration condition was optimized.

c) I modified the side chains of our ε-oligolysines and investigated their ability to transfect cells. LYR side chain was used to facilitate delivery on the basis of improved DNA compaction and cell surface binding due to increased charge; LYH side chain was

designed since the imidazole head group in histidine residue with its pK_a being within the acidity range of endosome lumen (pH 5.5-6.5) acted as a proton sponge while inside the endosome compartment which promoted endosomal release; RGDP side chain was explored to achieve cell type selectivity due to the selective binding of RGD motif.

d) MTT assay was conducted to measure the cytotoxicity of all ε-peptides and their mixture with DOTAP.

1.10 Biophysical methods

1.10.1 Dynamic Light Scattering (DLS) and Static Light Scattering (SLS)

A very sensitive photon counting laser light-scattering instrument enables the rapid determination of the conditions required for DNA condensation even at the very low concentrations used to avoid intermolecular association. Dynamic light scattering is also known as Quasi Elastic Light Scattering (QELS) or photon correlation spectroscopy (PCS).

When a beam of light passes through a colloidal dispersion, the particles or droplets scatter some of the light in all directions. When the particles are very small compared with the wavelength of the light, the intensity of the scattered light is uniform in all directions (Rayleigh scattering); for larger particles (above approximately 250 nm diameter), the intensity is angle dependent (Mie scattering). If the light is coherent and monochromatic, as from a laser, it is possible to observe time-dependent fluctuations in the scattered intensity using a suitable detector such as a photomultiplier capable of operating in photon counting mode.

These fluctuations arise from the fact that the particles are small enough to undergo random thermal (Brownian) motion and the distance between them is therefore constantly varying. Constructive and destructive interference of light scattered by neighbouring particles within the illuminated zone gives rise to the intensity fluctuation at the detector plane which, as it arises from particle motion, contains information about this motion. Analysis of the time dependence of the intensity fluctuation can therefore yield the diffusion coefficient of the particles from which, via the Strokes Einstein equation, knowing the viscosity of the medium, the hydrodynamic radius or diameter of the particles can be calculated.

The random motion of the small particles in a liquid gives rise to fluctuations in the time intensity of the scattered light. The fluctuation signal is processed by forming the autocorrelation function, $C(t)$, t being the time delay. As t increases, correlation is lost, and the function approaches the constant background term B. For short times the correlation is high. In between these two limits the function decays exponentially for a monodisperse suspension of rigid, globular particles and is given by

$$C(t) = A \, e^{-2\,\Gamma\,t} + B \tag{1}$$

Where A is an optical constant determined by the instrument design, and Γ is related to the relaxation of the fluctuations by

$$\Gamma = Dq^2 \qquad [\text{rad/sec}] \tag{2}$$

The value of q is calculated from the scattering angle θ (eg. 90º), the wavelength of the laser light λ_0 (eg. 0.635 μm), and the index of refraction n (eg. 1.33) of the suspending liquid. The equation relating these quantities is

$$q = (2\pi n / \lambda_0) \, 2 \, \text{Sin} \, (\theta/2)$$

The translational diffusion coefficient, D, is the principle quantity measured by DLS. It is an inherently interesting property of particles and macromolecules.

Particle size is related to D for simple common shapes like a sphere, ellipsoid, cylinder and random coil. Of these, the spherical assumption is most useful in the greatest number of cases. For a sphere,

$$D = (k_B T) / [3\pi\eta d] \tag{4}$$

Where k_B is Boltzmann's constant (1.38054×10^{-16} ergs/deg), T is the temperature in K, η (in centi poise) is the viscosity of the liquid in which the particle is moving, and d is the particle diameter. This equation assumes that the particles are moving independently of one another.

The DLS instrument measures the autocorrelation function and then fit it to equation (1) to determine Γ. D will be calculated from equation (2) given n, θ and Γ, then particle diameter d can be extracted from equation (4) given T and η. Figure 6 shows an example of DLS correlation function curve and particle size distribution.

In contrast to dynamic light scattering, in static light scattering time averaged scattering intensities are detected and observed at one specific scattering angle. In my project a standard fluorescence instrumentation is also used for this because it allows the detection of the intensity of the scattered light by measuring the intensity of light at 90 degree to the incident light.
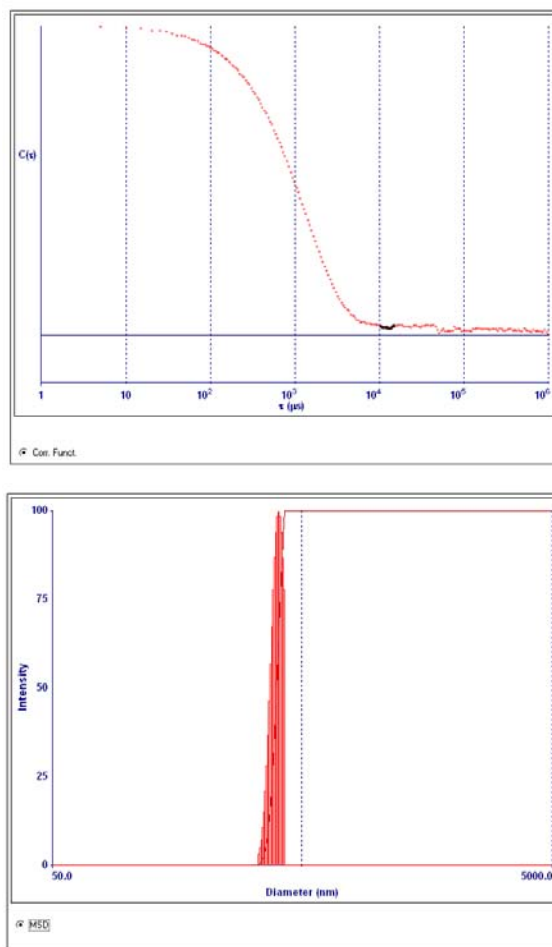
Figure 6. An example of DLS data.

1 µg/mL T4 DNA solution titrated by 7.6 µg/mL ε-K10 in 100 mM KCl and 1mM tris buffer. Top figure shows the correlation function C(t) plotted against the time delay. Bottom graph illustrates the distribution of particle size in diameter.

1.10.2 Fluorescence Microscopy (FM)

The fluorescence microscope is based on the phenomenon that certain material emits energy detectable as visible light when irradiated with the light of a specific wavelength. The sample can either be fluorescing in its natural form like chlorophyll and some minerals, or treated with fluorescing chemicals.

The basic task of the fluorescence miscroscope is to let excitation light radiate the specimen and then sort out the much weaker emitted light to make up the image. First, the microscope has a filter that only lets through radiation with the desired wavelength that matches the fluorescing material. The radiation collides with the atoms in the specimen and electrons are excited to a higher energy level. When they relax to a lower level, they emit light.

To become visible, the emitted light is separated from the much brighter excitation light in a second filter. Here, the fact that the emitted light is of lower energy and has a longer wavelength is used. The fluorescing areas can be observed in the microscope and shine out against a dark background with high contrast.

1.10.3 Isothermal Titration Calorimetry (ITC)

The ITC (Isothermal Titration Calorimetry) unit directly measures heat evolved or absorbed in liquid samples as a result of mixing precise amounts of reactants.

Temperature differences between the reference cell and the sample cell are measured, calibrated to power units. The data channel is referred to as the DP signal, or the differential power between the reference cell and the sample cell. This signal is sometimes referred to as the "feedback" power used to maintain temperature equilibrium. Calibration of this signal is obtained electrically by administering a known quantity of power through a resistive heater element located on the cell.

The syringe containing a "ligand" is titrated (injected) into the cell containing a solution of the "macromolecule". An injection which results in the evolution of heat (exothermic) within the sample cell causes a negative change in the DP power since the heat evolved chemically provides heat that the DP feedback is no longer required to provide. The

opposite is true for endothermic reactions. Since the DP has units of power, the time integral of the peak yields a measurement of thermal energy, ΔH. This heat is released or absorbed in direct proportion to the amount of binding that occurs. When the macromolecule in the cell becomes saturated with added ligand, the heat signal diminishes until only the background heat of dilution is observed. Figure 7 shows an example of ITC data.
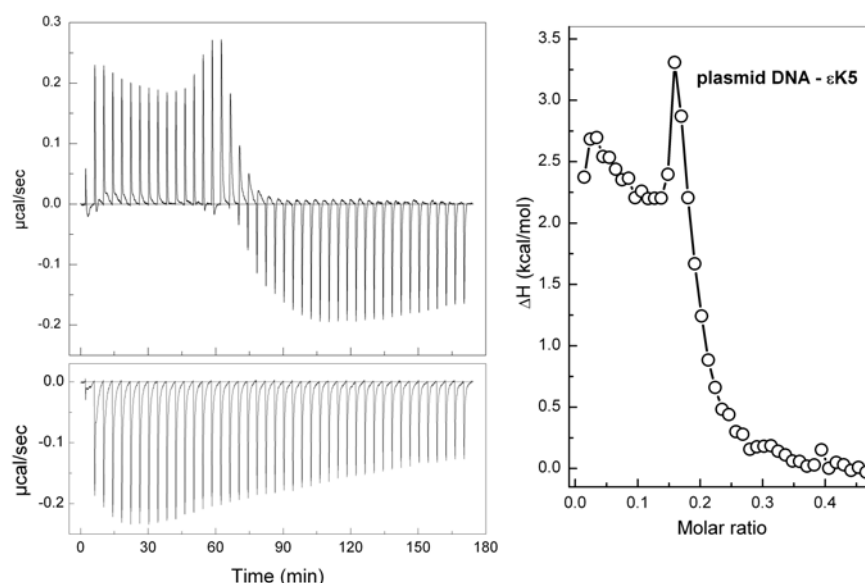
Figure 7. An example of ITC data.

Titration of 0.4 mM solution of plasmid DNA by 0.8 mM solution of ε-K5 in 10 mM KCl. Top left graph shows titration of the DNA solution, bottom left data presents reference titration of 10 mM KCl by 0.8 mM ε-K5. Graph on the right side displays the results of the ITC data analysis: dependence of ΔH of ε-K5 - DNA interaction on molar ε-K5/DNA ratio.

1.10.4 Precipitation Assay

Precipitation of the NCP was studied by UV absorption monitored assay using NanoDrop ND-1000 (NanoDrop Technologies Inc, Wilmington, DE, USA). The NanoDrop ND-1000 is a full-spectrum (220-750nm) spectrophotometer that measures 1 μL samples with high accuracy and reproducibility. It utilizes a patented sample retention

technology that employs surface tension alone to hold the sample in place. This eliminates the need for cumbersome cuvettes and other sample containment devices and allows for clean up in seconds.

Different quantities of salts (KCl, NaCl, $MgCl_2$ or $CaCl_2$) were added to the NCP solution. The samples were incubated at room temperature for 30 min and then centrifuged for 20 min at 11,000 x g. The NCP supernatant concentration was determined by absorbance measurements at 260 nm. When measured, a 1 µL sample is pipetted onto the end of a fiber optic cable (the receiving fiber). A second fiber optic cable (the source fiber) is then brought into contact with the liquid sample causing the liquid to bridge the gap between the fiber optic ends. The gap is controlled to both 1 mm and 0.2 mm paths. A pulsed Xenon flash lamp provides the light source and a spectrometer utilizing a linear CCD array is used to analyze the light after passing through the sample.

1.10.5 Solid Phase Peptide Synthesis (SPPS)

The revolutionary principle behind solid phase peptide synthesis (SPPS) as conceived by Merrifield in 1959 is that if the peptide is bound to an insoluble support then any unreacted reagent left at the end of any synthetic step can be removed by a simple wash procedure, greatly decreasing the time required for synthesis.

During the synthesis, the C-terminal amino acid is attached to a cross-linked polystyrene resin. The N-terminus is protected with the Fmoc group, which is stable in acid, but removable by base. Any side chain functional groups are protected with base stable, acid labile groups.

To begin each coupling, the Fmoc group on the resin bound amino acid is removed. It is then rinsed and a protected amino acid is added which has been activated at its α-

carboxyl group. The activated amino acid and the resin bound amino acid are allowed to react in the presence of base to form a new peptide bond. This process is repeated until the desired peptide is assembled at the resin.

Once the peptide is complete, it is ready to be cleaved from the resin. The peptide on the resin is allowed to react with the cleavage mixture for several hours, which affords the peptide in solution. It can then be precipitated and washed and analyzed or purified as desired.

1.10.6 Flow Cytometry (FACS)

Flow cytometry uses the principles of light scattering, light excitation, and emission of fluorochrome molecules to generate specific multi-parameter data from particles and cells in the size range of 0.5 μm to 40 μm diameter. Cells are hydro-dynamically focused in a sheath of PBS (phosphate-buffered saline) before intercepting an optimally focused light source. Lasers are most often used as a light source in flow cytometry.

The sample is injected into the center of a sheath flow. The combined flow is reduced in diameter, forcing the cell into the center of the stream, thus, the laser irradiates one cell at a time. As the cells or particles of interest intercept the light source, they scatter light and fluorochromes are excited to a higher energy state. This energy is released as a photon of light with specific spectral properties unique to different fluorochromes.

One unique feature of flow cytometry is that it measures fluorescence per cell or particle. This contrasts with spectrophotometry in which the percent absorption and transmission of specific wavelengths of light is measured for a bulk volume of sample.

Scattered and emitted light from cells and particles are converted to electrical pulses by optical detectors. Collimated light is picked up by confocal lenses focused at the

intersection point of cells and the light source. Light is sent to different detectors by using optical filters. The most common type of detector used in flow cytometry is the photomultiplier (PMT).

The electrical pulses originating from light detected by the PMTs are then processed by a series of linear and log amplifiers. Logarithmic amplification is most often used to measure fluorescence in cells. This type of amplification expands the scale for weak signals and compresses the scale for strong or specific fluorescence signals. After the different signals or pulses are amplified, they are processed by an Analog to Digital Converter (ADC) which in turn allows for events to be plotted on a graphical scale. An example of FACS Dotplot is shown in Figure 8.
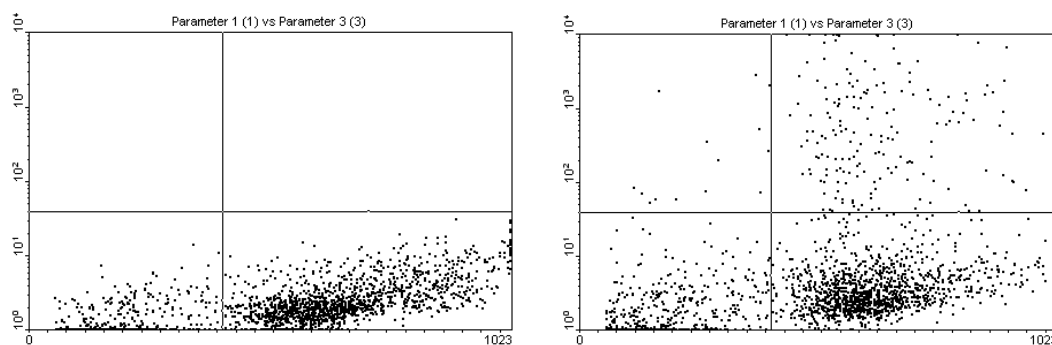
Figure 8. An example of FACS Dotplot.

293F cells transfected by ε-(LYH)K10. Parameter of X axis is FSC-H and of Y axis is FL1-H. Left graph shows negative control (only cells); right picture represents cells transfected by ε-(LYH)K10, the concentration of ε-(LYH)K10 is 60 μg/mL and plasmid DNA is 1.1 μg/mL. A total of 3×10^4 events were counted for each sample. Data were analyzed with WinMIDI (version 2.5) software with 30,000 counts in each measurement. Quadrants were drawn according to negative control and the tranfection efficiency was then calculated as UR/ (UR+LR). (UR represents transfected cell number at the upper right, LR represents the untransfected cell number at the lower right, cells at the left were regarded as debris or noise).

55

1.10.7 MTT Assay

Measurement of cell viability and proliferation forms the basis for numerous *in vitro* assays of a cell population's response to external factors. The reduction of tetrazolium salts is now widely accepted as a reliable way to examine cell proliferation. The yellow tetrazolium MTT (3-(4, 5-dimethylthiazolyl-2)-2, 5-diphenyltetrazolium bromide) is reduced by metabolically active cells, in part by the action of dehydrogenase enzymes, to generate reducing equivalents such as NADH and NADPH. The resulting intracellular purple formazan can be solubilized and quantified by spectrophotometric means.

Chapter 2. Materials and methods

2.1 DNA compaction by novel ε-peptides

2.1.1 Materials

DNA. Highly purified coliphage T2 DNA, 164 kilobase pairs (kbp), was purchased from Sigma-Aldrich (St. Louis, MO, USA). DNA was dissolved in Tris buffer (5 mM Tris, pH 7.3). The concentration of the stock solution was adjusted to 0.5 mg/mL. The absorbance ratio (A_{260}/A_{280}) was above 1.8, indicating absence of protein contamination. The stock solution was further diluted in 1 mM Tris buffer to give a concentration of 2 µg/mL. Bacteriophage T4GT7 DNA, 166 kilobase pairs, was purchased from Nippon Gene (Toyama, Japan). The T4GT7 DNA stock solution is 0.32 µg/µL in 10 mM Tris-HCl (pH 7.9) and 1.0 mM EDTA (ethylenediamine tetraacetic acid) buffer. Plasmid pEGFP-N1 (4.7 kbp), encoding green fluorescent protein, GFP, was a gift from Lu Yanning at Nanyang Technological University. The plasmid was amplified in E.coli DH5α strain and isolated using QIAGEN (Valencia, CA, USA) HiSpeed Plasmid Purification Giga Kit (plasmid stock solution is 2.75 mM in 10 mM KCl).

Peptides. α-Poly(L-lysine), namely α-PLL, (Mw=~8,300 − ~14,600 Da, degree of polymerization 40−70) was purchased from Sigma-Aldrich (St. Louis, MO, USA) and used without further purification. Two types of peptides have been designed; unsubstituted ε-oligo(L-lysine) of varying length and α-substituted ε-oligo(L-lysine) (the notation "L" is henceforth omitted) (Figure 9). ε-Poly(L-lysine), ε-PLL, with degree of polymerization 31 was purchased from Chisso Corporation (Tokyo, Japan). The

unsubstituted ε-peptides ε-K5, ε-K6, ε-K7, ε-K8, ε-K9, ε-K10, and the substituted ε-(R)K10, ε-(Y)K10, ε-(L)K10, ε-(YR)K10, ε-(LYR)K10 were synthesized by my co-supervisor Professor Tam's lab at Vanderbilt University using solid-phase peptide synthesis. All amino acids and coupling reagents were purchased from Novabiochem (San Diego, CA, USA). The MBHA (4-methylbenzhydrylamine) resin (0.2 mmol/g substitution) was purchased from Advanced ChemTech (Louisville, KY, USA). All solvents used were of the highest commercial grade. The ε-Kn homologues were constructed on the MBHA resin using Boc-Lys(Fmoc)-OH and Boc-Lys(2-Cl-Z)-OH for protection of the final epsilon amine. They were prepared by Fmoc chemistry using 20% piperidine in DMF (dimethylformamide) for 30 min at the deprotection step. Deprotection of the Boc-α-amines by 50% trifluoroacetic acid in DCM (dichloromethane) for 30 min generated the free α-amine for coupling in the α-substituted ε-K10 homologues. Each coupling steps for ε-Kn homologues was achieved in 2 h through a combination of coupling reagents, DCC (N,N'-dicyclohexylcarbodiimide) / HOBt (N-hydroxybenzotriazole·water), in DMF and DCM (1:1, v/v). However, the α-substituted amino acids on the ε-K10 homologues required a longer time or double coupling for complete coupling reaction. Each coupling steps was confirmed by the Kaiser test. The α-substituted and ε-Kn homologues were then cleaved from the resin using a standard method of HF (anisole:HF, 1:10, v/v) for 1 h and for 2-4 h in the case of arginine containing peptides. The crude peptides were purified by preparative RP-HPLC (reversed phase-high performance liquid chromatography) on a Waters 600 system using a C_{18} Vydac column 22x250 mm). All HPLC (high performance liquid chromatography) was carried out with a linear gradient of buffer A [0.05% TFA (trifluoroacetic acid) in H_2O]

and buffer B (60% CH_3CN in H_2O with 0.04% TFA). Products were confirmed by matrix-assisted laser desorption ionization mass spectrometry (MALDI-MS) using a PerSeptive Biosystems Voyager instrument. Measurements were taken in the linear mode with α-cyano-4-

hydroxycinnamic acid as the matrix. The concentration and purity of the ε-oligolysines were checked by HPLC analysis. The chemical structures of these polypeptides are given in Figure 9. The peptide stock solutions (5 mg/mL) were prepared in sterile, double-distilled water, and appropriate dilutions were made in 1 mM Tris buffer.

Chemical reagents. Tris and DAPI (4,6-diamidino-2-phenylindole) were obtained from Sigma-Aldrich (St. Louis, MO, USA). All other chemicals for buffers were purchased from Fisher Scientific (Pittsburgh, PA, USA).

Buffers. All experiments were performed in a buffer containing potassium chloride (5mM or 100mM) and 1mM tris (pH=7.3).

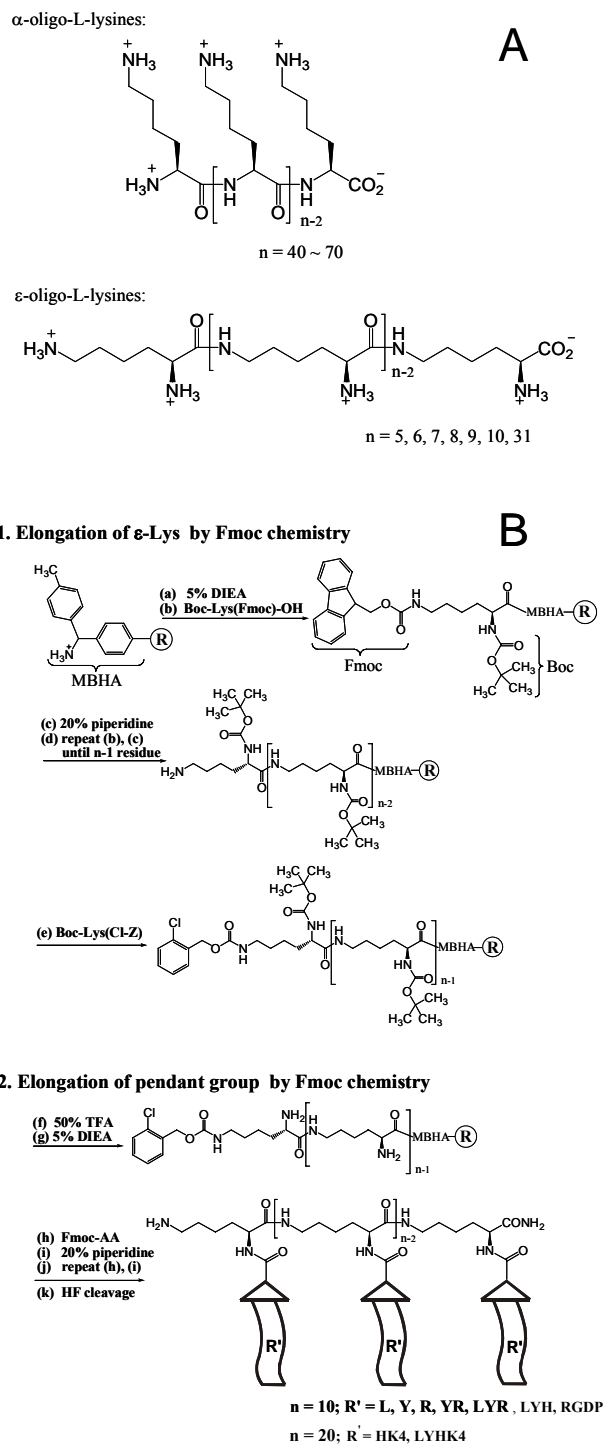**Figure 9. Chemical structure and synthetic scheme for ε-oligolysines.**

(**A**) Chemical structure of linear α-oligolysines and ε-oligolysines. (**B**) Synthetic scheme for solid phase chemistry preparation of dendrimeric ε-oligolysine α-amino acid derivatives (L, Y, R, H, G, D and K represent amino acid residue leucine, tyrosine, arginine, histidine, glycine, aspartic acid and lysine respectively).

2.1.2 Methods

Static light scattering. Light scattering experiments were performed using a Varian Cary eclipse fluorescence spectrophotometer (Palo Alto, CA, USA) by detection of the intensity of the scattered light at 90 degree to the incident light. The excitation wavelength was set to 350 nm. The compaction experiment was performed in 1 mM Tris buffer, pH 7.3. All buffers were filtered through 0.45 µm filters. Samples were prepared by titrating 3 mL of a solution containing T2 or T4 DNA in the appropriate buffer with the solution containing the peptides. The titration was done in the quartz cuvettes which are used as light-scattering cells. The filtration effectively reduces the scattering from dust and impurities. Every point in the figures shown was got from three separate experiments with reproducibility within 5%.

Dynamic light scattering (DLS). Dynamic light scattering (DLS) experiments were conducted using a Brookhaven 90plus particle size analyzer (Long Island, NY, USA). A laser beam were passed through a PMMA (polymethylmethacrylate) cell containing the samples (peptides/DNA mixture), and the scattered light was measured at a 90 degree angle to the incident beam. The particle sizes were calculated applying standard theory connecting light scattering autocorrelation function, translational diffusion coefficient and particle size using software provided by equipment manufacturer. Particle sizes are expressed as effective diameter assuming a lognormal distribution.

Fluorescence microscopy. A Nikon eclipse 90i fluorescence microscope (Tokyo, Japan) equipped with a 100× oil-immersed objective lens was used studying the conformational change of DNA induced by peptides. DNA molecules were visualized using DAPI (1:1 DNA:DAPI molar ratio was used). The final concentrations were as

follows: DNA in nucleotide, 0.5 μM and DAPI, 0.5 μM. The concentrations were kept constant throughout the experiment. In this condition, the binding number of DAPI per one base pair is estimated to be equal to 0.05 (Matsuzawa and Yoshikawa, 1993), and the persistent length is expected to remain nearly the same as in the absence of DAPI (Matsuzawa *et al.*, 1991). To prevent DNA degradation and precipitation to the glass surface, special care was taken to clean the glass microscope slides and cover slips thoroughly before observations. They were soaked in hydrogen peroxide for more than 1 h, washed repeatedly with distilled water, and then immersed in ethanol for 1 h and dried at 35 °C for 30 min (Mel'nikov *et al.*, 1995).

Isothermal titration calorimetry (ITC). A VP-ITC microcalorimeter from MicroCal (Northampton, MA, USA) was used at 25.0 °C. The calorimeter was checked and calibrated applying procedures provided in device documentation. All DNA and cationic ligand solutions were contained in 10 mM KCl and prepared using the same stock solvent. The same plasmid (pEGFP-N1 4.7 kb) as in transfection experiments was used. Stock solutions of the cationic ligands were prepared gravimetrically. At the beginning of titration, concentration of the plasmid DNA in the cell was 0.40 mM DNA phosphate groups. Concentration of the ligand in the injection syringe was chosen to ensure 2-3 time excess of the positive charge of the ligand over negative charge of the DNA in the sample cell at the end of titration. The ligand was added in 42 portions of 7.0 µl each from a 300 µl injection syringe, at three minute intervals. Each ITC measurement of ligand-DNA binding consisted of two titrations; the first one was carried with DNA solution in the cell, the second (blank) titration was performed with sample cell containing only solvent without DNA (10 mM KCl). The peaks in both titration curves

were integrated and the heats of ligand dilution were subtracted. Origin7.0 graphic and analysis program integrated in VP-ITC calorimeter by VPViewer 2000 ITC software was used for data collection, analysis, and presentation.

2.2 NCP aggregation studied by DLS and precipitation assay

2.2.1 Materials

NCP, HMGN2 and XN2-1. These materials were obtained from Dr. Curt Davey's laboratory at School of Biological Sciences in Nanyang Technological University. The stock concentration is as follows: 21.5 mg/mL NCP (~200 KDa) in 20 mM potassium cacodylate, 3 mg/mL HMGN2 (~9.5 KDa) in 20 mM tris-1mM EDTA and 300 μM XN2-1 in 20 mM potassium cacodylate. NCP was assembled from recombinant *Xenopus laevis* histones and a 147 bp palindromic DNA fragment (Dyer *et al.*, 2004). Recombinant *Xenopus laevis* HMGN2 was expresses in *E. coli* and purified to homogeneity by chromatographic methods (Vasudevan and Davey, unpublished data). A synthetic peptide which forms the Nucleosome Binding Domain of *Xenopus laevis* HMGN2 (XN2; a.a. 17 to 48) was purchased from Mimotopes (Australia).

Chemical reagents. Spermine was obtained from Sigma-Aldrich (St. Louis, MO, USA). All other chemicals for buffers were purchased from Fisher Scientific (Pittsburgh, PA, USA).

2.2.2 Methods

Dynamic light scattering (DLS). The same equipment used for T4 DNA compaction (shown in 2.1.2) was also used in this part.

63

Precipitation assay. A ND-1000 Spectrophotometer from NanoDrop (Wilmington, DE, USA) was used to measure NCP concentration. NCP, magnesium, calcium, sodium and potassium solutions were prepared in 10 mM Tris-HCl buffer, pH 7.5. Here, "starting concentration" will refer to the concentrations in the sample after mixing NCP and cation solutions. The starting concentration was 132 μg/mL for NCPs, from 0 mM to 3 mM for magnesium and calcium, and from 0 mM to 300 mM for potassium and sodium.

For a given precipitation curve, the starting NCP concentration was kept constant while cation solution concentration were varied. After mixed and put at room temperature for 30 minutes, samples were centrifuged for 20 min at 11,000 x g. For each experiment point, the fraction of NCPs remaining in the supernatant was determined by ultraviolet absorbance measurement at 260 nm.

The integrity of NCPs with various amounts of cation solutions ranging from 0 mM to 3 mM for magnesium and calcium, and from 0 mM to 300 mM for potassium and sodium, was checked with 5% polyarylamide electrophoresis gels (data not shown).

2.3 *In vitro* transfection with ε-peptide vectors

2.3.1 Materials

DNA. Plasmid pEGFP-N1 (4.7 kbp), encoding green fluorescent protein, GFP, was a gift from Lu Yanning at Nanyang Technological University. The plasmid was amplified in E.coli DH5α strain and isolated using QIAGEN (Valencia, CA, USA) HiSpeed Plasmid Purification Giga Kit (plasmid stock solution is 2.75 mM in 10 mM KCl).

Cell culture. Hela human cervical carcinoma cells (CCL-2), 293F human embryonic kidney cells (PEAKrapid, CRL-2828), Mewo human melanoma cells (HTB-65) and

A549 human lung carcinoma (CCL-185) were purchased from ATCC (Manassas, VA, USA). Cells were grown in Dulbecco's modified Eagle's medium (DMEM; Gibco, Eggenstein, Germany) supplemented with 10% fetal bovine serum (FBS; Invitrogen, Carlsbad, CA, USA) at 37 °C in a humidified 5% CO_2 atmosphere. Cells were fed every 2-3 days and split when almost confluent employing tripsin/EDTA (Gibco).

Peptides. The substituted ε-peptides, ε-(LYH)K10, ε-(RGDP)K10, ε-(HK$_4$)K20 and ε-(LYHK$_4$)K20 were synthesized by my co-supervisor Professor Tam's lab at Nanyang Technological University using solid-phase peptide synthesis (same method as described in 2.1.1). All amino acids and coupling reagents were purchased from Novabiochem (San Diego, CA, USA). The MBHA resin (0.2 mmol/g substitution) was purchased from Advanced ChemTech (Louisville, KY, USA). All solvents used were of the highest commercial grade.

Chemical reagents. DOTAP (1 µg/µL) solution was purchased from Roche (Basel, Switzerland). Tris, DMSO (dimethylsulfoxide), MTT were obtained from Sigma-Aldrich (St. Louis, MO, USA). All other chemicals for buffers were purchased from Fisher Scientific (Pittsburgh, PA, USA).

2.3.2 Methods

In vitro **gene expression.** Cells were plated on 60-mm tissue culture dishes (TPP, Trasadingen, Switzerland) at an initial density of $3x10^5$ cells per dish and grown to 80% confluency at the time of transfection, which was 24 h after plating, in 5 mL DMEM supplemented with 10% FBS, sodium pyruvate (100 mM), and L-glutamine (200 mM). To compare transfection efficiency of the tested peptides with commercial transfection

agents, DOTAP was used. Transfections with DOTAP were carried out according to the manufacturer's instructions. The DOTAP-DNA complexes were prepared by adding 50 μL (6.0 μg) of plasmid DNA from stock solution to 30 μL DOTAP in 70 μL HBS. HBS solution is 21 mM Hepes-NaOH buffer containing 135 mM NaCl, 5.0 mM KCl, and 0.76 mM Na_2HPO_4, pH 7.4. The data of transfection experiments carried out with DOTAP are indicated as "control" in corresponding figures presented in the Results section. In transfection experiments with peptides, stock DNA solution (concentration 1.4 mg/mL) was diluted 13 times by HBS buffer prior to addition of transfection agent. When both DOTAP and peptide were used in transfection (typically at 1:1 peptide:DOTAP volume ratio), they were mixed before addition of the DNA solution. Mixture of DNA with transfection agents was incubated at room temperature for 30 min. Amount of the DNA added per one 60-mm dish was typically 5.6 μg (unless otherwise specified). For a number of transfection experiments, 5 times lower concentration of DNA in solution was used (keeping the same amount of DNA per dish; stock DNA solution was diluted 5 times by HBS prior to addition of transfection agent). Before addition of transfection mixture, the cell growth medium was removed and cells were washed once with PBS buffer. Transfections were then performed in DMEM (5 mL/60-mm dish) without FBS. After incubating the cells with the complexes for 5 h at 37°C in humidified 5% CO_2 atmosphere, the complex-containing medium was removed and replaced with 5 mL of growth medium. Following an additional 48 h of incubation, the cells were collected for flow cytometric analysis.

Flow cytometric analysis. Cell transfection analysis was carried out with pEGFP-N1 plasmid complexes, following the procedure described above. After the final 48 h

incubation, cells in each well were harvested by trypsinization and washed once with PBS and then resuspended to a final volume of 1 mL in PBS buffer. Cells expressing green fluorescent protein were enumerated by fluorescence-activated cell sorting (FACSCalibur, BD Biosciences, San Jose, CA, USA) using the green channel FL-1H. A total of $3x10^4$ events were counted for each sample. Data were analyzed with WinMIDI (version 2.5) software with 30,000 counts in each measurement.

Cytotoxicity assay. Cytotoxicity was evaluated by using MTT (3-(4,5-dimethylthiazol-2-yl)-2,5-diphenyl tetrazolium bromide) assay. Cells were grown in 96-well plates (Iwaki, Tokyo, Japan) at an initial density of $1.5x10^5$ cells per well in 75 µL of growth medium for 16 h at 37°C, after which the growth medium was removed and cells were washed with PBS twice. Then 75 µL DMEM without FBS and 25 µL solution containing peptide or peptide (5 mg/mL) + DOTAP were added to each well; 75 µL DMEM + 25 µL PBS solution without peptide was applied in control wells. After incubation (37°C, 1 h), medium and peptide were removed and 12.5 µL of a 5-mg/mL MTT stock in sterile PBS was added to each well. Following an additional incubation at 37°C for 4 h, the MTT solution was removed and 100 µL DMSO was added to each well to dissolve crystals. Optical densities of each well were measured at 590 nm using a microplate reader from Bio-Rad (Hercules, CA, USA) and expressed as a percentage relative to control cells.

Chapter 3. Results and discussion

3.1 DNA compaction by novel ε-peptides

3.1.1 Design and synthesis

The work exploits a repeated branching design that uses the linear ε-oligolysine as an extended scaffold and their α-amino groups for functionalization with pendent groups of short α-peptides. Such a design has the advantages of design flexibility and synthetic expediency. The design flexibility is the ability to adjust the side-chain functionalities of the branching α-peptide motifs. The peptides contain an ε-peptide hydrophobic backbone tethered with a basic oligopeptide that can be synthesized unambiguously and honed with arbitrary net charge, hydrophobicity and chain length. The design provides synthetic expediency by allowing a concurrent synthesis of all branched α-peptides tethered on the ε-peptide backbone during the solid-phase synthesis to save many synthetic steps.

Figure 9A illustrates the linear ε-oligolysine peptide in comparison with the normal α-oligolysine. Envisioned biophysical advantages of having this architecture include a flexible backbone derived from ε-oligolysine to facilitate DNA compaction and the pendent oligopeptide moiety at the α-amino side chain to enable optimization of delivery efficiency as well as cell targeted delivery. These peptides are also expected to be more stable in the cell as compared to a backbone based on natural α-peptides, due to the resistance of the ε-peptide bond to protease degradation (Tam *et al.*, 2002). The hydrophobic methylene chain can be considered lipid-like and would favour penetration

of a lipid membrane. These properties, combined with the known nontoxic and safe nature of microbially produced ε-PLL (Shih *et al.*, 2006) as well as our own unpublished finding of high membrane penetrating capacity of these chemically synthesized ε-peptides (Tam et al., unpublished observation), makes these molecules attractive as a basis for a non-viral cationic gene delivery vehicle. Compared with α-oligolysines, ε-oligolysines have more rigid side chains. Since the charged amino group is closer to the carbonyl in ε-oligolysines, H^+ will shift more. That is why ε-oligolysines have lower pKa than α-oligolysines. The interior of endosomes is mildly acidic (pH~6) and the pH of cytosol is about 7.2 (Alberts *et al.*, 1994), therefore, ε-oligolysines is less positively charged in cytosol compared with α-oligolysines. This may make DNA release from the condensed particles more easy after entering the cells in the gene delivery process. α-Oligolysines are recognized by proteases and easily degradable in the cytoplasm. In contrast, ε-oligolysines can escape degradation because epsilon peptide bonds are different from usual alpha peptide bonds so that they may not be easily degraded. The linear ε-oligolysines of chain length varying from five to ten in comparison with the higher molecular weight ε-PLL (degree of polymerization n = 31) and α-PLL (n = 40-70) were studied. α-amino derivatives containing either of the side chains L, Y, R, YR, LYR, LYH, RGDP, HK_4 and $LYHK_4$ (Figure 9B) were synthesized and all peptides were further investigated by physicochemical characterization of DNA compaction. The LYR side chain motif was chosen because of the favorable membrane penetration capacity (coupled with antimicrobial activity) of the resulting molecules (Tam *et al.*, 2002), while the shorter side chains serve to test effects of amino acids with additional charge and/or of hydrophobic nature. The side chain LYH includes histidine for improved endosomal

release (Pichon *et al.*, 2001; Vinod Kumar *et al.*, 2003) and the side chain RGDP has cell targeting motifs RGD for cell binding specificity (Scott *et al.*, 2001; Kim *et al.*, 2006; Martin and Rice, 2007) while a block polymeric design would enable a flexible relative amount of such motifs to be introduced. These elements will be discussed later in this chapter.

The peptides were prepared using Fmoc-chemistry on a TFA-stable resin support as illustrated in Figure 9B. In brief, the synthesis was performed in two stages: stepwise synthesis of the ε-lysine backbone and then concurrent synthesis of all pendent α-peptides to complete the branched molecules, followed by final deprotection and the release of the peptide by a strong acid. As an example, I describe the synthesis of ε-(LYR)K10 to illustrate our synthetic scheme. In the first stage, this synthesis encompasses having the ε-lysine backbone on 4-methylbenzhydrylamine (MBHA) resin which is stable to TFA but cleavable by HF or trifluoromethanesulfonic acid (TFMSA). Stepwise elongation by Fmoc chemistry of Boc-L-Lys(Fmoc)-OH to ε-Lys$_9$ which was then capped by Boc-L-Lys(2-Cl-Z)-OH for protection of the final epsilon amine afforded the ε-(Boc-Lys)$_{10}$ backbone. In the second stage while still attached to the resin support, all the protected Boc-groups of ε-(Boc-Lys)$_9$-ε-Boc-Lys(2-Cl-Z) were then removed under 50% TFA conditions. The deprotected α-amines were utilized for generation of α-amino acid derivatives again by Fmoc chemistry using a "controlled polymerization" approach in which all branching α-peptides are elongated simultaneously. For the pendant tripeptide branches of ε-(LYR)K10, α-amino acid derivatives Fmoc-L-Arg(Pbf)-OH, Fmoc-L-Tyr(tBu)-OH, and Fmoc-Leu-OH were coupled consecutively by DCC/HOBt·H$_2$O in a

mixed solution of DMF and DCM. HF cleavage or 10% TFMSA in TFA removed all protecting groups and ε-(LYR)K10 from the resin support.

3.1.2 Static light scattering

Characterization of the compaction ability of the peptides has been performed with biophysical methods. Effectiveness in compaction is compared by using static light scattering to detect the amount of peptide needed for compaction of DNA. Fluorescence microscopy is used to visualize DNA compaction and the size of the particles is investigated by dynamic light scattering. Finally, compaction is verified by isothermal titration calorimetry which gives information on the thermodynamics of cations binding to DNA.

Figure 10A shows typical curves for titration of peptides into DNA solutions. Formation of compact DNA structures is accompanied by steep increase of scattered light. The log EC_{50} values (the charge concentration of peptide at the midpoint of the scattering intensity curve) of the linear unsubstituted ε-oligolysines plotted against their degree of polymerization (n) are displayed in Figure 10B for experiments conducted at two different concentrations of monovalent salt (5 and 100 mM KCl). There is a decrease in the EC_{50} values with the increase of ε-oligolysine charge, with most of the change in compaction efficiency occurring in the range n = 5-7 for both salt concentrations. The EC_{50} value of the lowest charged ε-oligolysine, ε-K5, is ~100-fold higher than that of ε-K10 (at the same oligopeptide charge concentration). Increased degree of polymerization from 10 to 31 produces a small but noticeable decrease in EC_{50} both at 5 and 100 mM KCl. For n > 7, compaction of DNA is more effective in 100 mM than in 5 mM KCl, i.e.

the salt dependence is reversed compared with the smaller peptides in agreement with observations for polyamines (Nayvelt *et al.*, 2007).

A

B
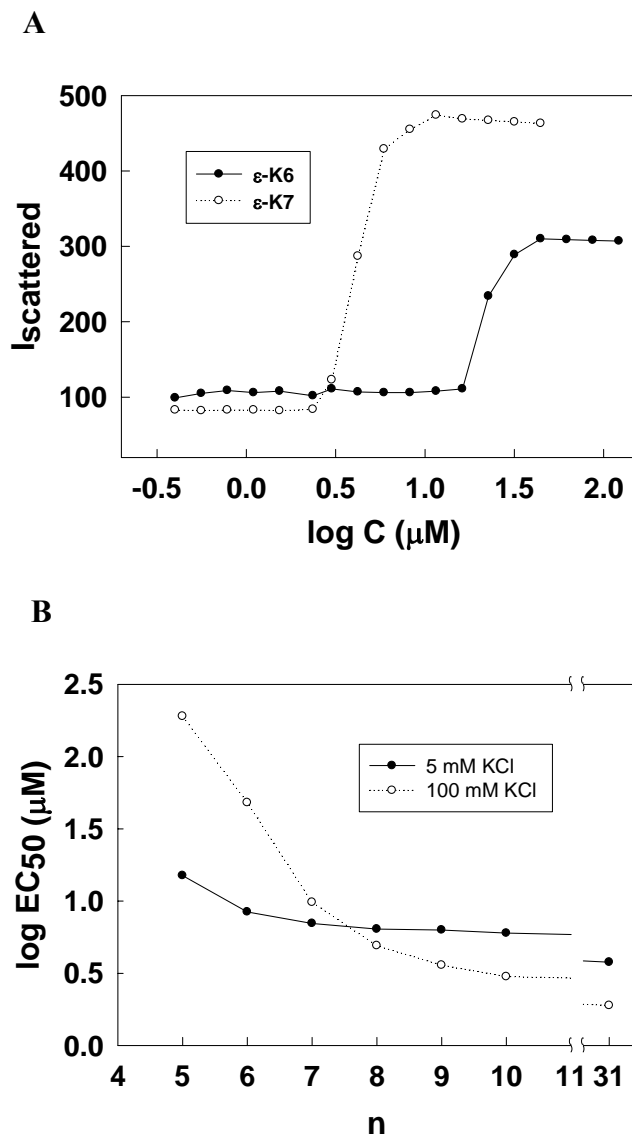
Figure 10. Dynamic light scattering measurements.

(**A**) Typical plots of the intensity of scattered light at 90º plotted against the concentration of added oligopeptides ε-K6 and ε-K7 (100 mM KCl, 4 μM T2 DNA, 1 mM Tris, pH 7.3; C – concentration of the ε-oligolysines expressed in micromoles/liter of amino acid). (**B**) Charge and salt effects of ε-oligolysines on DNA compaction. The midpoint concentration (EC_{50}) of ε-oligolysines necessary to induce T2 DNA condensation is plotted against the number of lysines in the ε-oligolysines. Two K^+ concentrations, 5 mM and 100 mM, are used (1 mM Tris, pH 7.3, T2 DNA concentration is 4 μM, the concentration used for EC_{50} is oligopeptide charge concentration in μM). Measurements were done in three separate experiments and the standard deviation is within 2%.

Table 1. EC50 and N/P ratio of α- and ε-oligolysines to compact T2 DNA[a, b]

Condensing agent	EC$_{50}$ (μM)	N/P
α-PLL	2.2	0.55
ε-PLL	1.9	0.48
ε-K10	3.0	0.75
ε-(L)K10	11.0	2.75
ε-(Y)K10	5.0	1.25
ε-(R)K10	4.2	1.05
ε-(YR)K10	3.6	0.90
ε -(LYR)K10	2.0	0.50

[a] The EC$_{50}$ values were obtained by DLS in three separated measurements, and the reproducibility is within 5%.

[b] T2 DNA concentration is 4 μM (100 mM KCl, 1 mM Tris, pH 7.3).

Table 1 compares the EC$_{50}$ values and N/P ratio (molar ratio of nitrogen to DNA phosphate) of α-PLL with ε-polylysines: ε-PLL and ε-K10 homologues: ε-(L)K10, ε-(Y)K10 (charge +10); ε-(R)K10, ε-(YR)K10 and ε-(LYR)K10 (charge +20). The condensing efficiency is: ε-(L)K10 < ε-(Y)K10 < ε-(R)K10 < ε-(YR)K10 < ε-K10 < α-PLL < ε-(LYR)K10 < ε-PLL. The higher compaction efficiency for the polymeric ε-PLL and the α-PLL as compared with ε-K10 is related to the higher charge of these more polymeric peptides. Addition of hydrophobic and aromatic amino acids to ε-K10 does not increase compaction capacity of the ε-oligolysines. The charged group of the arginine

73

side chain is also seen to be less effective in DNA compaction than the amino group in the ε-oligolysine. Only the combination of arginine, tyrosine and leucine results in more efficient compaction potential for ε-(LYR)K10 compared with that of ε-K10 and α-PLL. Most interestingly, the compaction efficiency of ε-(LYR)K10 is very comparable to that of ε-PLL which has charge +31.

In general, the EC_{50} and N/P values listed in Table 1 present a fragment of complex picture of DNA condensation induced by cationic ligands which depends on not only the charge and chemical composition of the ligand but also the concentration of monovalent salt and DNA. The ε-oligolysines studied in the present work were also used in our laboratory to carry out broad biophysical investigation of DNA condensation in dependence on those parameters (charge and nature of the peptide, DNA and salt concentration). The results obtained in that general study are in full agreement with the data presented here. However, comprehensive biophysical studies of DNA coil-globule transition is outside the scope of this thesis since the major objective of the biophysical section of the present work was to study DNA condensation under conditions relevant to those applied in transfection of eukaryotic cells.

Effect of pH was studied for ε-K10 and ε-(LYR)K10 (Figure 11). Increase of pH exerts a major influence on ε-K10 at pH > 7.5 with little effect on the other ε-oligolysine, ε-(LYR)K10. The value of pKa of ε-lysine is about 8.9 which implies almost full positive charge at pH below 7.5. As pH value increases to 8.2 and 9.1, some of the positive charge will be neutralized so that more ε-oligolysines are needed to collapse DNA. The contribution from the highly basic guanidinium groups of arginine ($pK_a = 12.0$) in the ε-(LYR)K10 preserves the compaction abilities of this peptide at high pH.
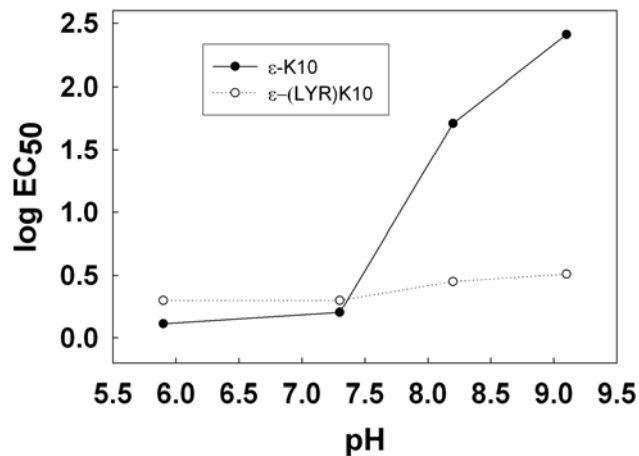
Figure 11. Effects of pH in the buffer on the midpoint concentration of ε-oligolysines (EC$_{50}$) to induce DNA compaction.

The EC$_{50}$ values were determined at pH 5.9, 7.3, 8.2 and 9.1. Data shown come from three separate experiments and the standard deviation is within 5%.

Figure 12 shows the efficiency of ε-K10, ε-(LYR)K10, ε-PLL and α-PLL in their ability to condense different type of DNA molecules. In all measurements, T2 DNA forms compact structures at lower concentration of condensing agent than plasmid DNA. The likely reason for the observed sensitivity of the EC$_{50}$ values to the source of DNA is that the higher molecular weight DNA from T2 (164 kbp) phage compared with the plasmid DNA (4.7 kbp) can more easily undergo condensation as shown theoretically by Post and Zimm (Post and Zimm, 1982).
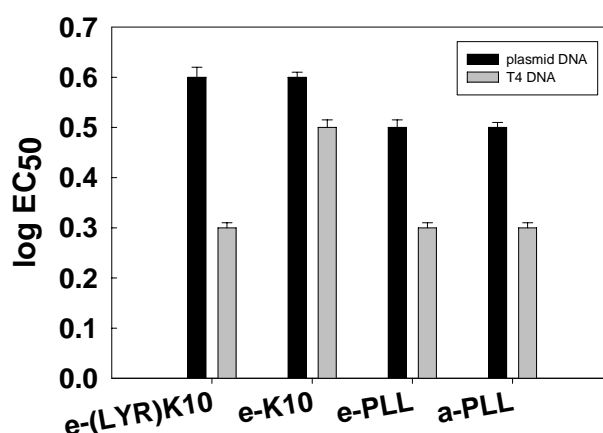
Figure 12. EC$_{50}$ of different polylysines necessary to induce T4GT7 and plasmid DNA condensation.

The concentration used for EC$_{50}$ is oligopeptide charge concentration in μM. DNA concentration is 4 μM; 100 mM KCl, 1 mM Tris, pH 7.3. Errors bars represent the standard deviation from three separate experiments.

3.1.3. Direct observation of conformational changes of single DNA molecules

Figure 13 shows the fluorescence images of T2 DNA molecules in the absence and in the presence of compaction agent, ε-(R)K10. In the absence of ε-(R)K10, double-stranded DNA molecules exist in the form of extended coil (Figure 13A). Addition of ε-oligolysines to concentration above the EC$_{50}$ value induces collapse of individual T2 DNA molecules to small compacted globules (Figure 13B). Similar behavior is observed for the other peptides (data not shown). My microscopic observation is in agreement (with respect to the DNA sizes free in solution and in compact form) with the data by Yoshikawa and co-workers obtained for similar viral DNA (Mel'nikov *et al.*, 1995; Takahashi *et al.*, 1997; Yoshikawa *et al.*, 1997; Murayama and Yoshikawa, 1999) but due to other compaction agents.
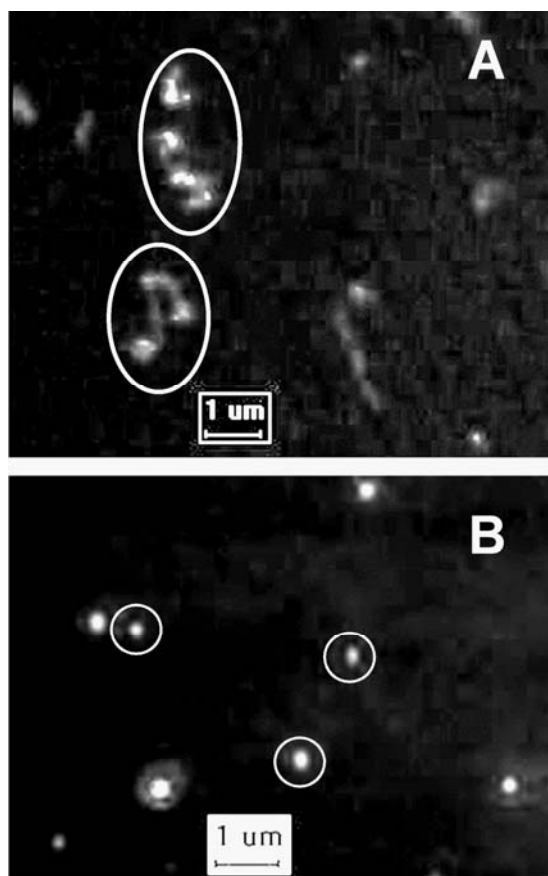
Figure 13. Fluorescence images of free DNA and compacted DNA.

(**A**) Fluorescence image of free T2 DNA molecules in extended coil conformation (0.5 µM DNA, 0.5 µM DAPI, 1 mM Tris, pH 7.3). (**B**) Fluorescence image of compacted T4 DNA molecules; the condensing agent used was ε-(R)K10 at concentration 0.1 µM. (0.5 µM DNA, 0.5 µM DAPI, 100 mM KCl, 1 mM Tris, pH 7.3). DNA molecules are marked by ovals.

3.1.4. Dynamic light scattering

The effective diameters of T4GT7 and plasmid DNA condensates formed in the presence of ε-oligolysines and α-polylysines were determined. Data on effective diameters measured at the plateau of the corresponding curves of the T4GT7 and plasmid DNA solutions are presented in Table 2. The effective diameters of fully compacted T4GT7 DNA are between 300 and 600 nm and depend on the compaction agent with the

most compact particles formed by ε-(LYR)K10. The DLS data are consistent with results obtained by static light scattering. For the plasmid DNA, DLS measurements were carried out at two different initial concentrations of DNA, 0.2 mM (70 µg/ml) and 0.04 mM (14 µg/ml). The effective diameter of the particles formed upon compaction of plasmid DNA depends on DNA concentration and is reduced when DNA concentration is decreased (Table 2). For plasmid DNA at low concentration (0.04 mM) it was possible to measure the size of uncondensed DNA molecules which was about 800 nm in agreement with estimation calculated from flexible worm-like chain model of the DNA. I also measured the size of plasmid DNA compacted using the commercial transfection agent, DOTAP, and using DOTAP + ε-(LYR)K10 at concentrations mimicking conditions of the transfection experiments (see Experimental Section) and the size was 163 nm and 198 nm with or without added ε-(LYR)K10 respectively. For plasmid DNA, the dependence of particle size on DNA concentration indicates that at the high concentration, aggregates of several DNA molecules are formed.

Table 2. Size of DNA condensates formed in the presence of α- and ε-oligolysines in 100 mM KCl[a]

Condensing agent	Size of T4GT7 DNA condensates[b] (nm)	Size of plasmid DNA condensates[c] (nm)	Size of plasmid DNA condensates[d] (nm)
ε -(LYR)K10	374	188	97
ε-PLL	455	254	138
ε-K10	487	293	140
α-PLL	556	367	131

[a] The particles sizes were obtained by DLS in three separated measurements, and the reproducibility is within 5%.

[b] T4 DNA concentration is 3.6 µM (1.3 µg/mL).

[c] Plasmid DNA concentration is 0.2 mM (70 µg/mL).

[d] Plasmid DNA concentration is 0.04 mM (14 µg/mL).

Table 3. Size of DNA condensates formed in the presence of some ε-oligolysines in

10 mM KCl[a]

Condensing agent	Size of plasmid DNA condensates[b] (nm)
ε -(LYH)K10	123.4
ε -(RGDP)K10	225.8
ε -(HK$_4$)K20	132.6
ε -(LYHK$_4$)K20	204.9

[a] The particles sizes were obtained by DLS in three separated measurements, and the

reproducibility is within 5%.

[b] Plasmid DNA concentration is 0.04 mM (14 µg/mL).

3.1.5. Isothermal titration calorimetry

I next measured the enthalpy of ligand-DNA interaction (ΔH) in dependence of charge ratio (positive charge of added ligand/negative charge of DNA). For comparison, values of ΔH are normalized by charge of the ligand. In Figure 14A, data determined for ε-oligolysines as a function of degree of polymerization is presented; Figure 14B compares the ε-K10 and its derivatives. Titrations using $[Co(NH_3)_6]^{3+}$ and spermine^{4+} (data shown in the Appendix, Figure 32) were conducted, demonstrating quantitative agreement with previous ITC studies of DNA binding and condensation by these and other cations (Matulis *et al.*, 2000).

The enthalpy of oligolysine-DNA interaction is always positive, i.e. the driving force of ligand binding is the entropic gain upon release of monovalent cations and water upon binding. A positive enthalpy is also a signature of ligand interaction with the DNA minor groove (Privalov *et al.*, 2007). Derivatives of ε-K10 containing leucine show more positive values of ΔH than the linear peptides; tyrosine- and arginine-containing ligands (except with leucine, LYR) display less positive enthalpy than ε-K5 − ε-K10 oligolysines. These differences in ΔH might reflect different contributions of electrostatic and hydrophobic ligand-DNA interactions (generally showing positive enthalpies in ITC measurements) (Matulis *et al.*, 2000; Matulis *et al.*, 2002; Patel and Anchodoquy, 2005) and specific binding which usually brings favorable (negative) contribution to the binding enthalpy. In particular, higher values of ΔH of the leucine-containing oligolysines correlate with high positive values of ΔH reported in ITC studies of DNA interaction with

the hydrophobic lipospermine (Patel and Anchodoquy, 2005) and with different cationic lipids (Matulis *et al.*, 2002).

All the ITC data demonstrate DNA condensation (Matulis *et al.*, 2000; Patel and Anchodoquy, 2005) by appearance of either a peak or a sharp discontinuity, both in raw data (heat capacity versus added titrant; data shown in the Appendix, Figure 33) and in ΔH. Significant contribution of the peak to the titration curves complicates the application of simple schemes (one or two site binding models) which would allow extraction of complete thermodynamic information from the ITC curves. The contribution of DNA condensation to the total heat effect is higher than similar effects reported for cobalt hexammine, and polyamines (Matulis *et al.*, 2000) (see also $Co(NH_3)_6Cl_6$ result in Appendix, Figure 32). The positions of the peaks are around a charge ratio 0.7-0.8 for the oligolysines ε-K5 - ε-K10 and around 1.0-1.1 for ε-PLL. The peak for DNA compaction is reduced and shifts to higher charge ratios (0.9-1.0) for the substituted ε-K10 derivatives.
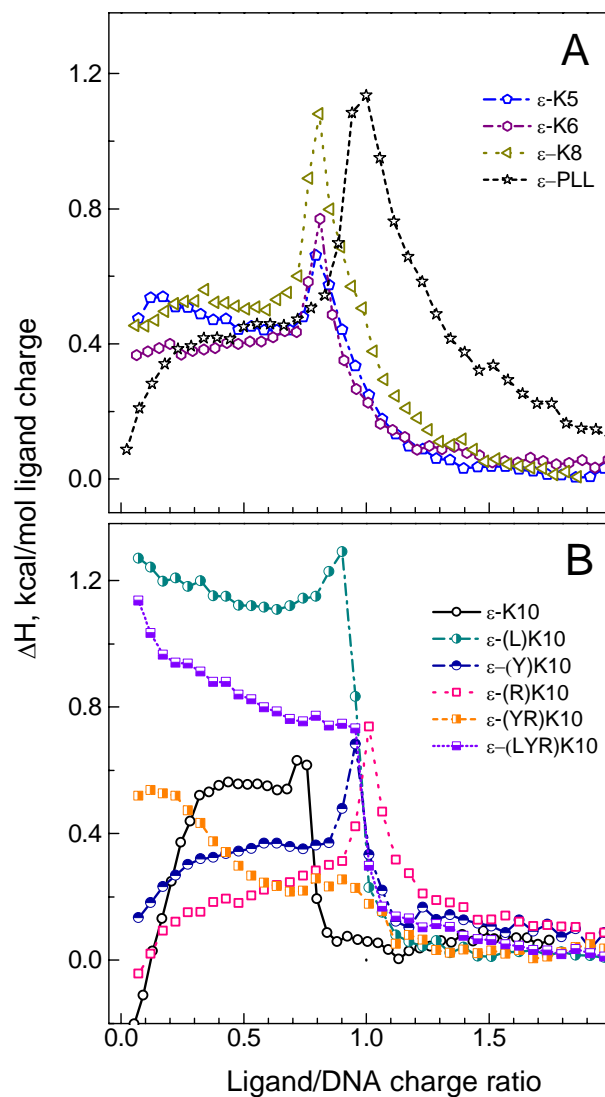
Figure 14. Results of isothermal titration calorimetry.

Values of enthalpy at 298 K calculated from titration curves were normalized relative to the charge of the cationic ligand and plotted versus ratio of added ligand charge to charge of the DNA. (**A**). Influence of degree of polymerization of ε-oligolysines on enthalpy of ligand-DNA interaction. (**B**). Influence of side chain of ε-K10 derivatives on enthalpy of ligand-DNA interaction.

3.1.6 Discussion

In physical characterizations, the ITC experiment showed that compaction of DNA occurred at an oligolysine/DNA charge ratio below 1.0 (Figure 14) which indicates that the degree of protonation of the ε-oligolysines is close to stoichiometric.

SLS results (Figure 10B and Table 1) and ITC data (Figure 14) are in general agreement and allow to explain some features of the ε-oligolysine−DNA interaction and compaction. For example, anomalously high value of logEC$_{50}$ observed for ε-(L)K10 in 100 mM KCl (Table 1) correlates with high positive enthalpy of ε-(L)K10−DNA interaction (Figure 14B). Positive enthalpy makes unfavorable contribution to the free energy of the ligand−DNA interaction and in this way reduces efficiency of the ligand to compact DNA. However, there is no straightforward correlation between enthalpies of the ε-oligolysine−DNA interaction and efficiency of DNA compaction by the ligands, e.g. high (relative to the other peptides except ε-(L)K10) enthalpy of ε-(LYR)K10−DNA interaction (Figure 14B) contradicts with the high efficiency of ε-(LYR)K10 in DNA compaction (Table 1).

The cause of this discrepancy between SLS and ITC results might originate from the complexity of dependence of the DNA compaction on ligand−DNA thermodynamic parameters, ligand charge and nature as well as on variation of the efficiency with concentration of monovalent salt. These issues have been recently addressed in our laboratory and the results of the present work have been extended. In particular, DLS and SLS studies of DNA compaction by the ε-oligolysines was extended to the wide range of salt concentration (from 10 to 400 mM KCl) and complemented with the data obtained by ITC titration in high KCl concentration (100 mM) (Korolev *et al.*, unpublished data).

Additionally, precipitation assay was used to confirm the data of DLS and ITC methods. Combination of all these techniques allowed to cover wide range of the DNA (5~400 µM), monovalent salt (KCl, 10~400 mM) and ε-oligolysines (from fraction of µM to tens mM) concentrations. The outcome of that extended study (which extends outside the scope of this PhD thesis) was creation of non-contradictory picture of the ε-oligolysine−DNA binding and DNA compaction in dependence on the variety of conditions (nature, charge and concentration of the ligand, DNA and monovalent salt concentration) (Korolev *et al*., manuscript in preparation).

ε-Oligolysines have a more flexible backbone and a more rigid charged side chain as compared with α-oligolysines. ε-Oligolysines also have lower pK_a than α-oligolysines. At physiological pH, the ε-oligolysines are only partially protonated and should have some lysosomotrophic effects similar to weak bases. This property may also enable DNA to be more easily released from the condensed particles after entering the cells. This hypothesis is supported by my data on pH dependence of EC_{50} for ε-oligolysines (Figure 11). In the case of α-lysines, the side chain amino groups (pKa = 10-11) are strongly charged at neutral pH and cannot buffer acidification of the endosome. It is known that nuclease degradation in the lysosomal compartment is a significant complication in developing the nonviral gene delivery systems. It was postulated that polymers containing pH sensitive groups with buffering abilities between pK_a 5.0 and 7.2, could buffer the endosome and induce its collapse and the release of the endosomal content into the cytoplasm to improve transfection efficiency (Remy *et al.*, 1998). On the basis of this finding, cationic polymer and liposome vectors containing histidine (pK_a = 5.0) have been designed and found to improve delivery *in vitro* as well as *in vivo* (Vinod Kumar *et*

al., 2003; Yu *et al.*, 2004). The present design with flexible and controlled synthesis enables this function by introducing histidine in the side chain which will be discussed later in this chapter.

In many studies the relation between the particle size for effective transfection has been established (Duguid *et al.*, 1998; Pouton and Seymour, 2001; Liu and Huang, 2002; Vijayanathan *et al.*, 2002; Jang *et al.*, 2006) with optimal size varying from 50 to 200 nm. My DLS results showed that under conditions of transfection recommended for application of DOTAP (DNA concentration about 50 μg/ml), plasmid DNA particles are around or larger than 200 nm with the substituted ε-(LYR)K10 forming the smallest particles and this correlates with the high transfection efficiency of this compound. Decreasing DNA concentration in solution before addition of the compaction agent produces smaller particles. Particles obtained at higher DNA concentration may be composed of aggregates of several plasmid molecules.

3.2 NCP aggregation

3.2.1 Results

The effect of cations on NCP aggregation has previously mainly been studied by the precipitation assay (de Frutos *et al.*, 2001; Bertin *et al.*, 2007). Here, it is proposed to use DLS for the purpose of detecting this cation induced aggregation. Before using this method for the systems of NCP with HMGN protein, I first investigate the Ca^{2+} and Mg^{2+} induced aggregation with DLS and compare results with precipitation assay.

Figure 15A shows NCP precipitation curves with starting NCP concentration 0.3 mg/mL in the presence of Mg^{2+} and Ca^{2+} respectively. The precipitation curves look

similar for both divalent cations. NCPs aggregate continuously. With increasing divalent cation concentrations, the fraction of precipitated NCPs increases to a maximum. At that point, a rather small NCP fraction (2-3%) remains soluble, regardless of the precipitating agent (magnesium or calcium).
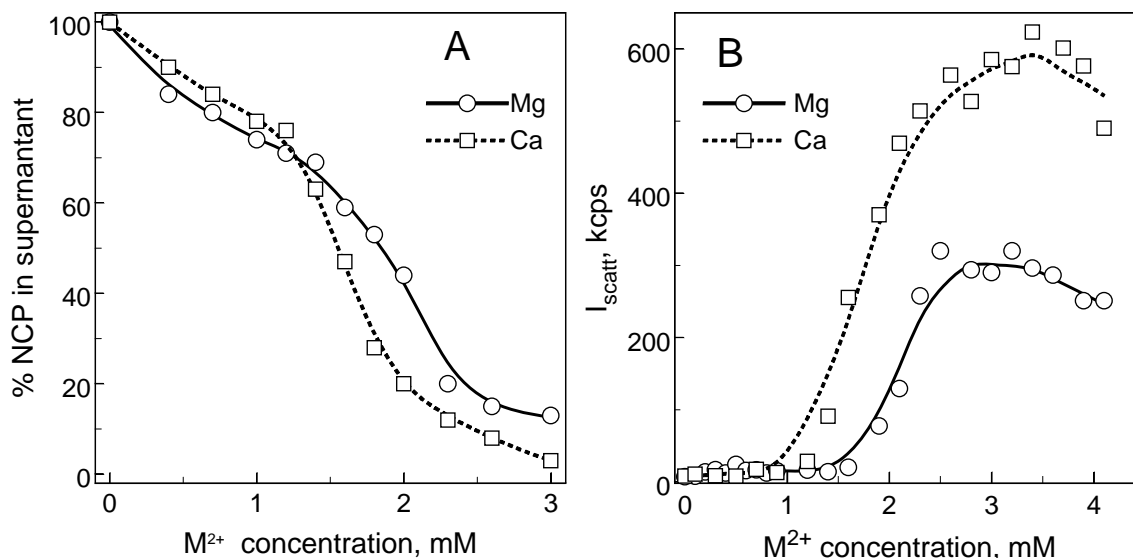

Figure 15. Comparison of the results of NCP (A) precipitation assay and (B) DLS.

Starting concentration of NCP is 132 μg/mL (or 182 μM of DNA phosphates) in **A** and 80 μg/mL (or 110 μM of DNA phosphates) in **B**. Either percentage of soluble NCP (in **A**) or intensity of scattered light (in **B**) is plotted against cation concentration added to the NCP solution. Both experiments are conducted in 10 mM Tris-HCl, pH 7.5.

DLS results of NCP compacted by Mg^{2+} or Ca^{2+} are shown in Figure 15B. Similarly to the curves for titration of peptides into T2 DNA solutions (shown in Figure 10A), the light scattering intensity of NCP solution is low and remains unchanged at low concentrations of divalent cations. However, at a critical concentration of the cations (1.7 mM for Ca^{2+} and 2.2 mM for Mg^{2+}), a rapid increase in the scattered light intensity occurs. The final intensity of scattered light for NCP-Ca^{2+} system is much higher than NCP-Mg^{2+}. The trend that Ca^{2+} is more effective in inducing NCP aggregation than Mg^{2+} in Figure

15B is very similar to that in Figure 15A (the cation concentration needed to induce 50% NCP aggregation is 1.6 mM for Ca^{2+} and 1.9 mM for Mg^{2+}).

Curves of NCP titration by Mg^{2+} in the presence of different concentration of KCl are shown in Figure 16. For both conditions, the intensity of scattered light increases slowly at first and then undergoes steep increase at 4 mM Mg^{2+} for 10 mM KCl and 7 mM Mg^{2+} for 100 mM KCl. The particle size of NCP aggregrates in 10 mM KCl is larger than in 100 mM KCl.
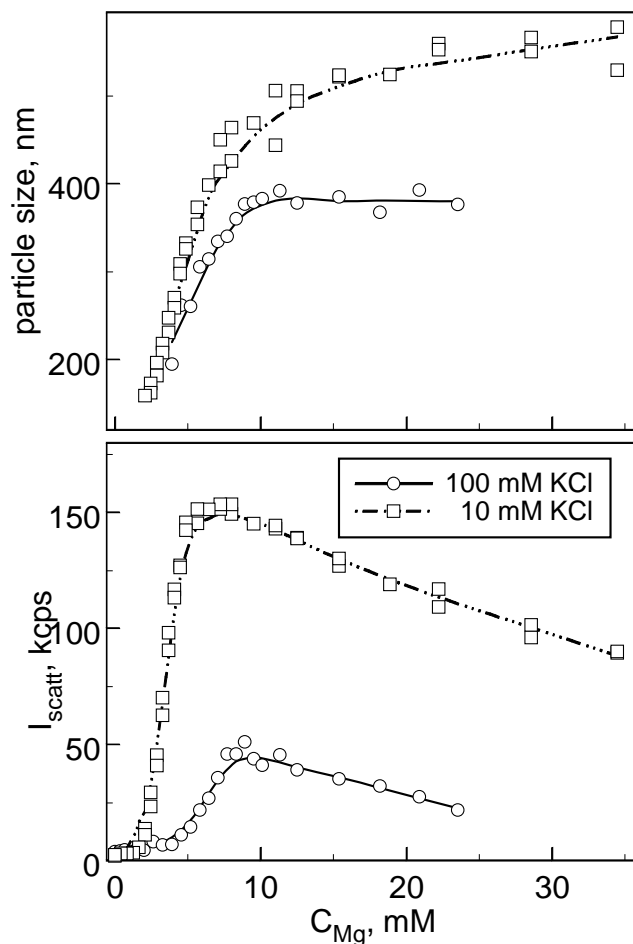

Figure 16. Data on NCP titration by Mg^{2+} in the presence of KCl.

The titrations were carried out at two KCl concentrations, 100 and 10 mM. NCP concentrations were slightly different, 7.4 and 8.3 μM respectively.

The influence of HMGN2 and XN2 on the NCP aggregation caused by addition of Mg^{2+} is shown in Figure 17. Particle size data gives limited information (Figure 17, top panels). This is due to kinetic effects and the aggregates may not be equilibrium structures. In the beginning of titration the intensity of light scattering was too low to get reliable values of particle size (However, there was some indication of particles with diameter around 10 nm in solutions of NCP, in agreement with the known size of NCP). For all NCP aggregates obtained in the presence of HMG proteins (both full length and truncated), the particle size is smaller than that of NCPs in the absence of HMG. Addition of proteins (both HMGN2 and XN2) to 2 and 4 molecules per NCP results in shift of NCP aggregation to higher Mg^{2+} concentration, lower values of $I_{scattered}$ and smaller particles.

For truncated HMG protein (XN2), scattering signal is lower than that obtained in the absence of XN2. It looks like there is consistent decrease of $I_{scattered}$ with increase of added XN2. 2 and 4 mole XN2 give equal signal while 10 moles added give very low signal. One can suggest that at high XN2:NCP ratio the aggregates are more loose (extended). For full length HMGN2 addition of 2 and 4 moles of the protein results in decrease of the $I_{scattered}$ similar (signal is a bit lower) to the picture seen for XN2.

Excess (10 moles per NCP) of protein HMGN2 or XN2 results in completely different titration curves: presence of the short fragment shifts formation of the NCP aggregates to higher C_{Mg} relative to 2 and 4 XN2 per NCP and dramatically reduces $I_{scattered}$ whereas excess of full length HMGN2 facilitates formation of the aggregates. To explain this contrasting behavior additional studies are needed with application of different techniques (e.g. gel shift analysis and other methods).

Figure 17. Influence of HMGN2 on the NCP aggregation caused by addition of Mg^{2+}.

Top panels: size of the particles (diameter in nm) vs Mg^{2+} concentration, C_{Mg}. Bottom panels: dependence of intensity of light scattering, I_{scatt} (kcps, kilocounts per second) is plotted against C_{Mg}. NCP concentration is 7.3 µM in DNA phosphates; salt concentration 100 mM KCl; moles of protein per mole of NCP are indicated in figures; titrant 200 mM MgCl$_2$ in 100 mM KCl. **A**. Full length HMGN2. **B**. XN2 is fragment of HMGN2 a.a. from 17 to 46.

The aa sequences of HMGN2 and its truncated form XN2-1 are listed below.

Xenopus laevis HMGN2 (N2)

   PKRKADGDSK AEKAKAKDEP QRRSARLSAK PAPPKPEAKP KKAAAPPKKA
   DKAPKGKKGK ADSGKDSSNA AENGEAKSDQ AQKAETGDTK

Xenopus laevis HMGN2 NBD (XN2-1)

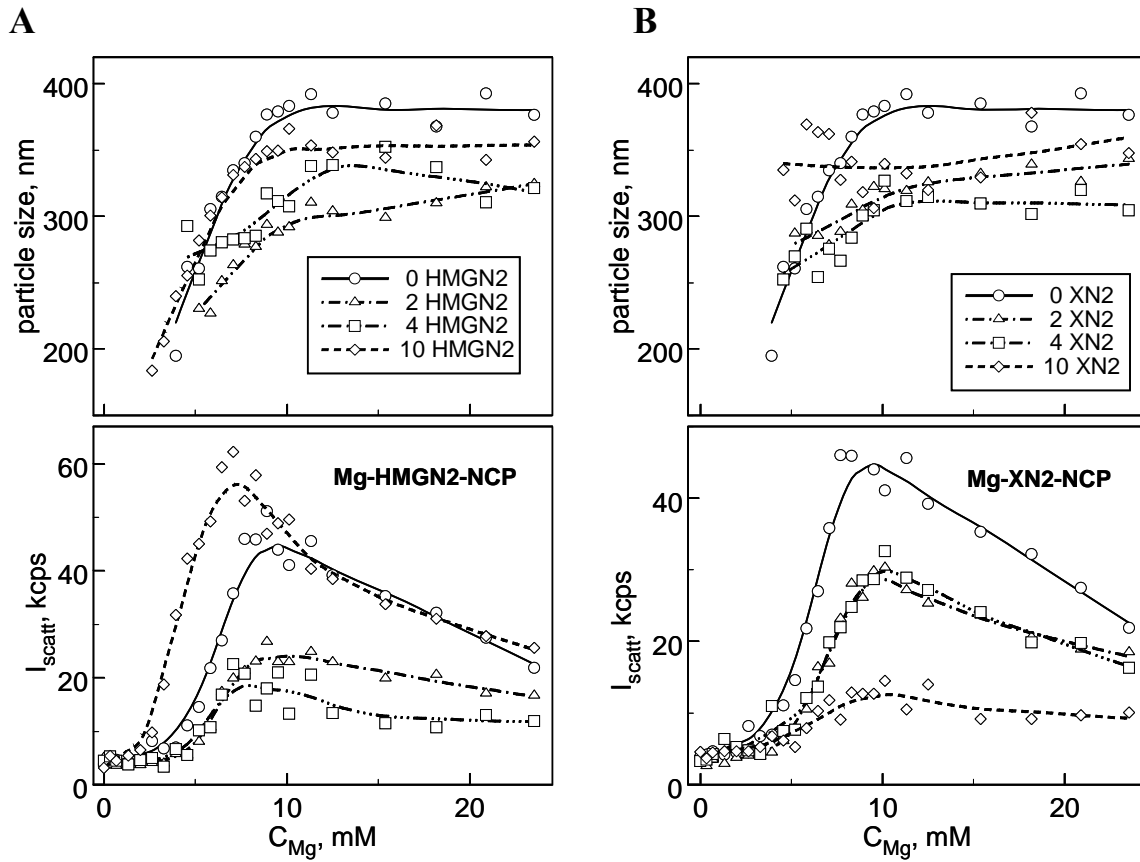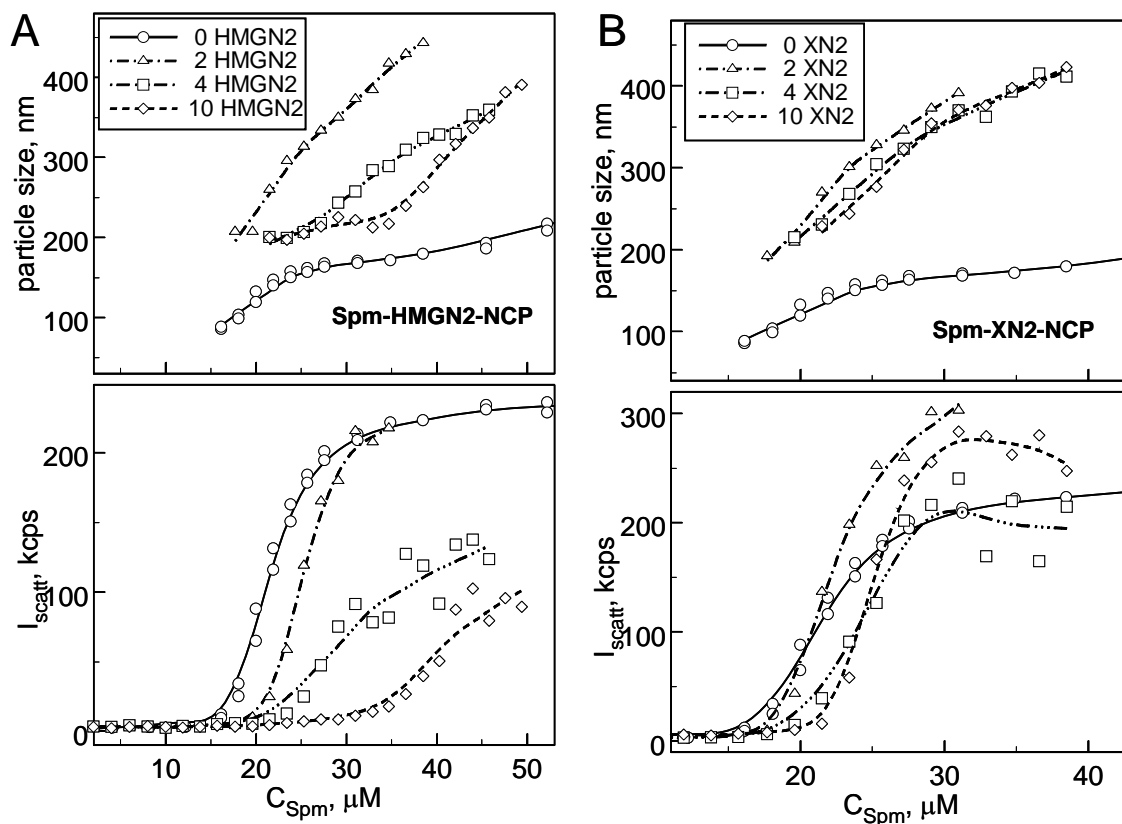   KDEP QRRSARLSAK PAPPKPEAKP KKAAAPPK

Figure 18. Influence of HMGN2 on the NCP aggregation caused by addition of spermine, Spm^{4+}.

Top panels: size of the particles (diameter in nm) vs Spm^{4+} concentration, C_{Spm}. Bottom panels: dependence of intensity of light scattering, I_{scatt} (kcps, kilocounts per second) is plotted against C_{Spm}. NCP concentration is 7.3 µM in DNA phosphates; salt concentration 10 mM KCl; moles of protein per mole of NCP are indicated in figures; titrant 500 µM Spm^{4+} in 10 mM KCl. **A**. Full length HMGN2. **B**. XN2 is fragment of HMGN2 a.a. from 17 to 46.

Figure 18 shows the effect of HMGN2 on the NCP aggregation caused by addition of spermine (Spm^{4+}). Comparing to the similar data obtained for Mg^{2+} titration, the influence of the protein presence on the NCP aggregation caused by addition of cationic species (Mg^{2+} or Spm^{4+}) is different. For full length protein (HMGN2), systematic trend in titration curves is obtained: increase of protein shifts NCP aggregation to the higher C_{spm} accompanied by decrease of $I_{scattered}$ and particle size (Figure 18, top panels).

Increase of XN2 from 2 to 4 protein molecules per NCP leads to the shift of aggregation to the higher C_{spm}, but in the presence of the excess of protein, 10 XN2/NCP, titration curve is similar to that of 4 XN2/NCP. Size of the particles is similar for all XN2/NCP ratios and higher than the values obtained in the absence of the protein (data not shown).

3.2.2 Discussion

NCP-NCP interaction was determined by the NCP precipitation assay (Figure 15A) and dynamic light scattering (Figure 15B). In both experiments Ca^{2+} shows slightly higher efficiency than Mg^{2+} in formation of the NCP aggregates and this is indicated by lower value of EC_{50}, higher percentage of NCP precipitated and higher intensity of light scattering. My result is in agreement with the data of the precipitation assay reported by de Frutos and co-workers (de Frutos *et al.*, 2001). With divalent cations, Mg^{2+} or Ca^{2+}, NCP precipitates continuously without redissolution and 80- 90% of NCP is aggregated. These are consistent with Bertin and co-workers' results (Bertin *et al.*, 2007).

Similar experiments were carried out to investigate NCP interaction in dependence of KCl or NaCl concentration in the range of 0-300 mM (data not shown). Neither precipitation assay nor DLS measurement shows significant formation of dense NCP aggregates (the aggregates which precipitate or show great light scattering). Some precipitation of the NCP occurs at the KCl or NaCl concentration higher than 50 mM, however, at all concentrations about 80% NCP remains in solution. Intensity of light scattering increases slightly from 5-10 kcps to 20-30 kcps (both values are within the uncertainty of the DLS measurements).

For NCP titration by Mg^{2+} in different concentration of KCl (Figure 16), addition of KCl shifts NCP aggregation to higher Mg^{2+} concentration. This is consistent with Bertin

and colleagues' finding that increasing the amount of monovalent salt in the solution induces a decrease in the fraction of precipitated NCPs. Therefore, more Mg^{2+} are needed to aggregate NCP. At initial stages of NCP aggregation, sizes of particles in 10 and 100 mM KCl are similar (300-400 nm) while scattering light intensity in 10 mM KCl is much higher than that in 100 mM KCl. It might indicate that denser particles are formed at the low salt condition. For NCP in 10 mM KCl, that increase in particle size is accompanied by decrease of I_{scatt} may due to swelling of aggregates which causes reduction of difference in refraction between solvent and aggregates.

Previously T2 DNA compaction by ε-K5~10 under two different KCl concentrations has been investigated (Figure 10B). Therefore, it is interesting to compare the effect of monovalent cation K^+ on DNA/peptide with NCP/ Mg^{2+} system. Taking ε-K5 which has the lowest positive charge among the ε-oligolysines for example, in Figure 10B, increasing KCl concentration from 5 mM to 100 mM increases EC_{50} from 16 μM to 200 μM. The same thing happens in NCP/Mg^{2+} system (Figure 16). The more KCl there is, the more Mg^{2+} is needed to induce NCP aggregation. Since ε-K5 has more positive charges than Mg^{2+}, EC_{50} of Mg^{2+} is always higher than ε-K5.

The behavior of NCP aggregation in the presence of HMGN2/XN2 in different cationic solutions seems to be complicated. To further understand it, more experiments need to be done.

One of the possible explanations for that excess HMGN2 or XN2 gives very different titration curves compared with lower amount is that the presence of acidic C-terminal in the full length HMGN2 enables this protein to form aggregates in the presence of Mg^{2+}. In a mixture of NCP and excess of HMGN2 complex aggregates (NCP+HMGN2) might

form by addition of Mg^{2+} with HMGN2 acting as additional compacting agent. Full length protein HMGN2 contains both DNA binding domain and negatively charged short "C-terminals", therefore it could form bridges between NCP molecules (for example by interacting with DNA on one NCP and forming contact with histone tails of the other NCP through its C-terminal). In that way, the system NCP plus excess of HMGN2 is more prone to aggregation than solution of NCP only and needs less Mg^{2+} to aggregate.

3.3 *In vitro* transfection with ε-peptide vectors

3.3.1 *In vitro* transfection

The transfection efficiency of ε- and α-oligolysines were investigated in four cells lines, Hela, 293F, Mewo and A549. Hela and 293F are commonly used cell lines for transfection. Mewo and A549 are optimal as positive and negative control for RGD-mediated transfection (Kunath *et al.*, 2003). For transfection experiments, I focus on one of unsubstituted ε-polylysines, ε-K10; two α-substituted ε-K10 homologues, ε-(YR)K10 and ε-(LYR)K10 and one α-oligolysine, α-PLL (based on the results in Figure 10 and Table 1). The results are presented according to peptides used. All data shown are based on three separate experiments and the standard deviation is within 5%. The standard deviation is calculated by the following formula:

$$\sigma = \sqrt{\frac{\sum_{k=1}^{n}\left(x_k - \mu\right)^2}{n}}$$

where σ is standard deviation, x_k is the value, μ is the arithmetic mean of the values and n is the total number of the values.

ε- and α-oligolysines, ε-(YR)K10 and ε-(LYR)K10. Figure 19 shows the transfection efficiency in HeLa cells mediated by the different ε-oligolysines and control transfection performed with DOTAP. Transfection was carried out using two different concentrations (but the same total amount) of plasmid DNA, 120 and 24 μg/mL. Among peptides investigated, only data for those demonstrating significant transfection are shown. For the substituted ε-oligolysine samples, the ε-(LYR)K10, can significantly increase transfection efficiency in HeLa cells as compared with the liposome transfection agent DOTAP. Combination of either of ε-(YR)K10 or ε-(LYR)K10 with DOTAP leads to considerably increased transfection in the HeLa cells.
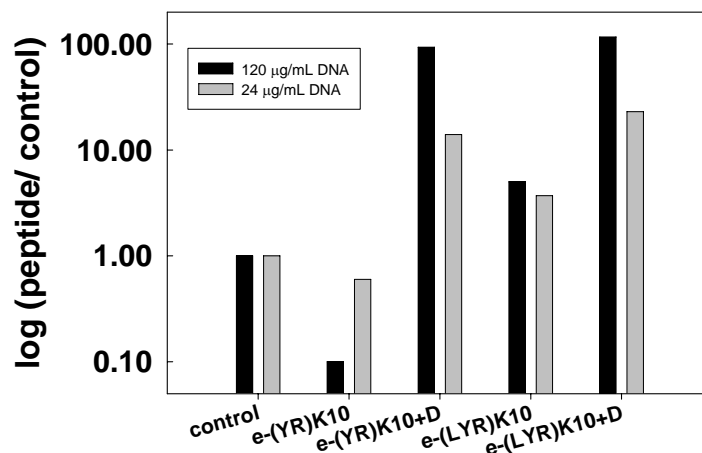
Figure 19. Transfection efficiency of the ε-peptides in Hela cells.

For peptides investigated, only those which show GFP transfection are displayed. The ε-peptide concentration was 2 mg/mL when ε-peptide only was applied, for mixtures of ε-peptide with DOTAP (indicated as "control" or "D" in the graphs), the peptide concentration was 1 mg/mL and the concentration of DOTAP was 0.2 mg/mL. A logarithmic scale is used for Y axes (the absolute transfection for control is 0.3%). All transfection experiments shown were repeated for three times separately and the standard deviation is within 5%.

Figure 20 shows the transfection efficiency in 293F cells mediated by the different ε-and α-oligolysines and control transfection performed with DOTAP. Transfection was carried out using two different concentrations (but the same total amount) of plasmid DNA, 120 and 24 μg/mL. Among peptides investigated, only data for those which demonstrate significant transfection are shown. Compared with results in the HeLa cells, several of the peptides tested in the first part of the work show noticeable transfection in the 293F cells. The linear unsubstituted ε-lysines ε-K10 and ε-PLL are more effective delivery vectors than α-oligolysines (which demonstrate negligible effect), albeit with small effect when used without DOTAP. In combination with DOTAP ε-lysines are relatively good transfection agents. For the substituted ε-lysines the system composed of DOTAP and ε-(LYR)K10 at a molar ratio of 3:2 is found to be optimal and can mediate up to 35 % of cell transfection when DNA concentration is 24 μg/mL; other derivatives of ε-K10 are less efficient. For all transfection agents, decrease of DNA concentration resulted increased GFP expression. For ε-(LYR)K10, the dependence of transfection on relative amount of the DOTAP and ε-(LYR)K10 in the DNA-condensing mixture has been studied (Figure 21). The molar ratio between DOTAP and ε-(LYR)K10 3:2 (equal to 1:1 volume ratio in Figure 21) displayes the highest transfection efficiency.
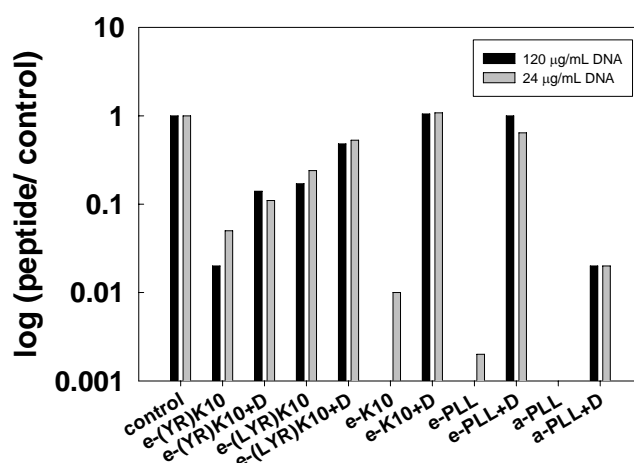
Figure 20. Transfection efficiency of the ε-peptides in 293F cells.

The ε-peptide concentration was 2 mg/mL when ε-peptide only was applied, for mixtures of ε-peptide with DOTAP (indicated as "control" or "D" in the graphs), the peptide concentration was 1 mg/mL and the concentration of DOTAP was 0.2 mg/mL. A logarithmic scale is used for Y axes (the absolute transfection for control is 42% for high concentration DNA and 66% for low concentration DNA). All transfection experiments shown were repeated for three times separately and the standard deviation is within 5%.

Figure 21. Dependence of transfection efficiency for 293F cells on the volume ratio between commercial transfection agent DOTAP and ε-(LYR)K10.

The stock concentration of DOTAP (indicated as "control" or "D") is 1 mg/mL and the stock solution of ε-(LYR)K10 is 5 mg/mL. DNA stock concentration is 50 µg/mL. All transfection experiments shown were repeated for three times separately and the standard deviation is within 5%.
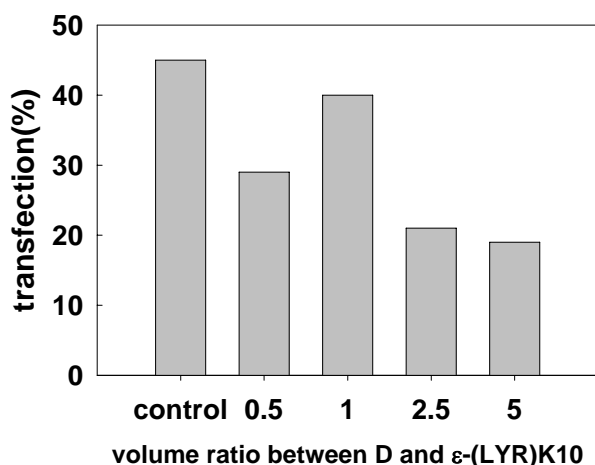
ε-(LYH)K10 and ε-(RGDP)K10. Figure 22 shows the transfection efficiency mediated

by ε-(LYH)K10, ε-(RGDP)K10 and their mixtures with DOTAP in four cell lines, Hela,

293F, Mewo and A549. As can be seen from Figure 22, the usage of only ε-(LYH)K10

did not result in noticeable transfection in Hela, Mewo and A549 cell lines but mediated

considerable transfection which was 15% in 293F cells. When used alone, ε-(RGDP)K10

had negligible transfection effect in all of the four cell lines. In combination with DOTAP,

ε-(LYH)K10 showed high (as for generally less potent cell lines) transfection which was

about 10% in both Hela and Mewo cell lines. The mixture of ε-(LYH)K10 and DOTAP

mediated considerably high transfection efficiency in both 293F and A549 cells, 66% and

35% respectively. ε-(RGDP)K10, when combined with DOTAP, induced negligible

transfection in Hela, Mewo and A549 cell lines whereas showed relatively high

transfection efficiency which was 32% in 293F cells.
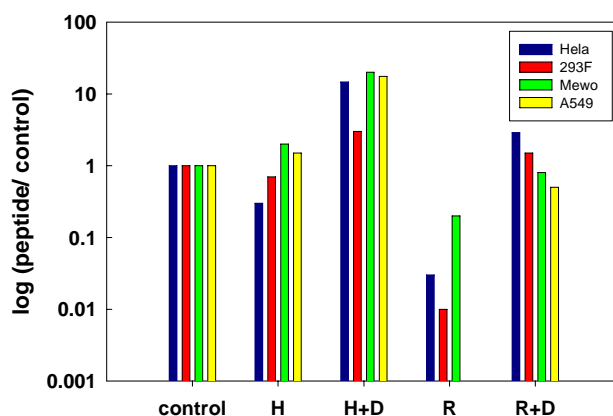
Figure 22. Transfection efficiency in four cell lines, Hela, 293F, Mewo and A549, mediated by ε-(LYH)K10 or ε-(RGDP)K10 or their mixtures with positive control DOTAP.

In this figure, H represents ε-(LYH)K10 and R represents ε-(RGDP)K10. The ε-peptide concentration was 2 mg/mL when ε-peptide only was applied, for mixtures of ε-peptide with DOTAP (indicated as "control" or "D" in the graphs), the peptide concentration was 1 mg/mL and the concentration of DOTAP was 0.2 mg/mL. A logarithmic scale is used for Y axes (the absolute transfection for control is 0.7%, 22%, 0.5% and 2% for Hela, 293F, Mewo and A549 respectively). All transfection experiments shown were repeated for three times separately and the standard deviation is within 5%.

Mixing ε-(LYH)K10 and ε-(RGDP)K10 did not result in noticeable transfection in Hela cells (Figure 23). Combination of all three species (DOTAP, ε-(LYH)K10 and ε-(RGDP)K10) produced variable transfection efficiency in dependence on different amount and ratio of peptides added. The amount of DOTAP used for transfection was 30 µL according to the recommended amount in the manual and kept constant throughout the whole experiments. The volume of peptides which was the same as the volume of DOTAP in control experiment was denoted as 1, and other amounts of peptides were denoted accordingly. First, the ratio between ε-(LYH)K10 and ε-(RGDP)K10 was modified to get better transfection. It was shown in Figure 23, 0.5H+0.5R+D [L:R 1:1 (µg:µg)] was more efficient than 0.7H+0.3R+D [H:R 2:1 (µg:µg)], so the ratio of H to R was subsequently fixed at 1:1 while the ratio of total volume of H+R to the volume of DOTAP was varied from 1:10 to 4:1 (µL:µL). The amount of cells transfected increased as the ratio of H+R to DOTAP increased except 2H+2R+D. The highest transfection efficiency was found at H+R+D and it was 11%.

For peptides ε-(LYH)K10 and ε-(RGDP)K10, the similar modification as which has been done in Hela cells was conducted in 293F cells. In Figure 24, mixing ε-(LYH)K10 and ε-(RGDP)K10 did not result in noticeable transfection. For mixtures of ε-(RGDP)K10 and ε-(LYH)K10 and DOTAP, when the ratio between ε-(RGDP)K10 and ε-(LYH)K10 was changed, the transfection efficiency was comparable among 0.5H+0.5R+D, 0.7H+0.3R+D and 0.8H+0.2R+D and they all mediated amazingly high transfection efficiency above 90%. Keeping the ratio of H to R at 1:1 while the ratio of total volume of H+R to the volume of DOTAP was varied from 1:10 to 4:1 (µL:µL), the

99

amount of cells transfected increased as the ratio of H+R to DOTAP increased except 2H+2R+D. The highest transfection efficiency was found at H+R+D and it was 94%.

Figure 25 shows the transfection efficiency in Mewo cells mediated by ε-(LYH)K10 and DOTAP, ε-(LYH)K10 and ε-(RGDP)K10 and their mixtures with DOTAP. The control transfection was also performed with DOTAP and the same modification as conducted on Hela cells has been done. The combination of ε-(LYH)K10 and ε-(RGDP)K10 together did not result in noticeable transfection. Mixtures of all three species (DOTAP, ε-(LYH)K10 and ε-(RGDP)K10) in different amounts while keeping the ratio H:R 1:1 produced transfection efficiency all around 10%. When the ratio of total volume of H+R to the volume of DOTAP was varied from 1:10 to 4:1 (µL:µL), the amount of cells transfected increased as the ratio of H+R to DOTAP increased except 2H+2R+D. The highest transfection efficiency was found at H+R+D and it was 12%.

The transfection efficiency in A549 cells mediated by ε-(LYH)K10 and DOTAP, ε-(LYH)K10 and ε-(RGDP)K10 and their mixtures with DOTAP is shown in Figure 26. The control transfection was also performed with DOTAP and the same modification as conducted in Hela cells has been applied. Mixing ε-(LYH)K10 and ε-(RGDP)K10 did not result in noticeable transfection. For mixtures of ε-(RGDP)K10 and ε-(LYH)K10 and DOTAP, when the ratio between ε-(RGDP)K10 and ε-(LYH)K10 was changed, the transfection efficiency increased as the ratio of H to R increased, and 0.8H+0.2R+D mediated the highest transfection efficiency 35%. Fixing the ratio of H to R at 1:1 while increasing the amount of H+R increased the amount of cells transfected from 1% at 0.01H+0.01R+D to 44% at 2H+2R+D.

The results in Figures 23-26 for the combination of the two peptides ε-(LYH)K10 and ε-(RGDP)K10 together with the positive control DOTAP, H+R+D, show that generally the combination of the peptide mixture H+R with DOTAP, results in increased transfection as compared with both the control D and the peptide mixture alone. However, this potentiating effect does not result in much significant increase in transfection, compared with the best combination H+D (see Figure 22 for the results of H+D, included in Figures 23-26). For most cases, the H+R+D combination is only slightly superior. The reason for this is probably the fact that R alone has insignificant transfection efficiency and its combination with D results in similar or decreased transfection compared with the control D alone (Figure 22). As for the possible origin of this low efficiency for the R peptide, see the discussion section below.

Figure 23. Transfection efficiency in Hela cells mediated by mixtures of ε-(LYH)K10 and positive control DOTAP, ε-(LYH)K10 and ε-(RGDP)K10 in different ratio or their mixtures with DOTAP.

In this figure, H represents ε-(LYH)K10, R represents ε-(RGDP)K10, "control" or "D" denotes DOTAP. Stock concentration of H or R is 5 mg/mL and of DOTAP is 1 mg/mL. The DOTAP concentration in positive control was 0.2 mg/mL. For H+R or H+R+D mixtures, the volume of peptides which was the same as the volume of DOTAP in the control experiment was denoted as 1, so other amounts of peptides were denoted accordingly by the numbers before the name. A logarithmic scale is used for Y axes (the absolute transfection for control is 0.7%). All transfection experiments shown were repeated for three times separately and the standard deviation is within 5%.
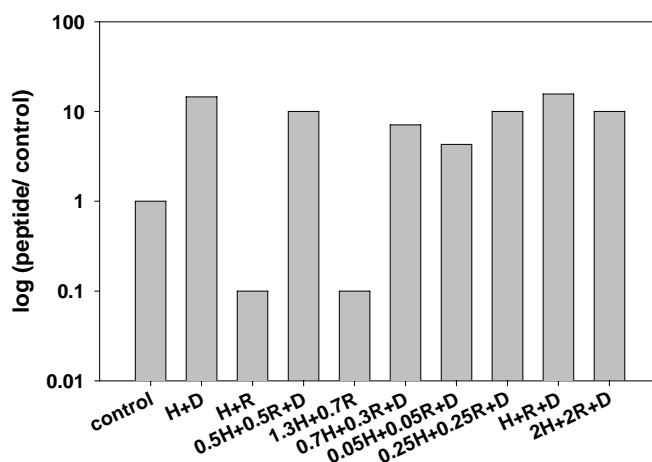
Figure 24. Transfection efficiency in 293F cells mediated by mixtures of ε-(LYH)K10 and positive control DOTAP, ε-(LYH)K10 and ε-(RGDP)K10 in different ratio or their mixtures with DOTAP.

In this figure, H represents ε-(LYH)K10, R represents ε-(RGDP)K10, "control" or "D" denotes DOTAP. Stock concentration of H or R is 5 mg/mL and of DOTAP is 1 mg/mL. The DOTAP concentration in positive control was 0.2 mg/mL. For H+R or H+R+D mixtures, the volume of peptides which was the same as the volume of DOTAP in the control experiment was denoted as 1, so other amounts of peptides were denoted accordingly by the numbers before the name. A logarithmic scale is used for Y axes (the absolute transfection for control is 22%). All transfection experiments shown were repeated for three times separately and the standard deviation is within 5%.
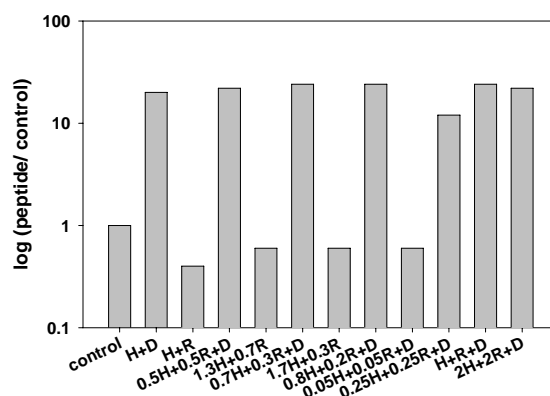
Figure 25. Transfection efficiency in Mewo cells mediated by mixtures of ε-(LYH)K10 and positive control DOTAP, ε-(LYH)K10 and ε-(RGDP)K10 in different ratio or their mixtures with DOTAP.

In this figure, H represents ε-(LYH)K10, R represents ε-(RGDP)K10, "control" or "D" denotes DOTAP. Stock concentration of H or R is 5 mg/mL and of DOTAP is 1 mg/mL. The DOTAP concentration in positive control was 0.2 mg/mL. For H+R or H+R+D mixtures, the volume of peptides which was the same as the volume of DOTAP in the control experiment was denoted as 1, so other amounts of peptides were denoted accordingly by the numbers before the name. A logarithmic scale is used for Y axes (the absolute transfection for control is 0.5%). All transfection experiments shown were repeated for three times separately and the standard deviation is within 5%.
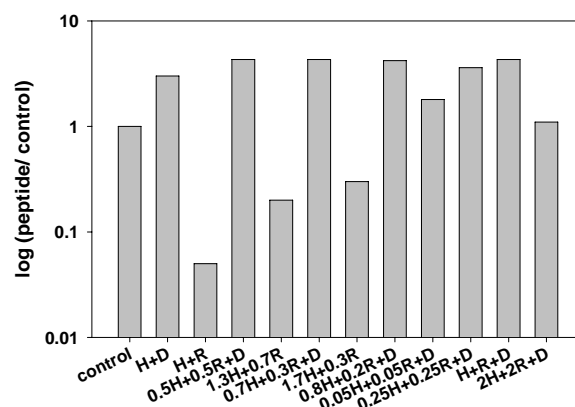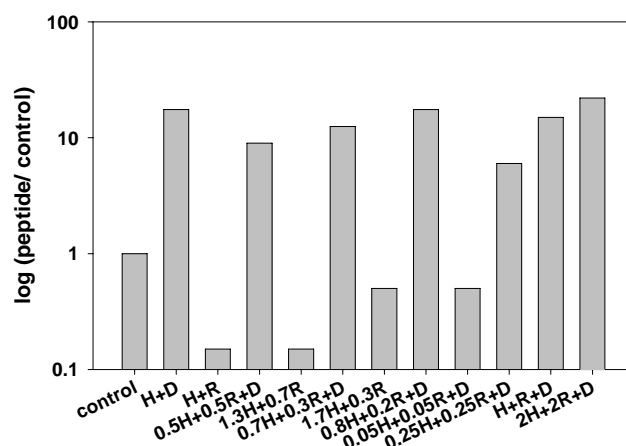
Figure 26. Transfection efficiency in A549 cells mediated by mixtures of ε-(LYH)K10 and positive control DOTAP, ε-(LYH)K10 and ε-(RGDP)K10 in different ratio or their mixtures with DOTAP.

In this figure, H represents ε-(LYH)K10, R represents ε-(RGDP)K10, "control" or "D" denotes DOTAP. Stock concentration of H or R is 5 mg/mL and of DOTAP is 1 mg/mL. The DOTAP concentration in positive control was 0.2 mg/mL. For H+R or H+R+D mixtures, the volume of peptides which was the same as the volume of DOTAP in the control experiment was denoted as 1, so other amounts of peptides were denoted accordingly by the numbers before the name. A logarithmic scale is used for Y axes (the absolute transfection for control is 2%). All transfection experiments shown were repeated for three times separately and the standard deviation is within 5%.

ε-(HK$_4$)K20 and ε-(LYHK$_4$)K20. The transfection efficiency in Hela cells mediated by ε-(HK$_4$)K20 and ε-(LYHK$_4$)K20 is shown in Figure 27. ε-(HK$_4$)K20 did not result in noticeable transfection. The transfection efficiency mediated by DOTAP is 1%, but addition of ε-(HK$_4$)K20 can significantly increase transfection efficiency to 11%. Another ε-peptide, ε-(LYHK$_4$)K20 can induce 6% transfection and 8% when combined with DOTAP.

Figure 28 shows the transfection efficiency in 293F cells mediated by ε-(HK$_4$)K20 and ε-(LYHK$_4$)K20. Commercial liposome transfection agent DOTAP can mediate 13% transfection efficiency. ε-(HK$_4$)K20 did not result in noticeable transfection but can induce 27% transfection when combined with DOTAP. ε-(LYHK$_4$)K20 can mediate

103

considerably high transfection efficiency which is 32%. However, when ε-(LYHK$_4$)K20

and DOTAP were used together, the transfection efficiency decreased to 22%.
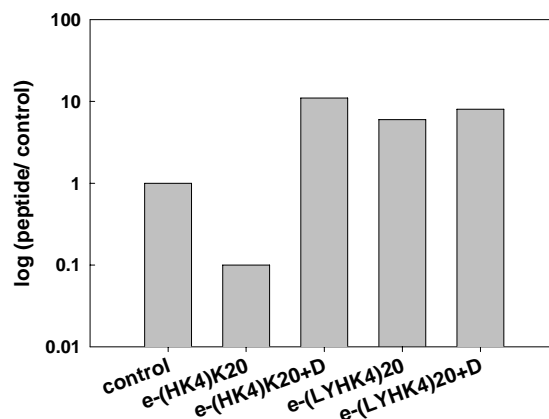
Figure 27. Transfection efficiency of the ε-(HK4)K20 and ε-(LYHK4)K20 in Hela cells.

The ε-peptide concentration was 2 mg/mL when ε-peptide only was applied, for mixtures of ε-peptide with DOTAP (indicated as "control" or "D" in the graphs), the peptide concentration was 1 mg/mL and the concentration of DOTAP was 0.2 mg/mL. A logarithmic scale is used for Y axes (the absolute transfection for control is 1%). All transfection experiments shown were repeated for three times separately and the standard deviation is within 5%.
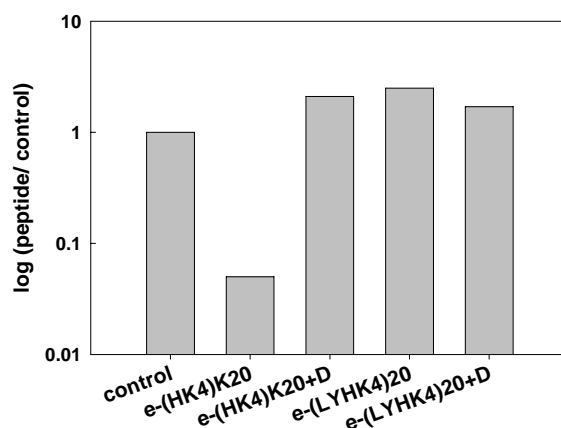
Figure 28. Transfection efficiency of the ε-(HK4)K20 and ε-(LYHK4)K20 in 293F cells.

The ε-peptide concentration was 2 mg/mL when ε-peptide only was applied, for mixtures of ε-peptide with DOTAP (indicated as "control" or "D" in the graphs), the peptide concentration was 1 mg/mL and the concentration of DOTAP was 0.2 mg/mL. A logarithmic scale is used for Y axes (the absolute transfection for control is 13%). All transfection experiments shown were repeated for three times separately and the standard deviation is within 5%.

3.3.2 Cell viability

The *in vitro* cytotoxicity of the ε-oligolysines and α-polylysines was measured for HeLa cells and results are displayed in Figure 29. All data shown are based on three separate experiments and the standard deviation is within 5%. The standard deviation is calculated using the same formula as shown on Page 93.

The cell viability has been measured for the same peptide concentrations as used in the *in vitro* transfection experiments. In literature, such data are sometimes presented for lower concentration (Putnam *et al.*, 2001; Jang *et al.*, 2006) of transfection agent or for conditions not precisely relevant to the transfection protocol (Vitiello *et al.*, 1996) for which control data on agents like polylysine and liposome (like DOTAP) display close to 100% cell viability. Under the present conditions, polylysine gives 40% and DOTAP 60% cell viability. The unsubstituted ε-lysines exhibit lower cytotoxicity compared with both the standard α-oligolysine and the liposome DOTAP. Cells incubated with ε-PLL and ε-K10 retain greater than 70% of their metabolic activity. The LYR substituted side chain displays 40% cell viability. As expected, increased peptide concentration leads to increased cytotoxicity. Adding 625 µg/ml of the LYR substituted ε-peptide to the control D (DOTAP) interestingly results in increased cell viability while in the case of adding unsubstituted ε-oligolysines, lower cell viability is observed, as expected on the basis of the increased total cation concentration. These results give confidence in this design based on the ε-lysine chain, demonstrating lower cytotoxicity as compared with the α-lysine chain. The decrease in cell viability for the LYR side chain substitution is not unexpected, given the introduction of the highly basic arginine.

Figure 29. Cytotoxic properties of some peptides.

Cytotoxicities were evaluated by MTT assay using Hela cells. Results are expressed as the percentage of dye reduction in cells treated with the transfection system compared with dye reduction in cells treated with HBS (used as negative control). The control is DOTAP and the concentration is 125μg/mL. For peptide only, the concentration is 1.25 mg/mL; for peptide+D (D=DOTAP), the concentration of peptide is 625 μg/mL and the concentration of DOTAP is 125 μg/mL; "2" indicates double amount of reagent added to the well. Cell viability measurements were done in three separate experiments and the standard deviation is within 5%.

Figure 30 showed the cytotoxicity of the substituted ε-polylysines, ε-(LYR)K10, ε-(LYR)K15, ε-(LYR)K20, ε-(LYH)K10, ε-(RGDP)K10, ε-(LYHK$_4$)K20 and ε-(HK$_4$)K20. The peptide concentration used was 1.25 mg/mL. For ε-(LYR)K10, ε-(LYR)K15 and ε-(LYR)K20, the cell viability decreased from 32% to 24% as the length of the lysine chain increased from 10 amino acids to 20 amino acids. The cytotoxicity of ε-(LYH)K10 or ε-(LYHK$_4$)K20 was similar as that of DOTAP which was around 60%. Cells incubated with ε-(RGDP)K10 or ε-(HK$_4$)K20 retained around 80% of their metabolic activity.
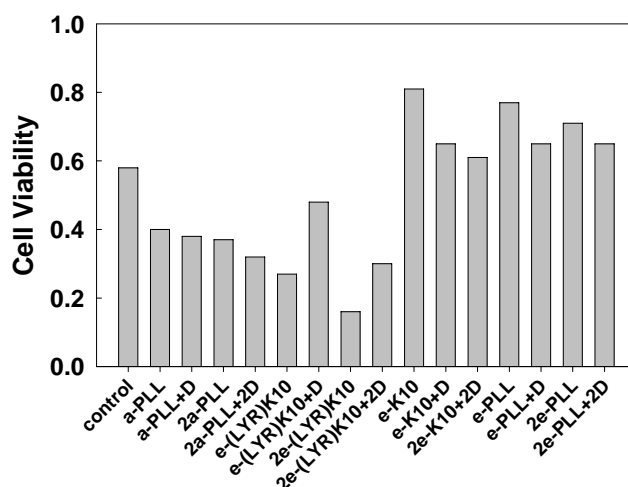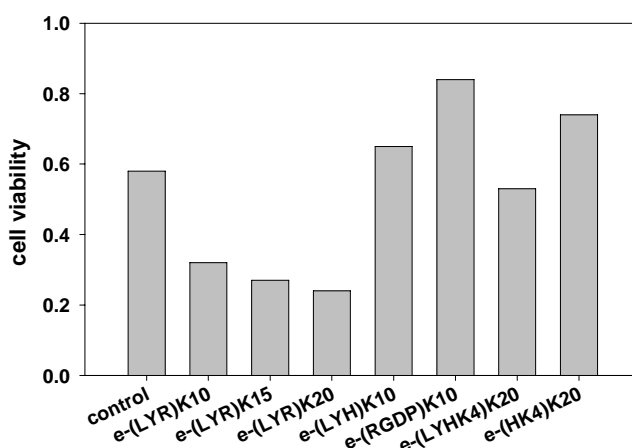
Figure 30. Cytotoxic properties of some substituted ε-peptides.

Cytotoxicities were evaluated by MTT assay using Hela cells. Results are expressed as the percentage of dye reduction in cells treated with the transfection system compared with dye reduction in cells treated with HBS (used as negative control). The control is DOTAP and the concentration is 250 µg/mL. For ε-peptides, the concentration is 1.25 mg/mL. Cell viability measurements were done in three separate experiments and the standard deviation is within 5%.

In some work (Putnam *et al.*, 2001; Jang *et al.*, 2006), very low concentration of transfection agent has been used to demonstrate high cell viability. Figure 31 shows the results of experiments carried out at low concentration of our oligolysines. For all samples, cytotoxicity increased with increasing polymer concentration but more than 70% of the cells were metabolically active at the highest polymer concentration (50 µg/mL). Addition of DOTAP increased the cell viability of α-PLL from 86% to 92%. DOTAP did not have noticeable effect in changing the cytotoxicity of ε-K10 with which more than 84% cells retained their metabolic activity. For ε-(LYR)K10, the cell viability decreased from 79% to 70% at the highest concentration shown.
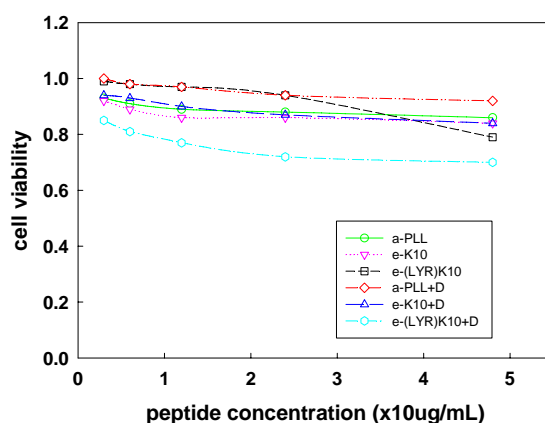
Figure 31. Cell viability of Hela cells at low oligolysine concentration.

Cell viability was evaluated by MTT assay using Hela cells. Results are expressed as the percentage of dye reduction in cells treated with the transfection system compared with dye reduction in cells treated with HBS (used as negative control). For peptide+D (D=DOTAP, the stock concentration is 1μg/μL), the volume ratio between DOTAP and peptide is 1:1. Cell viability measurements were done in three separate experiments and the standard deviation is within 5%.

3.3.3 Discussion

The substituted ε-(LYR)K10 show superior transfection compared with ordinary α-polylysine as well as linear ε-polylysines for both Hela and 293F cell lines. In one case (HeLa) they are considerably more effective than the liposome DOTAP. Enhanced delivery to the cells is also observed when the peptides are combined with DOTAP. However, in the case of the 293F cell line, the addition of ε-(LYR)K10 does not improve transfection for DOTAP. This result is in agreement with observations that low-molecular-weight polycations comparable to the length of our peptides generally demonstrate low potentiation when added to liposome (Gao and Huang, 1996). The results for the HeLa cell line are interesting because generally compared with other cell lines, transfection is low for liposomes and completely absent for standard α-peptides and the increase upon adding high molecular weight oligopeptides to liposome is moderate (Gao and Huang, 1996). This hints that the LYR side chain motif exhibits some cell

108

receptor specificity in the case of HeLa cells, an issue which motivates further future studies.

For both Hela and 293F cell lines, ε-(HK$_4$)K20, when combined with DOTAP, can mediate considerably high transfection efficiency compared with DOTAP. The transfection results are consistent with the small particle size obtained in Table 3 in which ε-(HK$_4$)K20 can form about 132 nm particles with plasmid DNA. As mentioned in many references, the size is suitable for fusion into the cells (Duguid *et al.*, 1998; Pouton and Seymour, 2001; Liu and Huang, 2002; Vijayanathan *et al.*, 2002; Jang *et al.*, 2006). ε-(LYHK$_4$)K20 forms particles bigger than 200 nm and this may explain why ε-(LYHK$_4$)K20 have lower transfection efficiency in Hela cells. However, for 293F cells, ε-(LYHK$_4$)K20 by itself induced very high transfection but decreased when combined with DOTAP. This may due to some special reason which needs to be further investigated.

Endosomal compartments are generally acidic in nature. Various methods have been developed to enhance the efficiency of liposomal payload delivery by exploiting this fact (Drummond *et al.*, 2000; Venugopalan *et al.*, 2002). These include incorporation of pH-sensitive components into liposomes. The selective destabilization of liposomes following acidification of the surrounding media, with resultant release of drug or DNA from the liposome, has been enhanced by inclusion of specific lipids, many based on phosphatidylethanolamine or modifications thereof (e.g. DOPE). The well-characterized lamellar to hexagonal phase transition that phosphatidylethanolamine undergoes at low pH, thus releasing the liposomal contents, is the most common mechanism employed to produce pH-triggered release. A number of pH-sensitive synthetic peptides have also

been designed in an attempt to develop molecules that can attach to, but do not perturb, the surface of the liposome at neutral pH, yet subsequently fuse adjacent bilayers at acidic pH. These include GALA, a 30 amino acid amphipathic peptide with a glutamic acid, alanine, leucine, alanine repeat unit (Drummond *et al.*, 2000; Turk *et al.*, 2002).

The established membrane fusion ability of histidine in weakly acidic conditions, such as the endosome, and the DNA compaction ability of lysine have been utilized to increase gene delivery efficiency (Chen *et al.*, 2000; Chen *et al.*, 2001; Chen *et al.*, 2002). Changing the histidine location and the ratio of histidine to lysine, a series of histidine/lysine (HK) peptides have been examined for their potential as gene delivery vehicles. Mixson and co-workers (Chen *et al.*, 2000; Chen *et al.*, 2001; Chen *et al.*, 2002) have designed a series of linear and branched HK peptides of varying lengths. The lysine in these co-polymer peptides can complex with and partially neutralize the negative charge of the plasmid DNA, while the histidine is believed to buffer and disrupt the endosomes. These co-polymer peptides contain a metabolizable peptide bond that, when combined with liposomes, can enhance transfection efficiency. They found that the inclusion of linear and branched co-polymer peptides (without conjugation) significantly increased the transfection efficiency over cationic liposomes alone (Chen *et al.*, 2000; Chen *et al.*, 2001; Chen *et al.*, 2002). Moreover, when used with liposomes, a 2:1 ratio of histidine to lysine was superior to a 1:1 ratio with respect to increases in transfection efficiency (Chen *et al.*, 2002).

Based on the idea that pH-sensitive peptides can enhance the transfection efficiency, ε-(LYH)K10 has been designed, 10 lysines connected by ε-peptide bonds with a group of leucine, tyrosine and histidine on every lysine. As seen clearly from the transfection

110

results (Figure 22), ε-(LYH)K10, when combined with DOTAP, can significantly increase the transfection efficiency in all of the four cell lines, Hela, 293F, Mewo and A549. These results are consistent with those observed by Mixson and co-workers (Chen *et al.*, 2000; Chen *et al.*, 2001; Chen *et al.*, 2002) and correspond very well with particle size data shown in Table 3 where ε-(LYH)K10 compacts plasmid DNA to 123 nm particles. This size falls into the range of 50~150 nm which is known suitable for transfection (Duguid *et al.*, 1998; Pouton and Seymour, 2001; Liu and Huang, 2002; Vijayanathan *et al.*, 2002; Jang *et al.*, 2006).

Previous studies (Kircheis *et al.*, 1997; Zanta *et al.*, 1997; Kren *et al.*, 1998) showed that additional cell targeting functions did not perturb endosome escape. The idea of using the integrin-mediated cell entry pathway for gene delivery comes from morphological and biochemical studies of viral infection. For example, serotype 1 and 5 adenoviruses sequentially bind to the fiber receptor (Bergelson *et al.*, 1997; Hong *et al.*, 1997) and to integrins (Wickham *et al.*, 1993) at the cell surface. In a multistep process involving integrins, viral particle rearrangement and coated pits, the virus becomes internalized. Previous work using targeted polylysine derivatives has shown that selectivity and efficiency depend upon the number of ligands and upon the N/P ratio (Erbacher *et al.*, 1995; Wadhwa *et al.*, 1997). More closely related work with a vector containing a RGD peptide coupled to an oligolysine showed epithelial cell lines to be transfected (Hart *et al.*, 1995). In this system, a minimum number of 5000 ligands per complex, an about 6:1 N/P ratio as well as extra endosomolytic agents such as chloroquine (Hart *et al.*, 1997; Harbottle *et al.*, 1998), polyethylenimine or inactivated adenovirus (Harbottle *et al.*, 1998) were required. Erbacher et al. (Erbacher *et al.*, 1999)

used PEI-CYGGRGDTP to mediate gene transfer and found that although epithelial (Hela) and fibroblast (MRC5) were already efficiently transfected with unmodified PEI-DNA complexes having a strongly positive surface charge via the "ionic" gene transfer mechanism (Behr *et al.*, 1989; Labat-Moleur *et al.*, 1996; Mislick and Baldeschwieler, 1996), grafting an RGD-containing peptide to PEI still improved transfection by two orders of magnitude. Also the transfection efficiency in Hela cells was higher than in MRC5 and this confirmed that MRC5 fibroblast-like normal human lung cells were not the easiest cells to transfect. (Boussif *et al.*, 1996; Erbacher *et al.*, 1999).

In order to achieve a similar goal with a nonviral system, we had planned to synthesize ε-(RGD)K10. However, during TFMSA cleavage in the process of solid phase peptide synthesis, the strong acidity caused aspartimide formation between the carboxyl group of aspartic acid in side chain and the α-amine group of the lysine residue in the backbone and there was little desired product observable (data not shown). Therefore, we added a proline residue which has no amide proton to form aspartimide. And this is why we obtained ε-(RGDP)K10.

For all of the four cell lines investigated, ε-(RGDP)K10 does not induce noticeable transfection and can only mediate considerable transfection efficiency when combined with DOTAP. This is different from what I had expected based on the results gained by other researchers. Kunath and coworkers (Kunath *et al.*, 2003) used fluorescence correlation spectroscopy to determine binding of the fluorescein-labeled $\alpha_v\beta_3$-specific peptide c(RGDfK) to Mewo and A549 cells. Their results correspond very well to immunofluorescence data from Nahde and coworkers where Mewo and A549 cells were stained with a monoclonal anti-$\alpha_v\beta_3$ integrin-specific antibody. From those results Kunath

and coworkers concluded that the combination of Mewo carcinoma cells and A549 lung adenocarcinoma cells seemed optimal as positive and negative control for RGD-mediated transfection.

One possible reason why our ε-(RGDP)K10 has low transfection efficiency in Mewo cells is that the prolines in the peptide side chain may play a negative role in the transfection process. This is consistent with Pierschbacher and Ruoslahti's results (Pierschbacher and Ruoslahti, 1987). They used a panel of peptides which had the structure Gly-Arg-Gly-Asp-Xaa-Pro-Cys in which each of the peptides had the Xaa position substituted with a different one of the 20 natural L-amino acids. They found that the peptides which have different residues in the position following the aspartic acid resulted in different binding affinity to fibronectin or vitronectin. Proline was the only substitution when placed in the position following the aspartic acid that rendered the resulting peptide inactive (Pierschbacher and Ruoslahti, 1987).

It is known that not all RGD-containing proteins mediate cell attachment, in fact, only a minority of the 2600 (per Swiss Plot database 9/15/95) sequenced proteins that contain the RGD sequence are likely to do so. This is because the RGD sequence may not always be available at the surface of the protein or may be presented in a context that is not compatible with integrin binding. Thus the surrounding sequences can silence the activity of RGD (Ruoslahti, 1996). Also, when looking at the particle size measured by dynamic light scattering in Table 3, ε-(RGDP)K10 formed about 225 nm particles with plasmid DNA that may be too big for fusion into cells. Cyclization of RGD peptide is known to increase receptor affinity and selectivity by providing conformational restraint (Ruoslahti,

1996) and it is more stable compared with linear RGD, so more and more interest has been put on cyclic-RGD (Ruoslahti, 1996; Juan *et al.*, 2006).

To combine the pH buffer effect of histidine and the property of binding receptor RGD together, I have used mixture of ε-(LYH)K10, ε-(RGDP)K10 and DOTAP to do transfection in all of our four cell lines. After concentration modification, the DOTAP-peptide complex can mediate up to 94% and 44% transfection for 293F cells and A549 cells while positive control DOTAP alone induces 22% and 2% transfection respectively. These results give us confidence in this design concept and enlighten the future work. For other two cell lines, Hela and Mewo, the mixture did not give noticeable enhancement in transfection efficiency. In order to explain this point, further studies need to be conducted in the future.

A standard MTT test was introduced to evaluate the cytotoxicity of α- and ε-peptides and the results was shown in Figure 29. The commercial transfection agent DOTAP was used as positive control and HBS was used as negative control. The cell viability of other samples was demonstrated as the percentage of the dye reduction in cells treated with the transfection system compared with dye reduction in cells treated with HBS. The linear ε-polylysines have cytotoxicity that is lower than comparable peptides such as α-polylysine and the liposome DOTAP. For the ε-polylysine substituted with the LYR side chain, cytotoxicity is, as expected higher, but still comparable to α-polylysine and in combination with DOTAP cytotoxicity is lower.

The cytotoxicity of different substituted ε-polylysines was shown in Figure 30. From ε-(LYR)K10 to ε-(LYR)K20, cytotoxicity increases as the length of peptide chain increases.

114

This is consistent with other researchers' work which showed the polycationic nature leads to the cytotoxicity of high molecular weight gene delivery vectors (Godbey and Mikos, 2001; Patil *et al.*, 2005). The other four substituted ε-polylysines, ε-(LYH)K10, ε-(RGDP)K10, ε-(HK$_4$)K20 and ε-(LYHK$_4$)K20 all showed cell viability comparable or higher than positive control DOTAP.

Figure 31 shows cell viability of Hela cells treated with different concentration of α- and ε-peptides or their complexes with DOTAP. Most of the samples showed higher cell viability above 90% in a concentration range of 1~50 µg/mL. Increasing the concentration of ε-(LYR)K10 from 24 µg/mL to 48 µg/mL induced decrease of cell viability from 94% to 79%. Among these samples, the complex of ε-(LYR)K10 and DOTAP displayed the highest cytotoxicity but still retained 70% cell viability even at 48 µg/mL. The results indicate that such design of ε-peptides can potentially improve cytotoxicity and has more favorable delivery properties.

Chapter 4. Conclusions and perspectives

Most of the polypeptide gene delivery systems present a heterogeneous, high-molecular-weight component. Such macromolecules, which are generally highly charged, have a propensity to elicit an immune response and are often cytotoxic. It has been suggested that biologically active regions of many proteins consist of residues that are only 10-20 amino acids in length (Gottschalk *et al.*, 1996). Thus, the use of high-molecular-weight polypeptides may not be necessary, because it has been shown that low-molecular-weight counterions with more than two positive charges are capable of inducing DNA condensation into compact structures (Gosule and Schellman, 1976; Chattoraj *et al.*, 1978; Wilson and Bloomfield, 1979; Widom and Baldwin, 1980; Widom and Baldwin, 1983; Bloomfield *et al.*, 1992).

Based on the background, a series of ε-polylysines with different chain length and side chains have been designed and characterized for their ability to condense DNA and thus been used as gene delivery vectors. My results generally validate the promises in designing chemically defined, medium-length, branched ε-lysines with pendent α-peptides as DNA delivery vectors. Although the unusual and microbially synthesized ε-PLL peptides have a safety record as food additives, they are yet to be exploited as building blocks in the design of biomolecules with unambiguous compositions. This chimeric branched design of using defined length of ε-oligolysines as flexible and hydrophobic backbone and α-peptides as pendent functional chains to improve on their versatility is novel. It should be emphasized that these branched peptides are fairly large peptides and can be appropriately called macromolecules. For example, ε-(LYR)K10 is

equivalent in size of an α-peptide of 63 amino acid residues. It contains 40 α- and ε-amino acid residues, 30 of which are α-amino acids as side chains and 10 as ε-Lys$_{10}$ backbone which contains 70 atoms, an equivalent in length of a 23-residue α-peptide backbone. The stepwise solid-phase synthesizing an all-α-peptide with 63 residues will require 63 repetitive coupling cycles. However, the solid-phase synthesis of ε-(LYR)K10 requires only 13 coupling cycles because their branched structure permits a "control polymerization" approach for elongating all α-amino-acid side chains simultaneously. Thus, the design bodes well in analog study for chemically defined peptides as delivery vectors which greatly reduces synthetic effort and manipulations (Huang *et al.*, 2008).

Generally, the linear ε-polylysines produce smaller particles than the corresponding α-PLL and they also exhibit better cell viability and better (albeit to a little extent) *in vitro* transfection. Furthermore, design with their α-amino groups having pendent groups of short α-peptides (such as LYR) demonstrated that this basic design can be improved for increased transfection. α-PLL or α-oligolysine peptide based vectors have been extensively used for DNA delivery, with interesting applications to receptor and cancer cell targeting delivery (Zauner *et al.*, 1998; Lochmann *et al.*, 2004) with some investigations showing promising *in vivo* transfection results in mouse model studies (Aoki *et al.*, 2001; Yu *et al.*, 2004). My results indicate that such α-oligolysine modified systems would potentially have more favorable delivery properties if they are instead based on ε-oligolysine peptides. It is clear our peptides in their present design have modest transfection capacity compared to the most promising polycationic systems in the literature. However, this work has demonstrated that this novel design using ε-

oligolysines can potentially improve cytotoxicity and delivery properties of existing vectors that presently are designed from α-oligolysine peptides. Therefore this study give confidence for the approach I have initiated and motivate further studies on improved design and with a wider range of cell lines to achieve cell targeted delivery.

In order to target the integrin receptors via the integrin selective binding tripeptide motif RGD, ε-(RGDP)K10 has been designed and synthesized in this study. *In vitro* transfection results show that ε-(RGDP)K10 alone does not induce noticeable transfection. However, when combined with ε-(LYH)K10 and DOTAP, ε-(RGDP)K10 can mediate up to 94% and 44% transfection for 293F and A549 cells compared with positive control DOTAP alone inducing 22% and 2% transfection respectively.

Recently, the RGD integrin targeting strategy has been used in conjuction with non-viral gene delivery systems targeting cells expressing integrin receptors (Scott *et al.*, 2001; Suh *et al.*, 2002; Kunath *et al.*, 2003; Kim *et al.*, 2005; Kim *et al.*, 2006). In the work by Scott et al., a RGDK$_{16}$ peptide was used. This contained only one RGD motif per vector and the oligolysine peptide in itself was not optimal due to its low delivery efficiency (Scott *et al.*, 2001). Kunath et al. and Kim and co-workers used RGD peptides attached to PEI and obtained good integrin targeting *in vitro* and also *in vivo* (Suh *et al.*, 2002; Kunath *et al.*, 2003; Kim *et al.*, 2005; Kim *et al.*, 2006). However, PEI has inherent cytotoxicity (Kircheis *et al.*, 2001) and the synthesis lacks specificity of RGD peptide attachment to PEI.

For those reasons, the recently developed novel flexible design in this study, allowing controlled synthesis of substituted ε-oligolysine vector ε-(RGDP)K10, serves as a promising starting point for integrin targeting delivery to tumour cells. Compared with

previous approaches of RGD integrin binding delivery, based on polylysine and PEI, the present design allows the synthesis of the ε-peptide with the incorporation of variable amount of the RGD motif per peptide and addition of pH sensitive amino acid such as histidine for optimized delivery in endosomal release. For example, a block copolymer containing both RGD and LYH (or other motifs of interest) side chains could be synthesized and investigated. In addition, linear RGD side chain could be changed to cyclic RGD since the latter one is proven to increase receptor affinity and selectivity by providing conformational restraint (Ruoslahti, 1996) and it is more stable compared with linear RGD (Ruoslahti, 1996; Juan *et al.*, 2006).

As an application of DNA condensation in nucleosome interactions, NCP aggregation has been studied under different cation concentrations and with HMGN2 or truncated form XN2. The results from NCP precipitation assay are in agreement with those of DLS. When divalent cation is used, Ca^{2+} is more efficient than Mg^{2+} to induce NCP aggregation. In the presence of monovalent salt KCl at two different concentrations (10 mM and 100 mM), the concentration of Mg^{2+} needed to aggregate NCP increases as KCl concentration increases and bigger particles are formed in 10 mM KCl solution. The effect of HMGN2 or XN2 on the NCP concentration caused by addition of Mg^{2+} or Spm^{4+} is rather complicated and further experiments are needed to establish effects of HMGN proteins on NCP and chromatin interactions. However, the approach DLS has shown great promise as a new experiment tool to study nucleosome interactions.

References

Nobel Prize: http://nobelprize.org/medicine/laureates/1962/index.html

What's a Genome:
http://www.genomenewsnetwork.org/resources/whats_a_genome/Chp1_1_1.shtml

Science Photo Library:
http://www.sciencephotogallery.co.uk/articles/DNA_50yearsArticle.php

Nature: http://www.sciencephotogallery.co.uk/articles/DNA_50yearsArticle.php

Biography of James Watson: http://www.cshl.org/public/SCIENCE/Watson.html

Biography of Francis Crick:
http://www.wellcome.ac.uk/en/genome/geneticsandsociety/hg13b001.html

Akiyama, S. K. and K. M. Yamada (1985). Synthetic peptides competitively inhibit both direct binding to fibroblasts and functional biological assays for the purified cell-binding domain of fibronectin. *J Biol Chem* **260**, 10402-10405.

Alberts, B., D. Bray, J. Lewis, M. Raff, K. Roberts and J. D. Watson (1994). Molecular biology of the cell. New York & London, Garland Publishing, Inc.

Alberts, B., A. Johnson, J. Lewis, M. Raff, K. Roberts and P. Walter (2002). DNA and chromosomes. In: Molecular Biology of the Cell, Garland Science, a member of the Taylor & Francis Group, New York. 191-234.

Alfonso, P. J., M. P. Crippa, J. J. Hayes and M. Bustin (1994). The footprint of chromosomal proteins HMG-14 and HMG-17 on chromatin subunits. *J Mol Biol* **236**, 189-198.

Ames, B. N. and D. T. Dubin (1960). The role of polyamines in the neutralization of bacteriophage deoxyribonucleic acid. *J Biol Chem* **235**, 769-775.

Anderson, W. F. (1972). Genetic therapy. In: Hamilton M, ed. The New Genetics and the Future of Man. Grand rapids: Eerdmans. 109-124.

Antonelli, M., J. Olate, C. C. Allende and J. E. Allende (1991). Polylysine activates membrane-bound adenylyl cyclase from Xenopus laevis oocytes through the Gs transducing protein. *Comp Biochem Physiol B* **99**, 827-832.

Aoki, Y., S. Hosaka, S. Kawa and K. Kiyosawa (2001). Potential tumor-targeting peptide vector of histidylated oligolysine conjugated to a tumor-homing RGD motif. *Cancer Gene Therapy* **8**, 783-787.

Arscott, P. G., A. Z. Li and V. A. Bloomfield (1990). Condensation of DNA by trivalent cations. 1. Effects of DNA length and topology on the size and shape of condensed particles. *Biopolymers* **30**, 619-630.

Arscott, P. G., C. Ma, J. A. Wenner and V. A. Bloomfield (1995). DNA condensation by cobalt hexaammine (III) in alcohol-water mixtures:dielectric constant and other solvent effects. *Biopolymers* **36**, 345-364.

Audouy, S., G. Molema, L. de Leij and D. Hoekstra (2000). Serum as a modulator of lipoplex-mediated gene transfection: dependence of amphiphile, cell type and complex stability. *J Gene Med* **2**, 465-476.

Behr, J. P., B. Demeneix, J. P. Loeffler and J. Perex-Mutul (1989). Efficient gene transfer into mammalian primary endocrine cells with lipopolyamine-coated DNA. *Proc Natl Acad Sci* **86**, 6982-6986.

Benns, J. M., A. Maheshwari, D. Y. Furgeson, R. I. Mahato and S. W. Kim (2001). Folate-PEG-folate-graft-polyethylenimine-based gene delivery. *J Drug Target* **9**, 123-139.

Bergelson, J. M., J. A. Cunningham, G. Droguett, E. A. Kurt-Jones, A. Krithivas, J. S. Hong, M. S. Horwitz, R. L. Crowell and R. W. Finberg (1997). Isolation of a common receptor for Coxsackie B viruses and adenoviruses 2 and 5. *Science* **275**, 1320-1323.

Berns, A. (2004). Good news for gene therapy. *N Engl J Med* **350**, 1679-1680.

Bertin, A., S. Mangenot, M. Renouard, D. Durand and F. Livolant (2007). Structure and phase diagram of nucleosome core particles aggregated by multivalent cations. *Biophys J* **93**, 3652-3663.

Birger, Y., Y. Ito, K. L. West, D. Landsman and M. Bustin (2001). HMGN4, a newly discovered nucleosome-binding protein encoded by an intronless gene. *DNA Cell Biol* **20**, 257-264.

Blaese, R. M., K. W. Culver, A. D. Miller, C. S. Carter, T. Fleisher, M. Clerici, G. Shearer, L. Chang, Y. Chiang, P. Tolstoshev, J. J. Greenblatt, S. A. Rosenberg, H. Klein, M. Berger, C. A. Mullen, W. J. Ramsey, L. Muul, R. A. Morgan and W. F. Anderson (1995). T lymphocyte-directed gene therapy for ADA-SCID: initial trial results after 4 years. *Science* **270**, 475-480.

Blessing, T., J. S. Remy and J. P. Behr (1998). Monomolecular collapse of plasmid DNA into stable virus-like particles. *Proc Natl Acad Sci* **95**, 1427-1431.

Bloomfield, V. A. (1991). Condensation of DNA by multivalent cations: considerations on mechanism. *Biopolymers* **31**, 1471-1481.

Bloomfield, V. A. (1996). DNA condensation. *Curr.Opin.Struct.Biol.* **6**, 334-341.

Bloomfield, V. A. (1997). DNA condensation by multivalent cations. *Biopolymers* **44**, 269-282.

Bloomfield, V. A., D. M. Crothers and I. J. Tinoco (1988). Nucleic Acids: Structures, Properties and Functions, University Science Press, Mill Valley, CA.

Bloomfield, V. A., S. He, A.-Z. Li and P. G. Arscott (1992). Light scattering studies of DNA condensation. In Laser Light Scattering in Biochemistry. The Royal Society of Chemistry, Cambridge, England.

Borchard, G. (2001). Chitosans for gene delivery. *Adv Drug Deliv Rev* **52**, 145-150.

Boussif, O., F. Lezoualc'h, M. A. Zanta, M. D. Mergny, D. Scherman, B. Demeneix and J. P. Behr (1995). A versatile vector for gene and oligonucleotide transfer into cells in culture and *in vivo*: Polyethyleneimine. *Proc Natl Acad Sci* **92**, 7297-7301.

Boussif, O., M. A. Zanta and J. P. Behr (1996). Optimized galenics improve in vitro gene transfer with cationic molecules up to 1000-fold. *Gene Ther* **3**, 1074-1080.

Buck, C. A. and A. F. Horwitz (1987). Cell surface receptors for extracellular matrix molecules. *Annu Rev Cell Biol* **3**, 179-205.

Budker, V., V. Gurevich, J. E. Hagstrom, F. Bortzov and J. A. Wolff (1996). pH-sensitive, cationic liposomes: a new synthetic virus-like vector. *Nat Biotechnol* **14**, 760-764.

Bustin, M. (1999). Regulation of DNA-dependent activities by the functional motifs of the high-mobility-group chromosomal proteins. *Mol Cell Biol* **19**, 5237-5246.

Bustin, M. (2001). Chromatin unfolding and activation by HMGN* chromosomal proteins. *Trends Biochem Sci* **26**, 431-437.

Bustin, M. (2001). Revised nomenclature for high mobility group (HMG) chromosomal proteins. *Trends Biochem Sci* **26**, 152-153.

Carmeliet, P. and R. K. Jain (2000). Angiogenesis in cancer and other diseases. *Nature* **407**, 249-257.

Cavazzana-Calvo, M., S. Hacein-Bey, G. de Saint Basile, F. Gross, E. Yvon, P. Nusbaum, F. Selz, C. Hue, S. Certain, J. L. Casanova, P. Bousso, F. L. Deist and A. Fischer (2000). Gene therapy of human severe combined immunodeficiency (SCID)-X1 disease. *Science* **288**, 669-672.

Chamberlain, J. S. (2002). Gene therapy of muscular dystrophy. *Hum Mol Genet* **11**, 2355-2362.

Chattoraj, D. K., L. C. Gosule and A. Schellman (1978). DNA condensation with polyamines. II. Electron microscopic studies. *J Mol Biol* **121**, 327-337.

Chen, Q. R., L. Zhang, P. W. Luther and A. J. Mixson (2002). Optimal transfection with the HK polymer depends on its degree of branching and the pH of endocytic vesicles. *Nucleic Acids Res* **30**, 1338-1345.

Chen, Q. R., L. Zhang, S. A. Stass and A. J. Mixson (2000). Co-polymer of histidine and lysine markedly enhances transfection efficiency of liposomes. *Gene Ther* **7**, 1698-1705.

Chen, Q. R., L. Zhang, S. A. Stass and A. J. Mixson (2001). Branched co-polymers of histidine and lysine are efficient carriers of plasmids. *Nucleic Acids Res* **29**, 1334-1340.

Cheresh, D. A. and R. C. Spiro (1987). Biosynthetic and functional properties of an Arg-Gly-Asp-directed receptor involved in human melanoma cell attachment to vitronectin, fibrinogen, and von Willebrand factor. *J Biol Chem* **262**, 17703-17711.

Choi, Y. H., F. Liu, J. S. Park and S. W. Kim (1998). Lactose-poly(ethylene glycol)-grafted poly-L-lysine as hepatoma cell-targeted gene carrier. *Bioconjug Chem* **9**, 708-718.

Clark, D. J. and T. Kimura (1990). Electrostatic mechanism of chromatin folding. *J Mol Biol* **211**, 883-896.

Cotten, M., F. Langle-Rouault, H. Kirlappos, E. Wagner, K. Mechtler, M. Zenke, H. Beug and M. L. Birnstiel (1990). Transferrin-polycation-mediated introduction of DNA into human leukemic cells: stimulation by agents that affect the survival of transfected DNA or modulate transferrin receptor levels. *Proc Natl Acad Sci* **87**, 4033-4037.

Cotten, M., E. Wagner and M. L. Birnstiel (1993). Receptor-mediated transport of DNA into eukaryotic cells. *Methods Enzymol* **217**, 618-644.

Crippa, M. P., P. J. Alfonso and M. Bustin (1992). Nucleosome core binding region of chromosomal protein HMG-17 acts as an independent functional domain. *J Mol Biol* **228**, 442-449.

Cristiano, R. J. and J. A. Roth (1995). Molecular conjugates: a targeted gene delivery vector for molecular medicine. *J Mol Med* **73**, 479-486.

Davey, C. A., D. F. Sargent, K. Luger, A. W. Maeder and T. J. Richmond (2002). Solvent mediated interactions in the structure of nucleosome core particle at 1.9 Å resolution. *J Mol Biol* **319**, 1097-1113.

de Frutos, M., E. Raspaud, A. Leforestier and F. Livolant (2001). Aggregation of nucleosomes by divalent cations. *Biophys J* **81**, 1127-1132.

de Kruijff, B., A. Rietveld, N. Telders and B. Vaandrager (1985). Molecular aspects of the bilayer stabilization induced by poly(L-lysines) of varying size in cardiolipin liposomes. *Biochim Biophys Acta* **820**, 295-304.

Ding, H.-F., M. Bustin and U. Hansen (1997). Alleviation of histone H1-mediated transcriptional repression and chromatin compaction by the acidic activation region in chromosomal protein HMG-14. *Mol Cell Biol* **17**, 5843-5855.

Dokka, S., D. Toledo, X. Shi, V. Castranova and Y. Rojanasakul (2000). Oxygen radical-mediated pulmonary toxicity induced by some cationic liposomes. *Pharm Res* **17**, 521-525.

Dowty, M. E. and J. A. Wolff (1994). Possible mechanisms of DNA uptake in skeletal muscle. In Gene Therapeutics: Methods and Applications of Direct Gene Transfer. Birkhäuser, Boston.

Drummond, D. C., M. Zignani and J. Leroux (2000). Current status of pH-sensitive liposomes in drug delivery. *Prog Lipid Res* **39**, 409-460.

Duguid, J. G., C. Li, M. Shi, M. J. Logan, H. Alila, A. Rolland, E. Tomlinson, J. T. Sparrow and L. C. Smith (1998). A physicochemical approach for predicting the effectiveness of peptide-based gene delivery systems for use in plasmid-based gene therapy. *Biophys J* **74**, 2802-2814.

Duzgunes, N. and P. L. Felgner (1993). Intracellular delivery of nucleic acids and transcription factors by cationic liposomes. *Methods Enzymol* **221**, 303-306.

Dyer, P. N., R. S. Edayathumangalam, C. L. White, Y. Bao, S. Chakravarthy, U. M. Muthurajan and K. Luger (2004). Reconstitution of nucleosome core particles from recombinant histones and DNA. *Methods Enzymol.* **375**, 23-44.

Elferink, J. G. (1985). Cytolytic effect of polylysine on rabbit polymorphonuclear leukocytes. *Inflammation* **9**, 321-331.

Elferink, J. G. (1991). Changes of plasma membrane permeability in neutrophils treated with polycations. *Inflammation* **15**, 103-115.

Erbacher, P., J. S. Remy and J. P. Behr (1999). Gene transfer with synthetic virus-like particles via the integrin-mediated endocytosis pathway. *Gene Ther* **6**, 138-145.

Erbacher, P., A. C. Roche, M. Monsigny and P. Midoux (1995). Glycosylated polylysine/DNA complexes: gene transfer efficiency in relation with the size and the sugar substitution level of glycosylated polylysines and with the plasmid size. *Bioconjug Chem* **6**, 401-410.

Evdokimov Iu, M., N. M. Akimenko, N. E. Glukhova, A. S. Tikhonenko and M. Varshavskii Ia (1973). Formation of the compact form of double-stranded DNA in solution in the presence of polyethylene glycol. *Mol Biol* **7**, 151-159.

Evdokimov Iu, M., T. L. Piatigorskaia, O. F. Polibtsv, N. M. Akimenko and D. Tsvankin (1976). DNA compact form. 8. X-ray diffraction study of DNA compact particles, formed in solutions containing polyethylene glycol. *Mol Biol (Mosk)* **10**, 1221-1230.

Fattal, E., J. Delattre, C. Dubernet and P. Couvreur (1999). Liposomes for delivery of nucleotides and oligonucleotides. *S.T.P. Pharma Sciences* **9**, 383-390.

Fattal, E., C. Dubernet and C. P. (2001). Liposome-based formulations for the delivery of oligonucleotides. *S.T.P. Pharma Sciences* **11**, 31-44.

Favre, D., N. Provost, V. Blouin, G. Blancho, Y. Cherel, A. Salvetti and P. Moullier (2001). Immediate and long-term safety of recombinant adeno-associated virus injection into the nonhuman primate muscle. *Mol Ther* **4**, 559-566.

Felgner, J. H., R. Kumar, C. N. Sridhar, C. J. Wheeler, Y. J. Tsai, R. Border, P. Ramsey, M. Martin and P. L. Felgner (1994). Enhanced gene delivery and mechanism studies with a novel series of cationic lipid formulations. *J Biol Chem* **269**, 2550-2561.

Felgner, P. L., T. R. Gadek, M. Holm, R. Roman, H. W. Chan, M. Wenz, J. P. Northrop, G. M. Ringold and M. Danielsen (1987). Lipofection: a highly efficient lipid mediated DNA transfection procedure. *Proc Natl Acad Sci* **84**, 7413-7417.

Filion, M. C. and N. C. Phillips (1997). Toxicity and immunomodulatory activity of liposomal vectors formulated with cationic lipids toward immune effector cells. *Biochim Biophys Acta* **1329**, 345-356.

Fletcher, T. M. and J. C. Hansen (1996). The nucleosomal array: structure/function relationships. *Crit Rev Eukaryot Gene Expr* **6**, 149-188.

Florea, B. I., C. Meaney, H. E. Junginger and G. Borchard (2002). Transfection efficiency and toxicity of polyethylenimine in differentiated Calu-3 and nondifferentiated COS-1 cell cultures. *AAPS PharmSci* **4**, E12.

Folkman, J. (1971). Tumor angiogenesis: therapeutic implications. *N Engl J Med* **285**, 1182-1186.

Folkman, J. and Y. Shing (1992). Angiogenesis. *J Biol Chem* **267**, 10931-10934.

Friedmann, T. and R. Roblin (1972). Gene therapy for human genetic disease? *Science* **175**, 949-955.

Gad, A. E., B. L. Silver and G. D. Eytan (1982). Polycation-induced fusion of negatively-charged vesicles. *Biochim Biophys Acta* **690**, 124-132.

Gao, X. and L. Huang (1996). Potentiation of cationic liposome-mediated gene delivery by polycations. *Biochemistry* **35**, 1027-1036.

Garcia-Ramirez, M. and J. A. Subirana (1994). Condensation of DNA by basic proteins does not depend on protein composition. *Biopolymers* **34**, 285-292.

Gatica, M., C. C. Allende, M. Antonelli and J. E. Allende (1987). Polylysine-containing peptides, including the carboxyl-terminal segment of the human c-Ki-ras 2 protein, affect the activity of some key membrane enzymes. *Proc Natl Acad Sci* **84**, 324-328.

Ghirlando, R., E. J. Wachtel, T. Arad and A. Minsky (1992). DNA packaging induced by micellar aggregates: a novel in vitro DNA condensation system. *Biochemistry* **31**, 7110-7119.

Godbey, W. T. and A. G. Mikos (2001). Recent progress in gene delivery using non-viral transfer complexes. *J Control Release* **72**, 115-125.

Gosule, L. C. and J. A. Schellman (1976). Compact form of DNA induced by spermidine. *Nature* **259**, 333-335.

Gosule, L. C. and J. A. Schellman (1978). DNA condensation with polyamines I. Spectroscopic studies. *J Mol Biol* **121**, 311-326.

Gottschalk, S., R. J. Cristiano, L. C. Smith and S. L. Woo (1994). Folate receptor mediated DNA delivery into tumor cells: potosomal and persistent expression of a foreign gene driven by disruption results in enhanced gene expression. *Gene Ther* **1**, 185-191.

Gottschalk, S., J. T. Sparrow, J. Hauer, M. P. Mims, F. E. Leland, S. L. Woo and L. C. Smith (1996). A novel DNA-peptide complex for efficient gene transfer and expression in mammalian cells. *Gene Ther* **3**, 448-457.

Griffioen, A. W. and G. Molema (2000). Angiogenesis: potentials for pharmacologic intervention in the treatment of cancer, cardiovascular diseases, and chronic inflammation. *Pharmacol Rev* **52**, 237-268.

Grosberg, A. and A. V. Zhestkov (1986). On the compact form of linear duplex DNA: globular states of the uniform elastic (persistent) macromolecule. *J Biomol Struct Dyn* **3**, 859-872.

Haensler, J. and F. C. Szoka, Jr. 2007 (1993). Polyamidoamine cascade polymers mediate efficient transfection of cells in culture. *Bioconjugate Chem* **4**, 372-379.

Hanahan, D. (1997). Signaling vascular morphogenesis and maintenance. *Science* **277**, 48-50.

Hansen, J. C. (2002). Conformational dynamics of the chromatin fiber in solution: determinants, mechanisms, and functions. *Annu.Rev.Biophys.Biomol.Struct.* **31**, 361-392.

Harbottle, R. P., R. G. Cooper, S. L. Hart, A. Ladhoff, T. McKay, A. M. Knight, E. Wagner, A. D. Miller and C. Coutelle (1998). An RGD-oligolysine peptide: a prototype construct for integrin-mediated gene delivery. *Hum Gene Ther* **9**, 1037-1047.

Hart, S. L., L. Collins, K. Gustafsson and J. W. Fabre (1997). Integrin-mediated transfection with peptides containing arginine-glycine-aspartic acid domains. *Gene Ther* **4**, 1225-1230.

Hart, S. L., R. P. Harbottle, R. Cooper, A. Miller, R. Williamson and C. Coutelle (1995). Gene delivery and expression mediated by an integrin-binding peptide. *Gene Ther* **2**, 552-554.

Haynes, M., R. A. Garrett and W. B. Gratzer (1970). Structure of nucleic acid-poly base complexes. *Biochemistry* **9**, 4410-4416.

Hermonat, P. L. and N. Muzyczka (1984). Use of adeno-associated virus as a mammalian DNA cloning vector: transduction of neomycin resistance into mammalian tissue culture cells. *Proc Natl Acad Sci* **81**, 6466-6470.

Hirschman, S., M. Leng and G. Felsenfield (1967). Interaction of spermine and DNA. *Biopolymers* **5**, 227-233.

Hock, R., F. Wilde, U. Scheer and M. Bustin (1998). Dynamic relocation of chromosomal protein HMG-17 in the nucleus is dependent on transcriptional activity. *Embo J* **17**, 6992-7001.

Hofland, H. E., L. Shephard and S. M. Sullivan (1996). Formation of stable cationic lipid/DNA complexes for gene transfer. *Proc Natl Acad Sci* **93**, 7305-7309.

Hong, S. S., L. Karayan, J. Tournier, D. T. Curiel and P. A. Boulanger (1997). Adenovirus type 5 fiber knob binds to MHC class I alpha2 domain at the surface of human epithelial and B lymphoblastoid cells. *Embo J* **16**, 2294-2306.

Horn, P. J. and C. L. Peterson (2002). Chromatin higher order folding: Wrapping up transcription. *Science* **297**, 1824-1827.

Hsiang, M. W. and R. D. Cole (1977). Structure of histone H1-DNA complex: effect of histone H1 on DNA condensation. *Proc Natl Acad Sci* **74**, 4852-4856.

Huang, D., N. Korolev, K. D. Eom, J. P. Tam and L. Nordenskiod (2008). Design and Biophysical Characterization of Novel Polycationic ε-Peptides for DNA Compaction and Delivery *Biomacromolecules* **9**, 321-330.

Huang, L., A. L. Klibanov, A. Mori and X. Gao (1993). Targeted delivery of drugs and DNA with liposomes. Proceedings of conference on "Liposomes as biomimetics", Rome, Italy, June 23-26. *J Liposome Res* **3**, 505-515.

Hynes, R. O. (1992). Integrins: versatility, modulation, and signaling in cell adhesion. *Cell* **69**, 11-25.

Jang, J. S., S. Y. Kim, S. B. Lee, K. O. Kim, J. S. Han and Y. M. Lee (2006). Poly(ethylene glycol)/poly(ε-caprolactone) diblock copolymeric nanoparticles for non-viral gene delivery: The role of charge group and molecular weight in particle formation, cytotoxicity and transfection. *J Contr Release* **113**, 173-182.

Johns, E. W. (1982). The HMG Chromosomal Proteins. Academic Press, London.

Joyner, A., G. Keller, R. A. Phillips and A. Bernstein (1983). Retrovirus transfer of a bacterial gene into mouse haematopoietic progenitor cells. *Nature* **305**, 556-558.

Juan, H.-F., I.-H. Wang, T.-C. Huang, J.-J. Li, S.-T. Chen and H.-C. Huang (2006). Proteomics analysis of a novel compound: Cyclic RGD in breast carcinoma cell line MCF-7. *Proteomics* **6**, 2991-3000.

Kabanov, A. V. and V. A. Kabanov (1995). DNA complexes with polycations for the delivery of genetic material into cells. *Bioconjug Chem* **6**, 7-20.

Kamiya, H., H. Tsuchiya, J. Yamazaki and H. Harashima (2001). Intracellular trafficking and transgene expression of viral and non-viral gene vectors. *Adv Drug Deliv Rev* **52**, 153-164.

Kang, S. H., E. L. Zirbes and R. Kole (1999). Delivery of antisense oligonucleotides and plasmid DNA with various carrier agents. *Antisense Nucleic Acid Drug Dev* **9**, 497-505.

Kato, T., S. Lee, S. Ono, Y. Agawa, H. Aoyagi, M. Ohno and N. Nishino (1991). Conformational studies of amphipathic alpha-helical peptides containing an amino acid with a long alkyl chain and their anchoring to lipid bilayer liposomes. *Biochim Biophys Acta* **1063**, 191-196.

Kay, M. A., J. C. Glorioso and L. Naldini (2001). Viral vectors for gene therapy: the art of turning infectious agents into vehicles of therapeutics. *Nat Med* **7**, 33-40.

Kim, J. S., A. Maruyama, T. Akaike and S. W. Kim (1998). Terplex DNA delivery system as a gene carrier. *Pharm Res* **15**, 116-121.

Kim, W. J., J. W. Yockman, J. H. Jeong, L. V. Christensen, M. Lee, Y.-H. Kim and S. W. Kim (2006). Anti-angiogenic inhibition of tumor growth by systemic delivery of PEI-g-PEG-RGD/pCMV-sFlt-1 complexes in tumor-bearing mice. *J.Contr.Release* **114**, 381-388.

Kim, W. J., J. W. Yockman, M. Lee, J. H. Jeong, Y.-H. Kim and S. W. Kim (2005). Soluble Flt-1 gene delivery using PEI-g-PEG-RGD conjugate for anti-angiogenesis. *J.Contr.Release* **106**, 224-234.

Kircheis, R., A. Kichler, G. Wallner, M. Kursa, M. Ogris, T. Felzmann, M. Buchberger and E. Wagner (1997). Coupling of cell-binding ligands to polyethylenimine for targeted gene delivery. *Gene Ther* **4**, 409-418.

Kircheis, R., L. Wightman and R. Wagner (2001). Design and gene delivery activity of modified polyethylenimines. *Adv.Drug Delivery Revs.* **53**, 341-358.

Kleinschmidt, J. H. and D. Marsh (1997). Spin-label electron spin resonance studies on the interactions of lysine peptides with phospholipid membranes. *Biophys J* **73**, 2546-2555.

Klimenko, S. M., T. I. Tikchonenko and V. M. Andreev (1967). Packing of DNA in the head of bacteriophage T2. *J Mol Biol* **23**, 523-533.

Koping-Hoggard, M., I. Tubulekas, H. Guan, K. Edwards, M. Nilsson, K. M. Varum and P. Artursson (2001). Chitosan as a nonviral gene delivery system. Structure-property relationships and characteristics compared with polyethylenimine in vitro and after lung administration in vivo. *Gene Ther* **8**, 1108-1121.

Korolev, N., A. P. Lyubartsev and L. Nordenskiod (2006). Computer modeling demonstrates that electrostatic attraction of nucleosomal DNA is mediated by histone tails. *Biophys J* **90**, 4305-4316.

Kren, B. T., P. Bandyopadhyay and C. J. Steer (1998). In vivo site-directed mutagenesis of the factor IX gene by chimeric RNA/DNA oligonucleotides. *Nat Med* **4**, 285-290.

Kunath, K., T. Merdan, O. Hegener, H. Haberlein and T. Kissel (2003). Integrin targeting using RGD-PEI conjugates for in vitro gene transfer. *J Gene Med* **5**, 588-599.

Labat-Moleur, F., A. M. Steffan, C. Brisson, H. Perron, O. Feugeas, P. Furstenberger, F. Oberling, E. Brambilla and J. P. Behr (1996). An electron microscopy study into the mechanism of gene transfer with lipopolyamines. *Gene Ther* **3**, 1010-1017.

Laemmli, U. K. (1975). Characterization of DNA condensates induced by poly(ethylene oxide) and polylysine. *Proc Natl Acad Sci* **72**, 4288-4292.

Lappalainen, K., I. Jaaskelainen, K. Syrjanen, A. Urtti and S. Syrjanen (1994). Comparison of cell proliferation and toxicity assays using two cationic liposomes. *Pharm Res* **11**, 1127-1131.

Lasic, D. D. (1997). Liposomes in Gene Delivery, CRC Press, Boca Raton, FL.

Ledley, F. D. (1994). Non-viral gene therapy. *Curr Opin Biotechnol* **5**, 626-636.

Ledley, F. D. (1995). Nonviral gene therapy: the promise of genes as pharmaceutical products. *Hum Gene Ther* **6**, 1129-1144.

Legendre, J. Y. and F. C. Szoka, Jr. (1992). Delivery of plasmid DNA into mammalian cell lines using pH-sensitive liposomes: comparison with cationic liposomes. *Pharm Res* **9**, 1235-1242.

LeHoux, J. G. and F. Grondin (1993). Some effects of chitosan on liver function in the rat. *Endocrinology* **132**, 1078-1084.

Lemkine, G. F. and B. A. Demeneix (2001). Polyethylenimines for in vivo gene delivery. *Curr Opin Mol Ther* **3**, 178-182.

Lerman, L. S. (1971). A transition to a compact form of DNA in polymer solutions. *Proc Natl Acad Sci* **68**, 1886-1890.

Lien, Y. H. and L. W. Lai (2002). Gene therapy for renal disorders: what are the benefits for the elderly? *Drugs Aging* **19**, 553-560.

Lim, J. H., M. Bustin, V. V. Ogryzko and Y. V. Postnikov (2002). Metastable macromolecular complexes containing high mobility group nucleosome-binding chromosomal proteins in HeLa nuclei. *J Biol Chem* **277**, 20774-20782.

Liu, F. and L. Huang (2002). Development of non-viral vectors for systemic gene delivery. *J Contr Release* **78**, 259-266.

Liu, F., H. Qi, L. Huang and D. Liu (1997). Factors controlling the efficiency of cationic lipid-mediated transfection in vivo via intravenous administration. *Gene Ther* **4**, 517-523.

Lochmann, D., E. Jauk and A. Zimmer (2004). Drug delivery of oligonucleotides by peptides. *Eur J Pharm Biopharm* **58**, 237-251.

Logan, D., R. Abu-Ghazaleh, W. Blakemore, S. Curry, T. Jackson, A. King, S. Lea, R. Lewis, J. Newman, N. Parry and et al. (1993). Structure of a major immunogenic site on foot-and-mouth disease virus. *Nature* **362**, 566-568.

Lollo, C. P., M. G. Banaszczyk and H. C. Chiou (2000). Obstacles and advances in non-viral gene delivery. *Curr Opin Mol Ther* **2**, 136-142.

Lollo, C. P., M. G. Banaszczyk, P. M. Mullen, C. C. Coffin, D. Wu, A. T. Carlo, D. L. Bassett, E. K. Gouveia and D. J. Carlo (2002). Poly-L-lysine-based gene delivery systems. Synthesis, purification, and application. *Methods Mol Med* **69**, 1-13.

Luger, K. and J. C. Hansen (2005). Nucleosome and chromatin fiber dynamics. *Curr Opin Struct Biol* **15**, 188-196.

Luger, K., A. W. Mader, R. K. Richmond, D. F. Sargent and T. J. Richmond (1997). Crystal structure of the nucleosome core particle at 2.8 Å resolution. *Nature* **389**, 251-260.

Luger, K. and T. J. Richmond (1998). The histone tails of the nucleosome. *Curr Opin Genet Dev* **8**, 140-146.

Luo, D. and W. M. Saltzman (2000). Synthetic DNA delivery systems. *Nat Biotechn* **18**, 33-37.

Ma, C. and V. A. Bloomfield (1994). Condensation of supercoiled DNA induced by $MnCl_2$. *Biophys J* **67**, 1678-1681.

Manning, G. S. (1978). The molecular theory of polyelectrolyte solutions with application of the electrostatic properties of polynucleotides. *Q Rev Biophys* **11**, 179-246.

Manning, G. S. (1996). The critical onset of counterion condensation: a survey of its experimental and theoretical basis. *Ber.Bunsengen.Phys.Chem.* **100**, 909-922.

Martin, K. R., R. L. Klein and H. A. Quigley (2002). Gene delivery to the eye using adeno-associated viral vectors. *Methods* **28**, 267-275.

Martin, M. E. and K. G. Rice (2007). Peptide-guided gene delivery. *AAPS J.* **9**, Article 3.

Marx, K. A. and G. C. Ruben (1983). Evidence for hydrated spermidine-calf thymus DNA toruses organized by circumferential DNA wrapping. *Nucleic Acids Res* **11**, 1839-1854.

Matsuzawa, Y., K. Minagawa, K. Yoshikawa, M. Matsumoto and M. Doi (1991). Conformational dynamics of DNA affected by intercalation and minor groove binding: direct observation of large DNA. *Nucleic Acids Symp Ser*, 131-132.

Matsuzawa, Y. and K. Yoshikawa (1993). Controlling the conformation of large DNA molecule in aqueous solution. *Nucleic Acids Symp Ser*, 147-148.

Matulis, D., I. Rouzina and V. A. Bloomfield (2000). Thermodynamics of DNA binding and condensation: isothermal titration calorimetry and electrostatic mechanism. *J Mol Biol* **296**, 1053-1063.

Matulis, D., I. Rouzina and V. A. Bloomfield (2002). Thermodynamics of cationic lipid to DNA and DNA condensation: roles of electrostatics and hydrophobicity. *J Amer Chem Soc* **124**, 7331-7342.

Mel'nikov, S. M., V. G. Sergeyev and K. Yoshikawa (1995). Discrete coil-globule transition of large DNA induced by cationic surfactant. *J Amer Chem Soc* **117**, 2401-2408.

Merdan, T., J. Kopecek and T. Kissel (2002). Prospects for cationic polymers in gene and oligonucleotide therapy against cancer. *Adv Drug Deliv Rev* **54**, 715-758.

Midoux, P., C. Mendes, A. Legrand, J. Raimond, R. Mayer, M. Monsigny and A. C. Roche (1993). Specific gene transfer mediated by lactosylated poly-L-lysine into hepatoma cells. *Nucleic Acids Res* **21**, 871-878.

Midoux, P. and M. Monsigny (1999). Efficient gene transfer by histidylated polylysine/pDNA complexes. *Bioconjugate Chem* **10**, 406-411.

Miller, A. D., D. J. Jolly, T. Friedmann and I. M. Verma (1983). A transmissible retrovirus expressing human hypoxanthine phosphoribosyltransferase (HPRT): gene transfer into cells obtained from humans deficient in HPRT. *Proc Natl Acad Sci* **80**, 4709-4713.

Mislick, K. A. and J. D. Baldeschwieler (1996). Evidence for the role of proteoglycans in cation-mediated gene transfer. *Proc Natl Acad Sci* **93**, 12349-12354.

Monsigny, M., A. C. Roche, P. Midoux and R. Mayer (1994). Glycoconjugates as carriers for specific delivery of therapeutic drugs and genes. *Adv Drug Delivery Rev* **14**, 1-24.

Montigny, W. J., C. R. Houchens, S. Illenye, J. Gilbert, E. Coonrod, Y. C. Chang and N. H. Heintz (2001). Condensation by DNA looping facilitates transfer of large DNA molecules into mammalian cells. *Nucleic Acids Res* **29**, 1982-1988.

Mumper, R. J. (1999). Polymeric Gene Delivery Systems for In-Vivo Gene Therapy", Advanced Gene Delivery: From Concepts to Pharmaceutical Products, AP Rolland (Ed.), Harwood Academic Publishers, Amsterdam, The Netherlands. 143-173.

Murayama, H. and K. Yoshikawa (1999). Thermodynamics of the collapsing phase transition in a single duplex DNA molecule. *J Phys Chem B* **103**, 10517-10523.

Nayvelt, I., T. Thomas and T. J. Thomas (2007). Mechanistic differences in DNA nanoparticle formation in the presence of oligolysines and poly-L-lysine. *Biomacromolecules* **8**, 477-484.

Olins, D. E., A. L. Olins and P. H. Von Hippel (1967). Model nucleoprotein complexes: studies on the interaction of cationic homopolypeptides with DNA. *J Mol Biol* **24**, 157-176.

Patel, M. M. and T. J. Anchodoquy (2005). Contribution of hydrophobicity to thermodynamics of ligand-DNA binding and DNA collapse. *Biophys J* **88**, 2089-2103.

Patil, S. D., D. G. Rhodes and D. J. Burgess (2004). Anionic liposomal delivery system for DNA transfection. *AAPS J* **6**, e29.

Patil, S. D., D. G. Rhodes and D. J. Burgess (2005). DNA-based therapeutics and DNA delivery systems: A comprehensive review. *AAPS J* **7**, E61-E77.

Pedroso de Lima, M. C., S. Simoes, P. Pires, H. Faneca and N. Duzgunes (2001). Cationic lipid-DNA complexes in gene delivery:from biophysics to biological applications. *Adv Drug Deliv Rev* **47**, 277-294.

Phair, R. D. and T. Misteli (2000). High mobility of proteins in the mammalian cell nucleus. *Nature* **404**, 604-609.

Pichon, C., C. Goncalves and P. Midoux (2001). Histidine-rich peptides and polymers for nucleic acids delivery. *Adv Drug Delivery Revs* **53**, 75-94.

Pichon, C., M. B. Roufai, M. Monsigny and P. Midoux (2000). Histidylated oligolysines increase the transmembrane passage and the biological activity of antisense oligonucleotides. *Nucleic Acids Res* **28**, 504-512.

Pierschbacher, M. D. and E. Ruoslahti (1984). Cell attachment activity of fibronectin can be duplicated by small synthetic fragments of the molecule. *Nature* **309**, 30-33.

Pierschbacher, M. D. and E. Ruoslahti (1984). Variants of the cell recognition site of fibronectin that retain attachment-promoting activity. *Proc Natl Acad Sci* **81**, 5985-5988.

Pierschbacher, M. D. and E. Ruoslahti (1987). Influence of stereochemistry of the sequence Arg-Gly-Asp-Xaa on binding specificity in cell adhesion. *J Biol Chem* **262**, 17294-17298.

Plank, C., B. Oberhauser, K. Mechtler, C. Koch and E. Wagner (1994). The influence of endosome-disruptive peptides on gene transfer using synthetic virus-like gene transfer systems. *J Biol Chem* **269**, 12918-12924.

Plank, C., K. Zatloukal, M. Cotten, K. Mechtler and E. Wagner (1992). Gene transfer into hepatocytes using asialoglycoprotein receptor mediated endocytosis of DNA complexed with an artificial tetra-antennary galactose ligand. *Bioconjug Chem* **3**, 533-539.

Plautz, G. E., Z. Y. Yang, B. Y. Wu, X. Gao, L. Huang and G. J. Nabel (1992). Immunotherapy of malignancy by in vivo gene transfer into tumors. *Hum Gene Ther* **3**, 399-410.

Plum, G. E. and V. A. Bloomfield (1988). Equilibrium dialysis study of binding of hexaamine Cobalt(III) to DNA. *Biopolymers* **27**, 1045-1051.

Post, C. B. and B. H. Zimm (1982). Theory of DNA condensation - collapse versus aggregation. *Biopolymers* **21**, 2123-2137.

Postnikov, Y. V., J. E. Herrera, R. Hock, U. Scheer and M. Bustin (1997). Clusters of nucleosomes containing chromosomal protein HMG-17 in chromatin. *J Mol Biol* **274**, 454-465.

Postnikov, Y. V., L. Trieschmann, A. Rickers and M. Bustin (1995). Homodimers of chromosomal proteins HMG-14 and HMG-17 in nucleosome cores. *J Mol Biol* **252**, 423-432.

Pouton, C. W. and L. W. Seymour (2001). Key issues in non-viral gene delivery. *Adv Drug Delivery Revs* **46**, 187-203.

Privalov, P. L., A. I. Dragan, C. Crane-Robinson, K. J. Breslauer, D. P. Remeta and C. A. S. A. Minetti (2007). What drives proteins into the major or minor grooves of DNA? *J Mol Biol* **365**, 1-9.

Putnam, D., C. A. Gentry, D. W. Pack and R. Langer (2001). Polymer-based gene delivery with low cytotoxicity by a unique balance of side-chain termini. *Proc Natl Acad Sci* **98**, 1200-1205.

Remy, J.-S., B. Abdallah, M. A. Zanta, O. Boussif, J. P. Behr and B. Demeneix (1998). Gene transfer with lipospermines and polyethylenimines. *Adv Drug Delivery Revs* **30**, 85-95.

Remy, J.-S., D. Goula, A.-M. Steffan, M. A. Zanta, O. Bousiff, J.-P. Behr and B. Demenix (1998). Self-assembling complexes for gene delivery, Kabanov, A.V., Felgner, P.L. and Seymour, L., Eds. (John Wiley & Sons).

Remy, J. S., A. Kichler, V. Mordvinov, F. Schuber and J. P. Behr (1995). Targeted gene transfer into hepatoma cells with lipopolyamine-condensed DNA particles presenting galactose ligands: a stage toward artificial viruses. *Proc Natl Acad Sci U S A* **92**, 1744-1748.

Ren, Q. and M. A. Gorovsky (2003). The nonessential H2A N-terminal tail can function as an essential charge patch on the H2A.Z variant N-terminal tail. *Mol Cell Biol* **23**, 2778-2789.

Rill, R. L. (1986). Liquid-crystalline phases in concentrated aqueous-solutions of Na+ DNA. *Proc Natl Acad Sci* **83**, 342-346.

Rolland, A. P. (1996). Controllable gene therapy: recent advances in nonviral gene delivery. In Targeting of Drugs, Vol. 5, Strategies for Oligonucleotide and Gene Delivery in Therapy. Plenum Press, New York.

Rolland, A. P. (1998). From genes to gene medicine: Recent advances in nonviral gene delivery, In Crit. Rev. Ther. Drug Carrier Syst., vol. 15. S. D. Bruck, editor. Begell House, New York.

Rolland, A. P. and E. Tomlinson (1996). Controllable gene therapy using nanoparticle systems. In Artificial Self-Assembling Systems for Gene Delivery. American Chemical Society, Washington, DC.

Ruoslahti, E. (1996). RGD and other recognition sequences for integrins. *Annu Rev Cell Dev Biol* **12**, 697-715.

Schellman, J. A. and N. Parthasarathy (1984). X-ray diffraction studies on cation-collapsed DNA. *J Mol Biol* **175**, 313-329.

Schmidt-Wolf, G. D. and I. G. Schmidt-Wolf (2003). Non-viral and hybrid vectors in human gene therapy: an update. *Trends Mol Med* **9**, 67-72.

Scott, E. S., J. W. Wiseman, M. J. Evans and W. H. Colledge (2001). Enhanced gene delivery to human airway epithelial cells using an integrin-targeting lipoplex. *J Gene Med* **3**, 125-134.

Shapiro, J. T., M. Leng and G. Felsenfeld (1969). Deoxyribonucleic acid-polylysine complexes. Structure and nucleotide specificity. *Biochemistry* **8**, 3119-3132.

Shih, I.-L., M.-H. Shen and Y.-T. Van (2006). Microbial synthesis of poly(ε-lysine) and its various applications. *Bioresour Technol* **97**, 1148-1159.

Shirakawa, H., D. Landsman, Y. V. Postnikov and M. Bustin (2000). NBP-45, a novel nucleosomal binding protein with a tissue-specific and developmentally regulated expression. *J Biol Chem* **275**, 6368-6374.

Shirikawa, H., J. E. Herrera, M. Bustin and Y. Postnikov (2000). Targeting of high mobility group-14/-17 proteins in chromatin is independent on DNA sequence. *J Biol Chem* **275**, 37937-37944.

Sikorav, J. L., J. Pelta and F. Livolant (1994). A liquid crystalline phase in spermidine-condensed DNA. *Biophys J* **67**, 1387-1392.

Singh, R. S., C. Goncalves, P. Sandrin, C. Pichon, P. Midoux and A. Chaudhuri (2004). On the gene delivery efficacies of pH-sensitive cationic lipids via endosomal protonation: A chemical biology investigation. *Chem Biol* **11**, 713-723.

Singla, A. K. and M. Chawla (2001). Chitosan: some pharmaceutical and biological aspects--an update. *J Pharm Pharmacol* **53**, 1047-1067.

Smith, A. E. (1995). Viral vectors in gene therapy. *Annu Rev Microbiol.* **49**, 807-838.

Smith, L. C., J. Duguid, M. S. Wadhwa, M. J. Logan, C.-H. Tung, V. Edwards and J. T. Sparrow (1998). Synthetic peptide-based DNA complexes for nonviral gene delivery. *Adv Drug Delivery Revs* **30**, 115-131.

Springer, T. A. (1990). Adhesion receptors of the immune system. *Nature* **346**, 425-434.

Strahl, B. D. and C. D. Allis (2000). The language of covalent histone modifications. *Nature* **403**, 41-45.

Suh, W., J. K. Chung, S. H. Park and S. W. Kim (2001). Anti-JL1 antibody-conjugated poly (L-lysine) for targeted gene delivery to leukemia T cells. *J Contr Rel* **72**, 171-178.

Suh, W., S. O. Han, L. Yu and S. W. Kim (2002). An angiogenic, endothelial-cell-targeted polymeric gene carrier. *Mol.Ther.* **6**, 664-672.

Takahashi, M., K. Yoshikawa, V. V. Vasilevskaya and A. R. Khokhlov (1997). Discrete coil-globule transition of single duplex DNAs induced by polyamines. *J Phys Chem B* **101**, 9396-9401.

Tam, J. P., Y. A. Lu and J. L. Yang (2002). Antimicrobial dendrimeric peptides. *Eur J Biochem* **269**, 923-932.

Tatum, E. L. (1967). Molecular biology, nucleic acids, and the future of medicine. In: Lyght CE, ed. Refections on Research and the Future of Medicine. New York: McGraw-Hill. 31-49.

Timme, T. L., S. J. Hall, R. Barrios, S. L. Woo, E. Aguilar-Cordova and T. C. Thompson (1998). Local inflammatory response and vector spread after direct intraprostatic injection of a recombinant adenovirus containing the herpes simplex virus thymidine kinase gene and ganciclovior therapy in mice. *Cancer Gene Ther* **5**, 74-82.

Tomlinson, E. and A. P. Rolland (1996). Controllable gene therapy: Pharmaceutics of non-viral gene delivery systems. *J Contr Rel* **39**, 357-372.

Tratschin, J. D., M. H. West, T. Sandbank and B. J. Carter (1984). A human parvovirus, adeno-associated virus, as a eucaryotic vector: transient expression and encapsidation of the procaryotic gene for chloramphenicol acetyltransferase. *Mol Cell Biol* **4**, 2072-2081.

Trieschmann, L., P. J. Alfonso, M. P. Crippa, A. P. Wolffe and M. Bustin (1995). Incorporation of chromosomal proteins HMG-14/HMG-17 into nascent nucleosomes induces an extended chromatin conformation and enhances the utilization of active transcription complexes. *Embo J* **14**, 1478-1489.

Trieschmann, L., B. Martin and M. Bustin (1998). The chromatin unfolding domain of chromosomal protein HMG-14 targets the N-terminal tail of histone H3 in nucleosomes. *Proc Natl Acad Sci* **95**, 5468-5473.

Trieschmann, L., Y. V. Postnikov, A. Rickers and M. Bustin (1995). Modular structure of chromosomal protein HMG-14 and HMG-17: definition of transcriptional enhancement domain distinct from the nucleosomal binding domain. *Mol Cell Biol* **15**, 6663-6669.

Trubetskoy, V. S., V. P. Torchilin, S. Kennel and L. Huang (1992). Cationic liposomes enhance targeted delivery and expression of exogenous DNA mediated by N-

terminal modified poly(L-lysine)-antibody conjugate in mouse lung endothelial cells. *Biochim Biophys Acta* **1131**, 311-313.

Turk, M. J., J. A. Reddy, J. A. Chmielewski and P. S. Low (2002). Characterization of a novel pH-sensitive peptide that enhances drug release from folate-targeted liposomes at endosomal pHs. *Biochim Biophys Acta* **1559**, 56-68.

Van Doren, K., D. Hanahan and Y. Gluzman (1984). Infection of eucaryotic cells by helper-independent recombinant adenoviruses: early region 1 is not obligatory for integration of viral DNA. *J Virol* **50**, 606-614.

Varner, J. A. and D. A. Cheresh (1996). Integrins and cancer. *Curr Opin Cell Biol* **8**, 724-730.

Vasilevskaya, V. V., A. R. Khokhlov, S. Kidoaki and K. Yoshikawa (1997). Structure of collapsed persistent macromolecule: toroid versus spherical globule. *Biopolymers* **41**, 51-60.

Venugopalan, P., S. Jain, S. Sankar, P. Singh, A. Rawat and S. P. Vyas (2002). pH-sensitive liposomes: mechanism of triggered release to drug and gene delivery prospects. *Pharmazie* **57**, 659-671.

Vijayanathan, V., T. Thomas and T. J. Thomas (2002). DNA nanoparticles and development of DNA delivery vehicles for gene therapy. *Biochemistry* **41**, 14085-14094.

Vinod Kumar, V., C. Pichon, M. Refregiers, B. Guerin, P. Midoux and A. Chaudhuri (2003). Single histidine residue in head-group region is sufficient to impart remarkable gene transfection properties to cationic lipids: evidence for histidine mediated fusion at acidic pH. *Gene Ther* **10**, 1206-1215.

Vitiello, L., A. Chonn, J. D. Wasserman, C. Duff and R. G. Worton (1996). Condensation of plasmid DNA with polylysine improves liposome mediated gene transfer into established and primary muscle cells. *Gene Ther.* **3**, 396-404.

Votavova, H., D. Kucerova, J. Felsberg and J. Sponar (1986). Changes in conformation, stability and condensation of DNA by univalent and divalent cations in methanol-water mixtures. *J Biomol Struct Dyn* **4**, 477-489.

Wadhwa, M. S., W. T. Collard, R. C. Adami, D. L. McKenzie and K. G. Rice (1997). Peptide-mediated gene delivery: influence of peptide structure on gene expression. *Bioconjug Chem* **8**, 81-88.

Wagner, E., M. Cotten, R. Foisner and M. L. Birnstiel (1991). Transferrin-polycation-DNA complexes: the effect of polycations on the structure of the complex and DNA delivery to cells. *Proc Natl Acad Sci* **88**, 4255-4259.

Wagner, E., C. Plank, K. Zatloukal, M. Cotten and M. L. Birnstiel (1992). Influenza virus hemagglutinin HA-2 N-terminal fusogenic peptides augment gene transfer by transferrin-polylysine-DNA complexes: toward a synthetic virus-like gene-transfer vehicle. *Proc Natl Acad Sci* **89**, 7934-7938.

Wagner, E., M. Zenke, M. Cotten, H. Beug and M. L. Birnstiel (1990). Transferrin-polycation conjugates as carriers for DNA uptake into cells. *Proc Natl Acad Sci* **87**, 3410-3414.

Wang, C. Y. and L. Huang (1989). Highly efficient DNA delivery mediated by pH-sensitive immunoliposomes. *Biochemistry* **28**, 9508-9514.

West, K. L., Y. Ito, Y. Birger, Y. Postnikov, H. Shirakawa and M. Bustin (2001). HMGN3a and HMGN3b, two protein isoforms with a tissue-specific expression pattern, expand the cellular repertoire of nucleosome-binding proteins. *J Biol Chem* **276**, 25959-25969.

Wheeler, C. J., P. L. Felgner, Y. J. Tsai, J. Marshall, L. Sukhu, S. G. Doh, J. Hartikka, J. Nietupski, M. Manthorpe, M. Nichols, M. Plewe, X. Liang, J. Norman, A. Smith and S. H. Cheng (1996). A novel cationic lipid greatly enhances plasmid DNA delivery and expression in mouse lung. *Proc Natl Acad Sci* **93**, 11454-11459.

Wickham, T. J., P. Mathias, D. A. Cheresh and G. R. Nemerow (1993). Integrins alpha v beta 3 and alpha v beta 5 promote adenovirus internalization but not virus attachment. *Cell* **73**, 309-319.

Widom, J. (1986). Physicochemical studies of the folding of the 100 A nucleosome filament into the 300 A filament. Cation dependence. *J Mol Biol* **190**, 411-424.

Widom, J. (1998). Structure, dynamics, and function of chromatin in vitro. *Annu Rev Biophys Biomol Struct* **27**, 285-327.

Widom, J. and R. L. Baldwin (1980). Cation-induced toroidal condensation of DNA studies with $Co^{3+}(NH_3)_6$. *J Mol Biol* **144**, 431-453.

Widom, J. and R. L. Baldwin (1983). Monomolecular condensation of lambda-DNA induced by cobalt hexamine. *Biopolymers* **22**, 1595-1620.

Wigler, M., S. Silverstein, L. S. Lee, A. Pellicer, Y. Cheng and R. Axel (1977). Transfer of purified herpes virus thymidine kinase gene to cultured mouse cells. *Cell* **11**, 223-232.

Willis, R. C., D. J. Jolly, A. D. Miller, M. M. Plent, A. C. Esty, P. J. Anderson, H. C. Chang, O. W. Jones, J. E. Seegmiller and T. Friedmann (1984). Partial phenotypic correction of human Lesch-Nyhan (hypoxanthine-guanine phosphoribosyltransferase-deficient) lymphoblasts with a transmissible retroviral vector. *J Biol Chem* **259**, 7842-7849.

Wilson, R. W. and V. A. Bloomfield (1979). Counterion-induced condensation of deoxyribonucleic acid. A light-scattering study. *Biochemistry* **18**, 2192-2196.

Wolf, J. K. and A. D. Jenkins (2002). Gene therapy for ovarian cancer (review). *Int J Oncol* **21**, 461-468.

Wolffe, A. P. (1998). Chromatin: Structure and function. San Diego, CA, Academic Press. 447.

Wolffe, A. P. and J. J. Hayes (1999). Chromatin disruption and modification. *Nucleic Acids Res* **27**, 711-720.

Woodcock, C. L. and S. Dimitrov (2001). Higher-order structure of chromatin and chromosomes. *Curr Opin Genet Dev* **11**, 130-135.

Wu, G. Y. and C. H. Wu (1987). Receptor-mediated *in vitro* gene transformation by a soluble DNA carrier system. *J Biol Chem* **262**, 4429-4432.

Wu, G. Y. and C. H. Wu (1988). Evidence for targeted gene delivery to Hep G2 hepatoma cells in vitro. *Biochemistry* **27**, 887-892.

Wu, G. Y. and C. H. Wu (1988). Receptor-mediated gene delivery and expression in vivo. *J Biol Chem* **263**, 14621-14624.

Xu, Y., S. W. Hui, P. Frederik and F. C. Szoka, Jr. (1999). Physicochemical characterization and purification of cationic lipoplexes. *Biophys J* **77**, 341-353.

Xu, Y. and F. C. Szoka, Jr. (1996). Mechanism of DNA release from cationic liposome/DNA complexes used in cell transfection. *Biochemistry* **35**, 5616-5623.

Yen, W. S. and B. R. Ware (1982). Counterion condensation of DNA studied by electrophoretic light scattering. *Biophys J* **37**, 291a.

Yoshikawa, K., Y. Yoshikawa, Y. Koyama and T. Kanbe (1997). Highly effective compaction of long duplex DNA induced by polyethylene glycol with pendant amino group. *J Amer Chem Soc* **119**, 6473-6477.

Yu, Q., W. C., J. Yang and J. P. Tam. A simple approach to design β-strand antimicrobial peptide mimetics through peptide dendrimers with ε-peptide scaffolds. In manuscript.

Yu, W., K. F. Pirollo, B. Yu, A. Rait, L. Xiang, W. Huang, Q. Zhou, G. Ertem and E. H. Chang (2004). Enhanced transfection efficiency of a systemically delivered tumor-targeting immunolipoplex by inclusion of a pH-sensitive histidylated oligolysine peptide. *Nucleic Acids Res* **32**, e48.

Zabner, J., A. J. Fasbender, T. Moninger, K. A. Poellinger and M. J. Welsh (1995). Cellular and molecular barriers to gene transfer by a cationic lipid. *J Biol Chem* **270**, 18997-19007.

Zanta, M. A., O. Boussif, A. Adib and J. P. Behr (1997). In vitro gene delivery to hepatocytes with galactosylated polyethylenimine. *Bioconjug Chem* **8**, 839-844.

Zauner, W., M. Ogris and E. Wagner (1998). Polylysine-based transfection systems utilizing receptor-mediated delivery. *Adv Drug Delivery Revs* **30**, 97-113.

Zhou, X. H., A. L. Klibanov and L. Huang (1991). Lipophilic polylysines mediate efficient DNA transfection in mammalian cells. *Biochim Biophys Acta* **1065**, 8-14.

Zuber, G., E. Dauty, M. Nothisen, P. Belguise and J. P. Behr (2001). Towards synthetic viruses. *Adv Drug Deliv Rev* **52**, 245-253.

Appendix

Publications:

Dandan Huang, Nikolay Korolev, Khee Dong Eom, James P. Tam and Lars Nordenskiöld, *"Design and Biophysical Characterization of Novel Polycationic ε-Peptides for DNA Compaction and Delivery"*. **Biomacromolecules,** 2008, 9, 321-330

Dandan Huang, Nikolay Korolev, Lars Nordenskiöld, *"Novel Polycationic ε-Peptides for DNA Compaction and Delivery"*. **Human Gene Therapy,** 2007, 18, 1058-1059
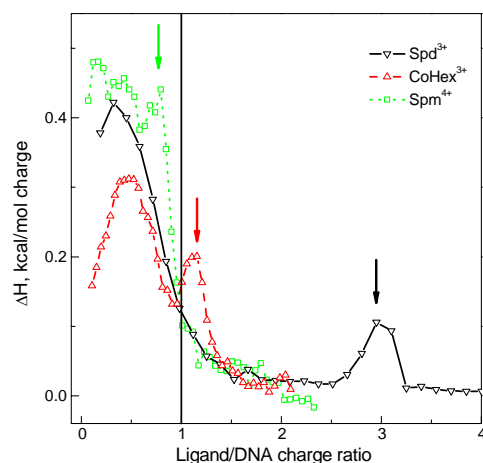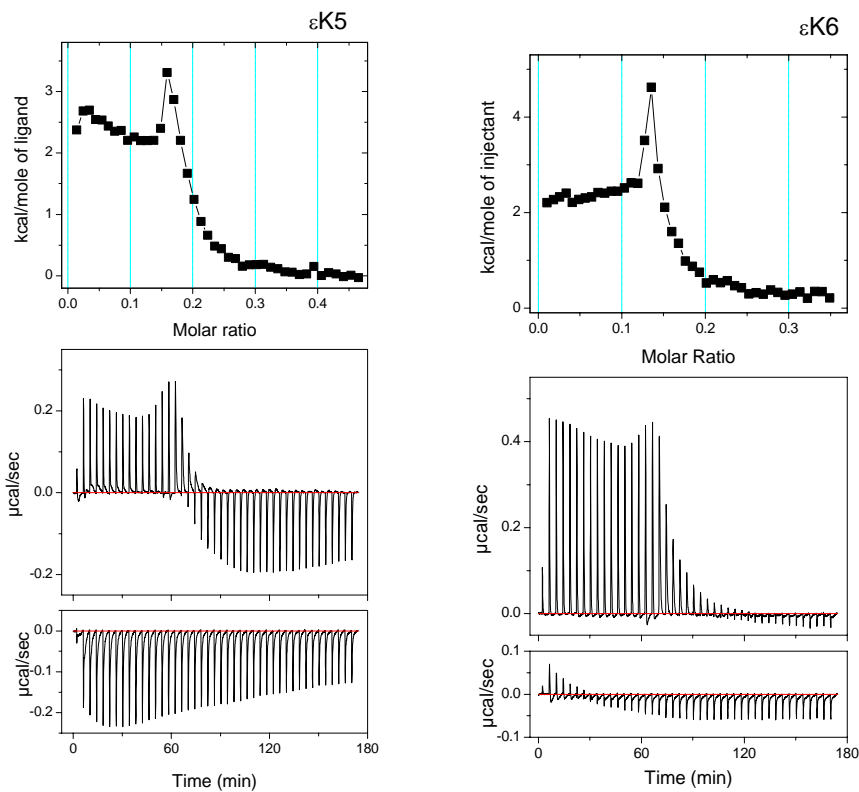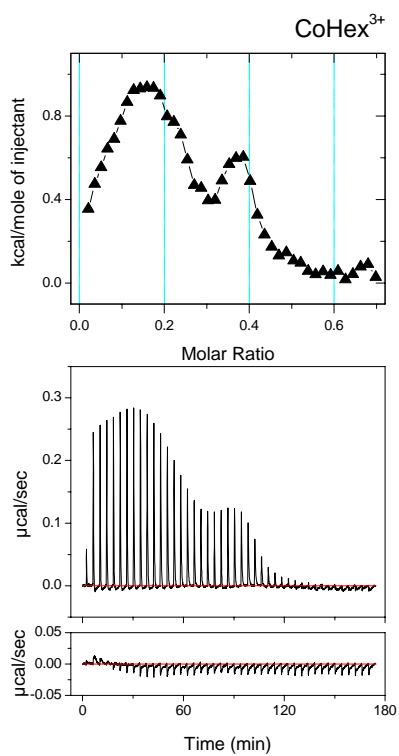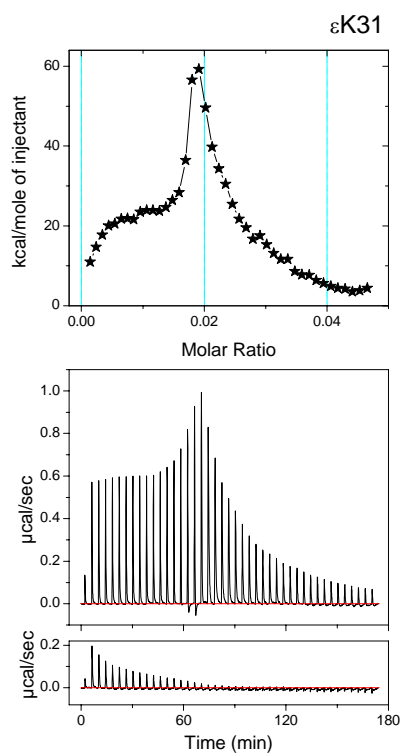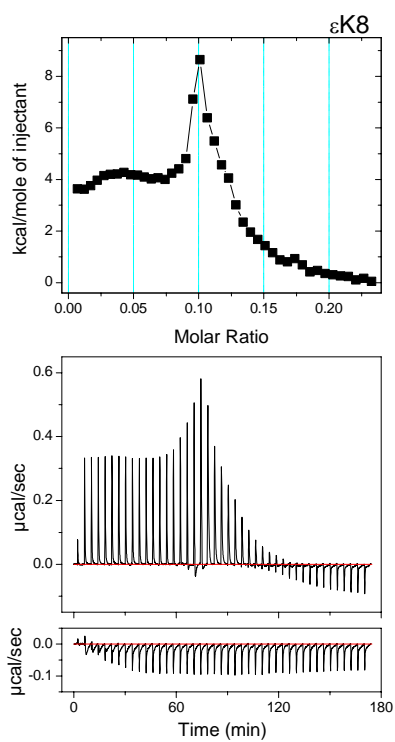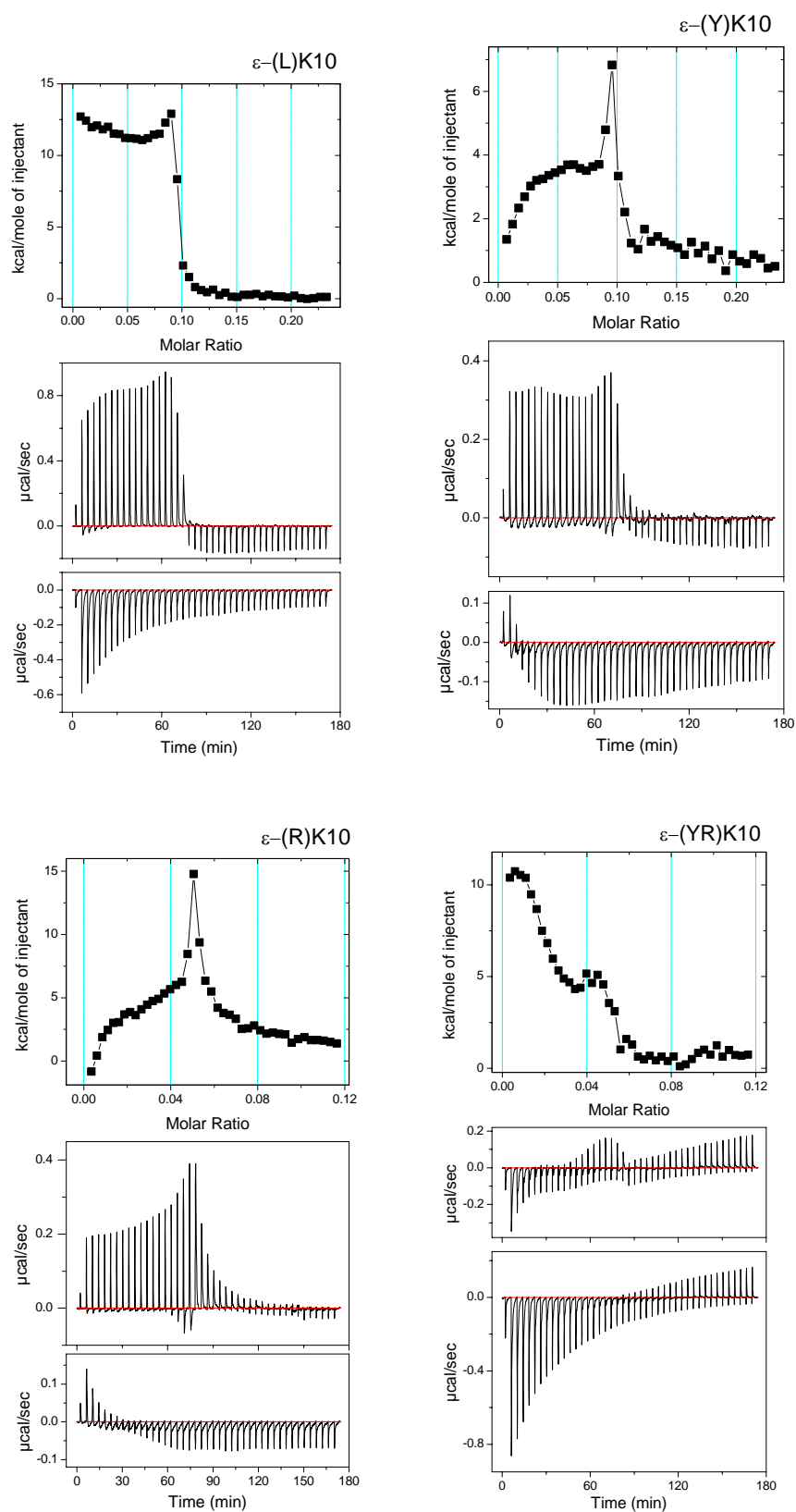
Supplementary Figures:

Figure 32. Results of isothermal titration calorimetry.

Values of enthalpy at 298 K calculated from titration curves were normalized relative to the charge of the cationic ligand and plotted versus ratio of added ligand charge to charge of the DNA. Titration of the same DNA sample by solutions of $Co(NH_3)_6Cl_6$, Spd^{3+} and Spm^{4+} are shown.
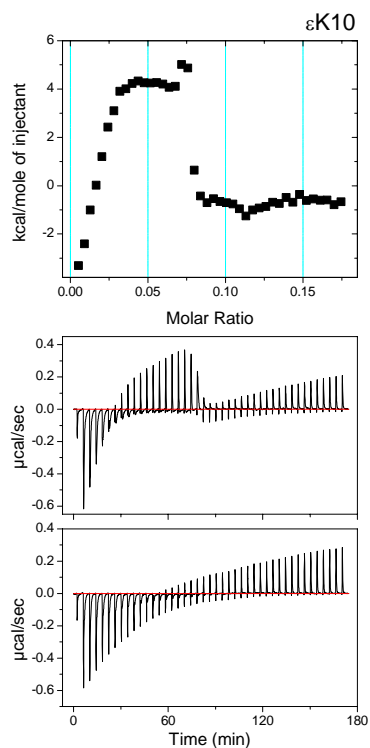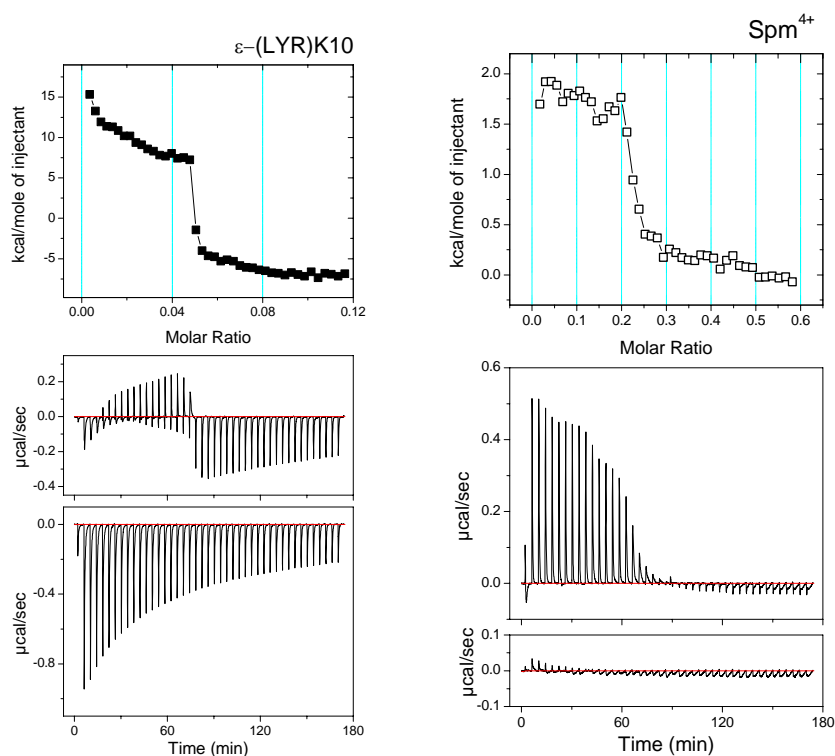
Figure 33. ITC raw data.

Titration of 0.4 mM solution of plasmid DNA by different titrants in 10 mM KCl. For every panel, top graph shows the results of the ITC data analysis: dependence of ΔH of ligand-DNA interaction on molar ligand/DNA ratio; middle graph displays titration of the DNA solution; bottom picture presents reference titration of 10 mM KCl by the same titrant.